

INVESTIGATING THE ^{13}C SUESS EFFECT IN THE NORTHWESTERN
NORTH ATLANTIC

by

Stefanie Mellon

Submitted in partial fulfillment of the requirements
for the degree of Master of Science

at

Dalhousie University
Halifax, Nova Scotia
September 2018

© Copyright by Stefanie Mellon, 2018

TABLE OF CONTENTS

List of Tables	v
List of Figures	vi
Abstract	ix
List of Abbreviations and Symbols Used	x
Acknowledgements	xii
Chapter 1 Introduction	1
Chapter 2 Background Information	5
2.1 The ^{13}C Suess Effect	5
2.2 Foraminifera as a proxy for $\delta^{13}\text{C}$ of DIC	10
2.3 Oceanographic Conditions in the Northwest Atlantic	13
Chapter 3 Methods	16
3.1 Core Collection	16
3.2 Laboratory Analysis	17
3.3 Statistical Analysis	19
Chapter 4 Age Models	21
4.1 Age Model Methods	21
4.1.1 ^{210}Pb	23
4.1.2 ^{14}C	27
4.2 Results from Bacon Age Models	29
4.2.1 KNR158	29

4.2.2	OCE326 MC29D and OCE400 MC44	30
4.2.3	Hg analysis and MSM46 Cores	31
Chapter 5	Results	35
5.1	Carbon Isotopes	35
5.1.1	Foraminiferal Records	35
5.1.2	Organic Matter	39
5.2	Results of Piecewise Regressions	41
5.2.1	MSM46 MC4	41
5.2.2	MSM46 MC2	42
5.2.3	KNR15 11BC/13GGC	43
5.2.4	OCE326 MC29	44
5.2.5	OCE400 MC44	45
5.2.6	MSM46 Organic Carbon	46
5.2.7	Time of Emergence of CIEs	47
5.3	Summary of Results	48
Chapter 6	Discussion	51
6.1	Effects on $\delta^{13}\text{C}$ of DIC	52
6.2	Disequilibrium effects between $\delta^{13}\text{C}$ DIC and carbonate	54
6.2.1	Calcification Temperature	55
6.2.2	Carbonate Ion Effect	58
6.2.3	Foraminiferal Diet	59
6.3	The northwestern North Atlantic Suess effect	60
6.4	Impact of Bioturbation	62
6.5	Estimates of Anthropogenic CO_2 Uptake	63
Chapter 7	Conclusion	65
Bibliography	67

Appendix 74

LIST OF TABLES

3.1	Locations of the cores investigated in my thesis.	16
3.2	Approximate sampling intervals of each core investigated in this study.	18
3.3	Foraminifera species and grain sizes picked from each core in this study.	18
4.1	Types of dating methods applied to each sediment core from this study.	23
4.2	Radiocarbon ages on foraminifera from OCE326 MC-29D, Emerald Basin (published in <i>Keigwin et al. (2003)</i>).	28
4.3	Radiocarbon ages on planktonic foraminifera (<i>G. bulloides</i>) from KNR158-4-11BC and KNR158-13GGC (unpublished Marchitto and deMenocal).	29
4.4	Radiocarbon ages on planktonic foraminifera from OCE400 MC44 (<i>Keigwin and Pilskałn, 2015</i>).	29
5.1	Change point year (AD) of each foraminifera record and corresponding 1σ uncertainties in the age-depth and broken line models, respectively.	47
5.2	Summary table of the piecewise linear regressions for each core, including carbon isotope excursions.	48
1	Foraminiferal $\delta^{13}\text{C}$, $\delta^{13}\text{O}$, and Bacon age output data from MSM46 MC2.	76
2	Foraminiferal $\delta^{13}\text{C}$, $\delta^{13}\text{O}$, and Bacon age output data from MSM46 MC4.	78

LIST OF FIGURES

1.1	Depth-integrated inventory of anthropogenic CO ₂ over the global ocean in moles m ⁻² , from <i>Sabine et al. (2004)</i>	2
1.2	A 1000 year record of atmospheric CO ₂ (red circles) and its δ ¹³ C composition (black circles).	3
2.1	Illustration from <i>Le Quéré et al. (2016)</i> of the mass flow rates between major carbon reservoirs over the last decade (2006-2015). .	7
2.2	Global Suess effect (‰) modeled at selected depths from <i>Eide et al. (2017a)</i>	9
2.3	Map from <i>Eide et al. (2017a)</i> displaying locations and Suess effect magnitudes of scleractinian corals (<i>Swart et al., 2010</i>) and sclerosponges (<i>Böhm et al., 1996; Worheide, 1998; Swart et al., 1996; Böhm et al., 2000</i>).	10
2.4	Record of planktonic foraminifera δ ¹³ C from the Caribbean Sea since 1725 (heavy black line) compared to Siple ice core (light blue square) and Mauna Loa atmospheric CO ₂ records (dark blue squares). 11	11
2.5	Bathymetric map and major current systems of the northwest Atlantic.	14
3.1	Map of core sites from this study on the northwestern shelf of the North Atlantic.	17
4.1	(a) Bacon default accumulation rate prior, which follows a gamma distribution.	23
4.2	²¹⁰ Pb activity profiles of core OCE400 MC44.	25
4.3	²¹⁰ Pb activity profiles of core OCE326 MC29.	26
4.4	Calibrated radiocarbon dates (purple) and corresponding age-depth model for KNR158 11BC/13GGC, where the darker grays represent more likely calendar ages.	30
4.5	Radiocarbon dates (purple), Pb-210 derived age points (green) and corresponding age-depth models for both (a) OCE326 MC29 and (b) OCE400 MC44.	31
4.6	The Hg profile from MSM46MC2 plotted with different age models. 33	33

4.7	(a) Hg ($\mu\text{g/g}$) vs. sediment depth (bottom axis) and ^{210}Pb date (top axis) of a non-bioturbated core from the Saguenay Fjord.	33
4.8	Hg profile of core MSM46 MC4 plotted with published sedimentation rates from nearby core sites in (<i>Jennane, 1993</i>) (red and black) and the constructed age model described in the text (green). . . .	34
4.9	Age markers (green) and corresponding age-depth models for both (a) MSM46 MC2 and (b) MSM46 MC4, where the darker grays represent more likely calendar ages.	34
5.1	Results of all foraminiferal $\delta^{13}\text{C}$ downcore records from the eastern Canadian continental margin.	36
5.2	Results of all foraminiferal $\delta^{13}\text{C}$ time series records from the eastern Canadian continental margin.	37
5.3	All $\delta^{13}\text{C}$ core records plotted versus age from 1700-2015 AD. . . .	38
5.4	Time series results of (a) $\delta^{13}\text{C}_{org}$ and (b) $\%C_{org}$ of the MSM46 cores in the Gulf of St. Lawrence.	40
5.5	$\delta^{13}\text{C}$ of organic carbon (red) and <i>N. pachyderma</i> (black) time series results of cores (b) MSM46 MC2 and (b) MSM46 MC4.	40
5.6	Piecewise linear regression results on foraminiferal $\delta^{13}\text{C}$ records from MSM46 MC4.	42
5.7	The MSM46 MC2 (a) two-piece and (b) three-piece linear regression results on $\delta^{13}\text{C}$ of planktic foraminifera, <i>N. pachyderma</i>	43
5.8	The KNR158 11BC/13GGC piecewise linear regression results on $\delta^{13}\text{C}$ of planktic foraminifera, <i>G. bulloides</i>	44
5.9	Piecewise linear regression results on foraminiferal $\delta^{13}\text{C}$ records from OCE326 MC29D.	45
5.10	OCE400 MC44 piecewise linear regression results on $\delta^{13}\text{C}$ of planktic foraminifera, <i>N. incompta</i>	46
5.11	Statistical analysis of CIEs on $\delta^{13}\text{C}_{org}$ of a.) MSM46 MC2 using a broken-line model and b) MSM46 MC4 using the difference between pre-industrial and modern day $\delta^{13}\text{C}$ values	47
5.12	Compilation of foraminiferal $\delta^{18}\text{O}$ records from all core sites in the study region.	49
5.13	Compilation of foraminiferal $\delta^{13}\text{C}$ records from all core sites in the study region.	50

6.1	Observed (black) and 2013-adjusted (purple) $\delta^{13}\text{C}$ excursions for all foraminiferal records.	52
6.2	$\delta^{18}\text{O}$ <i>G. auriculata</i> downcore records from cores MD99-2220, CR02-23, and COR0503-37BC (Retreived from <i>Thibodeau et al.</i> (2010) with permission by John Wiley and Sons).	57
6.3	A compilation of foraminiferal based temperature proxies from three cores on the Northwest Atlantic Slope (Emerald Basin, Gulf of St. Lawrence, and Laurentian Fan.	57
6.4	Effect of different $\delta^{13}\text{C}$ food sources on chamber $\delta^{13}\text{C}$ of <i>G. bulloides</i> . 60	60
6.5	Observed (black) and 2013-adjusted (purple) Suess effect magnitudes for the atmosphere and all foraminiferal records.	61
6.6	A high resolution $\delta^{13}\text{C}_{\text{CO}_2}$ record compiled from ice core, firn, and direct atmospheric CO_2 samples that cover 1000 to 2015 AD (<i>Graven et al.</i> , 2017).	62

ABSTRACT

The carbon isotope signature ($\delta^{13}\text{C}$) of atmospheric CO_2 has decreased as a direct result of anthropogenic CO_2 emissions since the industrial revolution. This climate phenomenon has been termed the ^{13}C Suess effect, and can be used to trace anthropogenic CO_2 penetration into the surface ocean. This thesis presents the first long-term $\delta^{13}\text{C}$ time series from the northwestern shelf region of the North Atlantic recorded in fossil foraminifera from five high-resolution sediment cores. These records reveal a Suess effect signal that emerges in the mid-twentieth century with a magnitude of -0.64 ± 0.32 ‰ (i.e., 40% of the atmospheric signal) and a $\delta^{13}\text{C}$ decrease rate of -0.014 ± 0.005 ‰ yr^{-1} (58% of the atmospheric rate), a $\delta^{13}\text{C}$ decrease unprecedented over the 4000 years sampled by the foraminifera records. The implications of these findings are discussed in the context of air-sea CO_2 exchange rates, foraminiferal calcification vital effects, and post-depositional processes in the sediments.

LIST OF ABBREVIATIONS AND SYMBOLS USED

Abbreviation/Symbol	Description
$\delta^{13}\text{C}$	carbon isotope signature
$\delta^{13}\text{C}_{foram}$	carbon isotope signature of foraminifera
$\delta^{13}\text{C}_{org}$	carbon isotope signature of organic matter
$\delta^{13}\text{C}_{PI}$	pre-industrial carbon isotope signature
$\delta^{13}\text{C}_{SE}$	^{13}C Suess effect
ΔC_t	anthropogenic CO_2 uptake rate
ΔRC	$\Delta\delta^{13}\text{C}/\Delta\text{C}_t$
$\%C_{org}$	percent organic carbon
1σ	1 standard deviation
^{14}C	Radiocarbon
AMOC	Atlantic Meridional Overturning Circulation
BP	before present (1950)
CaCO_3	calcium carbonate
CFC/pCFC-12	chlorofluorocarbons
CF-CS	Constant Flux-Constant Supply
CIE	carbon isotope excursion
CO_2	carbon dioxide
$[\text{CO}_3^{2-}]$	carbonate ion concentration
CP	change point
CRS	Constant Rate of Supply
DIC	dissolved inorganic carbon
GGC	Giant Gravity Core
GoM	Gulf of Maine
GoSL	Gulf of St. Lawrence
Hg	Mercury
IRMS	Isotope Ratio Mass Spectrometer
LC	Labrador Current

Abbreviation/Symbol	Description
LCW	Labrador Current Water
LSLE	Lower St. Lawrence Estuary
MC	Multi Core
NACW	North Atlantic Central Water
NAO	North Atlantic Oscillation
NSC	Nova Scotia Current
ToE	Time of Emergence

ACKNOWLEDGEMENTS

I first and foremost would like to thank my supervisor, Markus Kienast, not only for providing me with countless opportunities and scientific guidance over the past five years, but for his endless optimism, for his reminders to keep looking “onwards and upwards”, and for teaching me the value of serendipity both in science and in life.

Thank you to my committee members, Helmuth Thomas and Stephanie Kienast, for their ideas and constructive comments throughout the research and writing processes. I am more than grateful to the entire Kienast Lab, whose advice, support, and company I couldn't have done without. Thank you to Peter DeMenocal, Tom Marchitto, and Lloyd Keigwin for sharing the data from cores KNR158 11BC/13GGC, OCE326 MC29D, and OCE400 MC44. Thank you to Ed Boyle for sharing ^{210}Pb data for core OCE400 MC44. Thanks to Matthias Moros for providing mercury measurements on MSM46 cores. Thank you to Claire Normandeau and the UC Santa Cruz Stable Isotope Facility for performing stable isotope analysis on the organic matter and foraminifera samples. Laboratory work was made much easier thanks to assistance from Lachlan Riehl and Chloe Younger. Thanks to Marit-Solveig Sidenkranz for hosting me in Aarhus and introducing me to the art of foram picking. Thank you to Delia Oppo and her lab group for hosting me at WHOI, assisting me with stable isotope analysis, and for the many helpful discussions. Thanks to Michael Dowd for all of his input on the statistical handling of my data. This research wouldn't have been possible without funding from MEOPAR, Environment and Climate Change Canada, NSERC, CMOS, and Clean NS – so thank you.

I am very appreciative of the many friends from DOSA and USSP 2017 who have inspired and supported me over these past years. Special thanks to Christoph Renkl, Jenna Hare, and Lorenza Raimondi for donating their time to help me over the many hurdles encountered with Latex and the Carbon Cycle. Thank you to the friends outside of my academic circle who helped me maintain a work-life balance over the past 2.5 years. Among them were Kevin Cox, Brooke Edwards, Nikki van der Waal, Ana Eguiren, Emily Higgins, and many more. Finally, thank you to my family – Dale Mellon, Gregg Mellon, Kathy Ure, Barry White, Spencer Mellon, and Sean White – for their ceaseless

love and support.

CHAPTER 1

INTRODUCTION

Anthropogenic activity involving the combustion of fossil fuels and land use change is perturbing the global carbon cycle. The atmospheric carbon dioxide (CO₂) concentration has increased from 280 ppm to 406 ppm (*Dlugokencky and Tans, 2017*) since the beginning of the industrial revolution in the mid-1800s. This increase in atmospheric CO₂, along with other gases, is enhancing a process called the “greenhouse effect” that traps heat in the Earth’s atmosphere. The greenhouse effect is the cause of the well documented increase in global temperature ($0.85 \pm 0.2^\circ\text{C}$ over the period 1880 to 2012), widely known as “global warming” (*IPCC, 2014*). Since the ocean is a major sink for CO₂, the CO₂ concentration in the ocean is also increasing (*Sabine et al., 2004*). Figure 1.1 illustrates the depth-integrated inventory of anthropogenic CO₂ (in moles m⁻²) over the global ocean.

The CO₂ that enters the ocean reacts with water to form carbonic acid, bicarbonate, and carbonate ions, and has led to a decrease in pH values compared to pre-industrial times (*Caldeira and Wickett, 2003*). This ocean acidification, often referred to as the “other CO₂ problem”, makes it more difficult for calcifying organisms to form their shells (*Hendriks et al., 2010*). Despite remaining uncertainties regarding the exact regions that will be affected by ocean acidification and the magnitude of pH change, there will likely be global impacts on marine ecosystems and living resources.

With the threat of ocean acidification from increased penetration of anthropogenic CO₂, there is a need to establish a historical record of the carbon cycle throughout the global ocean to distinguish natural variability from secular trends. Since there are few extensive, in-situ time series measurements, paleoclimate proxies are an important tool for reconstructing climate parameters further back in time. The time at which a

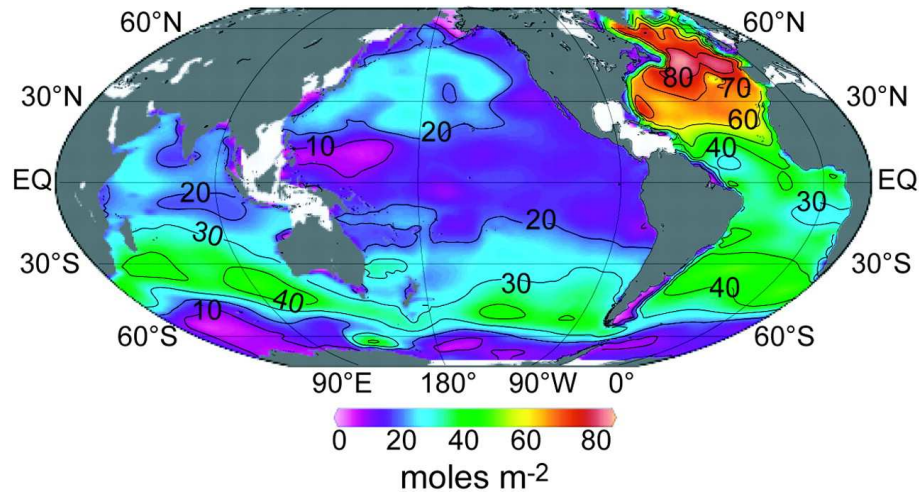


Figure 1.1: Depth-integrated inventory of anthropogenic CO_2 over the global ocean in moles m^{-2} . Higher values indicate a larger total water column inventory of anthropogenic CO_2 , associated with regions of deep water formation in the North Atlantic, and intermediate and mode water formation at mid-latitudes. From *Sabine et al.* (2004). Reprinted with permission from AAAS.

climate change signal emerges from the background natural climate variability is called the Time of Emergence (ToE), which is a key variable in climate predictions (Hawkins & Sutton, 2012). My thesis project uses paleoceanographic techniques to investigate the influence of anthropogenic CO_2 on the carbon isotope signature of the dissolved inorganic carbon (DIC) pool ($\delta^{13}\text{C}_{\text{DIC}}$) in the ocean and to determine the ToE of this climate signal.

The release of ^{13}C and ^{14}C depleted anthropogenic CO_2 since the industrial revolution has decreased the carbon isotope signature of the atmosphere ($\delta^{13}\text{C}_{\text{CO}_2}$) (Figure 1.2). Ice cores and modern atmospheric measurements reveal an abrupt decrease in global $\delta^{13}\text{C}_{\text{CO}_2}$ since preindustrial times of -2.2‰ (*Keeling et al.*, 2001; *Francey et al.*, 1999; *Rubino et al.*, 2013). This ubiquitous perturbation, first observed by Hans Suess in tree ring ^{14}C records, has been termed the ‘‘Suess effect’’. Since the ocean absorbs a large portion of anthropogenic CO_2 , it is expected that the (^{13}C) Suess effect is detectable in the $\delta^{13}\text{C}_{\text{DIC}}$ of waters that are well-ventilated with respect to the atmosphere. This implies that surface waters should express a larger amplitude Suess effect than older, deeper waters that have not recently exchanged gases with the atmosphere. Previous studies have modeled the full global ocean Suess effect based on modern $\delta^{13}\text{C}$ measurements, modern chlorofluorocarbon (CFC) concentrations, ie. anthropogenic pollutants

that have a strong correlation with preindustrial $\delta^{13}\text{C}_{DIC}$, and $\delta^{13}\text{C}$ calcite records of tropical corals and sclerosponges (eg. *Quay et al.*, 2007; *Eide et al.*, 2017a; *Swart et al.*, 2010). These studies reveal a spatially varying distribution, not dissimilar to *Sabine et al.* (2004)'s depth integrated inventory of anthropogenic CO_2 , whereby the deep water formation regions of the North Atlantic have both the highest Suess effect and largest anthropogenic CO_2 inventory.

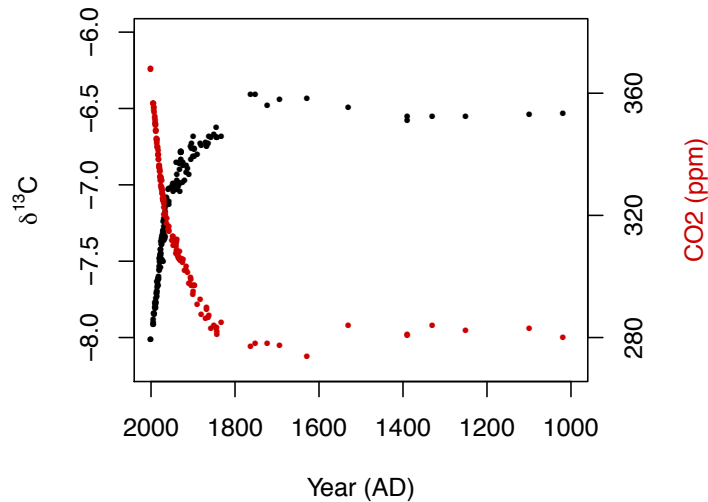


Figure 1.2: A 1000 year record of atmospheric CO_2 (red circles) and its $\delta^{13}\text{C}$ composition (black circles). These data were compiled from a high resolution ice core at Law Dome (East Antarctica), combined with firm records from Law Dome and the South Pole. Data from *Graven et al.* (2017).

Despite the northwestern North Atlantic being such an important anthropogenic CO_2 sink, few historical records of $\delta^{13}\text{C}$ exist, none of which extend back before the 1980s. My thesis presents the first long-term time series of $\delta^{13}\text{C}$ for the northwestern shelf region of the North Atlantic. I analyzed $\delta^{13}\text{C}$ records of foraminifera from five marine sediment cores spanning the Gulf of St. Lawrence, Halibut Channel, Scotian Shelf, and Gulf of Maine. Assuming that the $\delta^{13}\text{C}$ of a foraminifera shell reflects the $\delta^{13}\text{C}_{DIC}$ of the water that it calcified in (*Ravelo and Hillaire-Marcel*, 2007), I quantified the magnitude and rate of change of the oceanic Suess effect since pre-industrial times. I take this one step further and relate $\delta^{13}\text{C}$ observations to accumulation rates of anthropogenic CO_2 into the northwestern shelf region of the North Atlantic.

The following research questions will be addressed in my thesis:

- Can we detect and unambiguously identify the Suess effect from marine sedimentary sequences?
- If so, when was the Time of Emergence of the Suess effect in northwestern shelf waters of the North Atlantic?
- What is the magnitude and rate of change since the onset of the $\delta^{13}\text{C}$ decline?
- Can we detect spatial variation of the Suess effect throughout these shelf waters?
- What is the rate of anthropogenic CO_2 penetration into the northwestern North Atlantic?

CHAPTER 2

BACKGROUND INFORMATION

2.1 The ^{13}C Suess Effect

Carbon exists in two stable isotopes, ^{12}C and ^{13}C . Approximately 98.9% of the carbon is ^{12}C and 1.1% is ^{13}C (*Farquhar et al.*, 1989). The distribution of these isotopes among and within different compounds can give insight into different processes controlling fractionation, such as temperature, biological activity, or carbon speciation (*Farquhar et al.*, 1989). To compare these distributions, the $^{13}\text{C}/^{12}\text{C}$ ratio is commonly expressed in delta (δ) notation relative to VPDB (Vienna Peedee belemnite), according to equation 2.1 (*Craig*, 1957):

$$\delta^{13}\text{C}(\text{‰}) = \frac{{}^{13}\text{C}_{\text{sample}}/{}^{12}\text{C}_{\text{sample}} - {}^{13}\text{C}_{\text{VPDB}}/{}^{12}\text{C}_{\text{VPDB}}}{{}^{13}\text{C}_{\text{VPDB}}/{}^{12}\text{C}_{\text{VPDB}}} \times 1000 \quad (2.1)$$

The CO_2 emissions from fossil fuel combustion and land use change are enriched in ^{12}C , and therefore have a more negative $\delta^{13}\text{C}$. This is because the plants that originally formed the fossil fuels took up ^{12}C preferentially during photosynthetic fixation of CO_2 (*O’Leary*, 1981).

As anthropogenic CO_2 concentrations increase in the atmosphere, the $\delta^{13}\text{C}$ of atmospheric CO_2 decreases. The atmospheric $\delta^{13}\text{C}$ has decreased from -6.4 ‰ before the industrial revolution (~1850 AD) (*Friedli et al.*, 1986; *Francey et al.*, 1999; *Rubino et al.*, 2013) to -8.6 ‰ in 2017 (Scripps CO_2 , http://scrippsco2.ucsd.edu/graphics_gallery/isotopic_data/; *Keeling et al.* 2001; *Rubino et al.* 2013). This sudden perturbation after 1850 is well illustrated in Figure 1.2, which shows the 1000

year atmospheric $\delta^{13}\text{C}$ record from the Law Dome ice core, spliced with firn and atmospheric samples (Rubino *et al.*, 2013; Francey *et al.*, 1999). This rapid decrease in $\delta^{13}\text{C}$ was termed the Suess effect after Hans Suess, who first identified it in 1955 (Keeling, 1979). Note that Suess actually first discovered the negative isotope excursion in $^{14}\text{C}/^{12}\text{C}$ of modern wood (Suess, 1955), but throughout my thesis the term Suess effect will be referring to the negative $\delta^{13}\text{C}$ excursion only. The Suess effect, denoted as $\delta^{13}\text{C}_{SE}$, can be defined by equation (2.2):

$$\delta^{13}\text{C}_{SE} = \delta^{13}\text{C} - \delta^{13}\text{C}_{PI} \quad (2.2)$$

where $\delta^{13}\text{C}$ is the observed stable carbon isotope ratio of the carbon species under investigation and $\delta^{13}\text{C}_{PI}$ is the pre-industrial stable carbon isotope ratio of the same carbon species (Eide *et al.*, 2017a). Air-sea gas exchange and biological processes allow for the transfer of the atmospheric Suess effect to the dissolved inorganic carbon (DIC) pool of the surface ocean (Quay *et al.*, 1992). These processes lead to a fairly complex distribution of $\delta^{13}\text{C}$ in surface waters and uncertainties in the regional expression of the oceanic Suess effect (Gruber *et al.*, 1999).

Quay *et al.* (1992) demonstrated that the net oceanic CO_2 uptake rate can be estimated using measured concentrations of atmospheric CO_2 , the $\delta^{13}\text{C}$ of atmospheric CO_2 , the $\delta^{13}\text{C}$ of DIC in the ocean, and knowledge of equilibration times. They found the ocean to be the dominant sink of anthropogenic CO_2 from the atmosphere, corroborated by a later study by Sabine *et al.* (2004). However, the 2016 Global Carbon Budget (Le Quéré *et al.*, 2016) suggests that over the last decade, the ocean sink accounted for only 25% of the total anthropogenic emissions, while the terrestrial biosphere accounted for 30%, and the remaining 45% stayed in the atmospheric reservoir. The discrepancy between older studies and the 2016 Global Carbon Budget is due to the exclusion of land use change emissions by the older studies (Le Quéré *et al.*, 2016). Figure 2.1 displays the overall perturbation of the global carbon cycle by illustrating the mass flow rates of CO_2 between the major reservoirs over the last decade (2006-2015). Provided that these fluxes change over time, the long-term records of $\delta^{13}\text{C}$ presented by this thesis will give further insight on the uptake of CO_2 by the ocean sink in northwestern shelf waters of the North Atlantic.

The distribution of $\delta^{13}\text{C}$ throughout the global ocean is a useful paleoceanographic

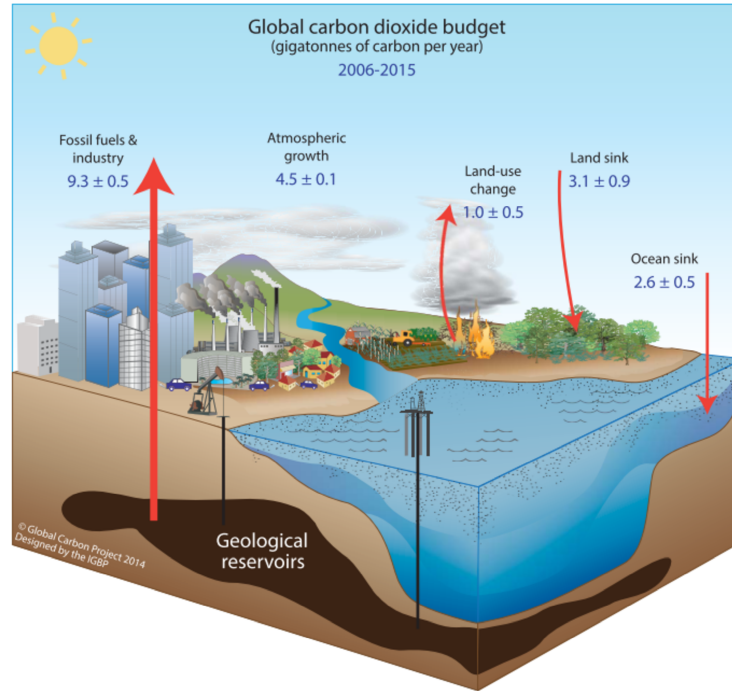


Figure 2.1: Illustration from *Le Quéré et al.* (2016) of the mass flow rates between major carbon reservoirs over the last decade (2006-2015). Mass flow rates are in units of $\text{GtC yr}^{-1} \pm 1\sigma$. Fossil fuels and land use change emissions account for the sources of carbon to the atmosphere, while the ocean and land are the major sinks. The imbalance between sources and sinks leads to the net growth of the atmospheric carbon reservoir. Reprinted with permission from *Le Quéré et al.* (2016).

proxy for determining past ocean ventilation, ie. transport of water that has recently exchanged gases with the atmosphere, into the ocean's interior. Penetration of isotopically light CO_2 has diminished the natural gradients between surface and deep ocean $\delta^{13}\text{C}$, causing misinterpretations of the past ocean $\delta^{13}\text{C}$ variations in sedimentary records (*Olsen and Ninnemann, 2010*). *Olsen and Ninnemann (2010)* show that a correction for the oceanic Suess effect can restore the pre-industrial $\delta^{13}\text{C}$ surface ocean values, which have a more detailed structure closely related to water mass distributions. The restored pre-industrial $\delta^{13}\text{C}$ values make a better reference framework to then compare with past $\delta^{13}\text{C}$ distributions.

Different methods have been used to establish the regional Suess effect by using in situ time series measurements (*Gruber et al., 1999*) or comparing data sets collected at different time periods from the same region (*Quay et al., 2007; Sonnerup et al., 2000; Olsen et al., 2006*). Models have also been useful to estimate the Suess effect. Relying

on established relationships between chlorofluorocarbons (pCFC-12) and the ocean Suess effect, *Eide et al.* (2017a) modeled the Suess effect over the global ocean from pre-industrial times to 1994. The total atmospheric Suess effect over this time period was -1.4‰ . *Eide et al.* (2017a) mapped the Suess effect over the global ocean using gridded GLODAPv1.1 pCFC-12 climatological data, the results of which are presented at various depths in Figure 2.2. It should be noted that the preformed $\delta^{13}\text{C}$ -pCFC-12 relationship breaks down above 200 m, so this technique is only used below that depth. At 200 m, they found the largest decrease in oceanic $\delta^{13}\text{C}$ in the subtropical gyres of the Northern Hemisphere, ie. -0.8‰ in the North Pacific and -0.6‰ in the North Atlantic. In the Southern Hemisphere, the Indian Ocean showed a $\delta^{13}\text{C}$ decrease similar to the North Atlantic around -0.6‰ , while there was a considerably weaker Suess effect in the South Atlantic and South Pacific Oceans of -0.3 to -0.4‰ (*Eide et al.*, 2017a). The differences in Suess effect magnitudes were explained to be mainly due to surface water residence times, vertical mixing with older water masses, and thermodynamic fractionation during air-sea gas exchange (*Eide et al.*, 2017a).

The data input to model the upper 200 m in *Eide et al.* (2017a) were compiled from previous studies of $\delta^{13}\text{C}$ records of sclerosponges (*Böhm et al.*, 1996; *Worheide*, 1998; *Swart et al.*, 1996; *Böhm et al.*, 2000) and scleractinian corals (*Swart et al.*, 2010). Long-lived calcite or aragonite forming organisms make great paleoproxies for $\delta^{13}\text{C}_{DIC}$ of the surface ocean because they precipitate calcium carbonate (CaCO_3) very close to isotopic equilibrium with the ambient seawater (*Druffel and Benavides*, 1986). Using these records, *Eide et al.* (2017a) found the mean surface ocean Suess effect to be $-0.9 \pm 0.1\text{‰}$ between the beginning of the industrial revolution and 1994, which is $65 \pm 10\%$ of the atmospheric signal. However, the paleoceanographic proxy data compiled in the *Eide et al.* (2017a) study are limited to regions displayed in Figure 2.3 (35°N to 35°S), where seasonal variability in $\delta^{13}\text{C}_{DIC}$ is low (*Quay et al.*, 1992; *Gruber et al.*, 1999). As shown in the top left panel of Figure 2.2, the largest Suess effect occurs in the mid-to-high latitude North Atlantic and Pacific, highlighting the need to validate these models with data from these regions. Since long-lived, shallow dwelling corals and sclerosponges are sparse at higher latitudes, foraminifera are a better archive for $\delta^{13}\text{C}_{DIC}$ in these regions and will be used in my thesis.

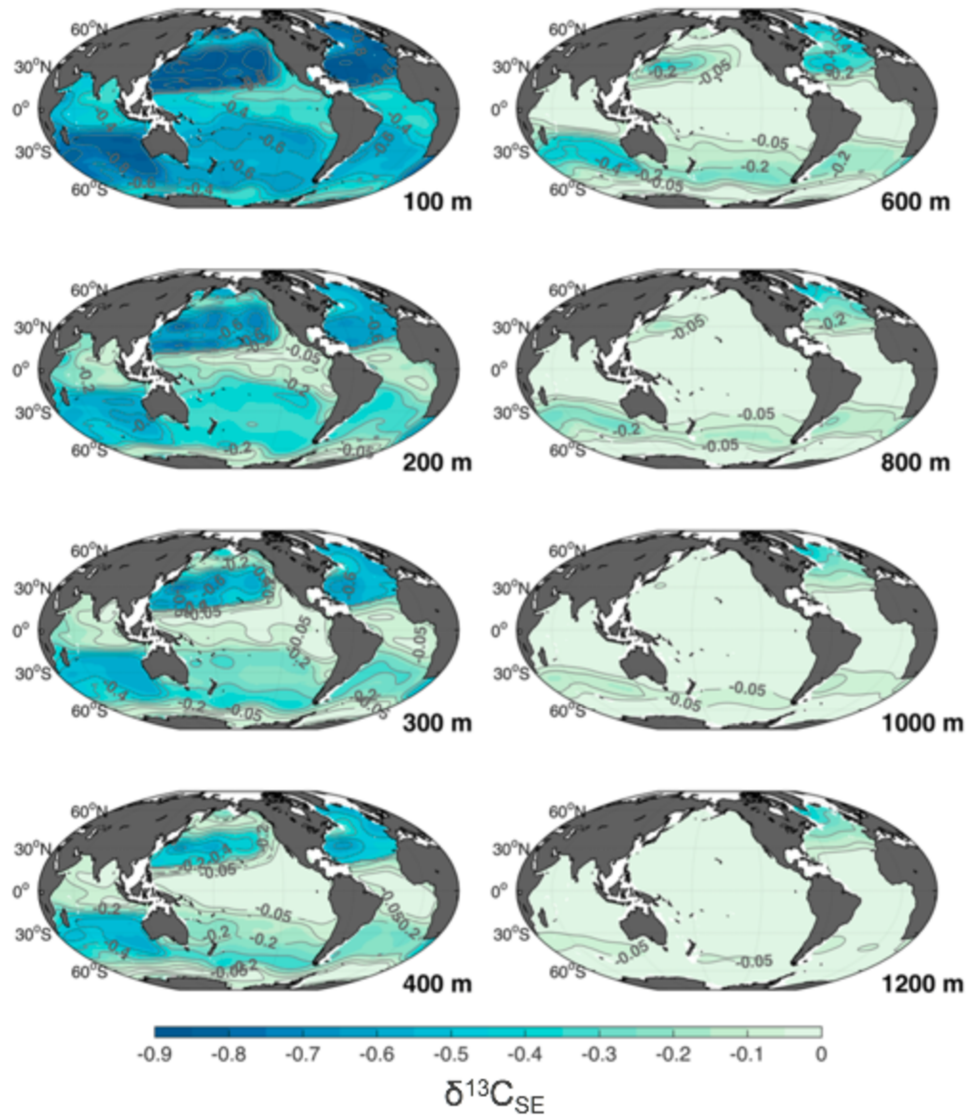


Figure 2.2: Global Suess effect (‰) modeled at selected depths from *Eide et al.* (2017a). The upper right panel (100 m) was constructed using interpolation from the coral and sclerosponge $\delta^{13}\text{C}$ records mapped in Figure 2.3. The remaining panels show the Suess effect using GLODAPv1.1 climatological chlorofluorocarbon (pCFC-12) gridded model data for water depths ranging from 200 to 1200 m.

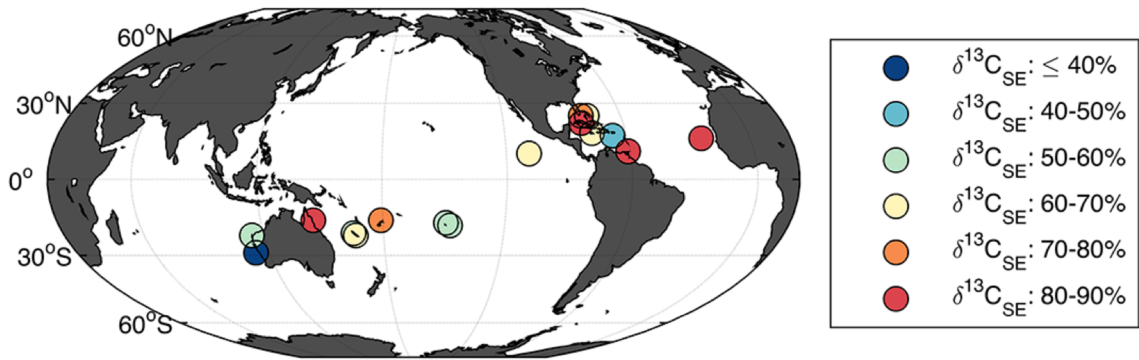


Figure 2.3: Map from *Eide et al.* (2017a) displaying locations and Suess effect magnitudes of scleractinian corals (*Swart et al.*, 2010) and sclerosponges (*Böhm et al.*, 1996; *Worheide*, 1998; *Swart et al.*, 1996; *Böhm et al.*, 2000), expressed as the percentage of the atmospheric Suess effect over the time period spanned by each record. From the *Swart et al.* (2010) data compilation, only statistically significant values at the 95% confidence interval were included.

2.2 Foraminifera as a proxy for $\delta^{13}\text{C}$ of DIC

Foraminifera precipitate dissolved inorganic carbon (DIC) to form their shells with little fractionation of $\delta^{13}\text{C}$, and have thus been used to observe the Suess effect. It is therefore assumed that $\delta^{13}\text{C}$ of CaCO_3 reflects the $\delta^{13}\text{C}_{\text{DIC}}$ over the lifespan of the foraminifera (*Ravelo and Hillaire-Marcel*, 2007). The CaCO_3 shells from both planktonic and benthic foraminifera are well preserved in marine sediments under most open ocean conditions. When planktonic foraminifera die, they sink to the sea floor and are buried together with benthic foraminifera by continuous sediment delivery from the sea surface. A sediment core from a particular site can be collected and foraminifera species selected at chosen depth intervals for stable isotope analysis. If an age model can be applied to the core, then these data will provide a $\delta^{13}\text{C}$ time series, similar to aforementioned archives from the atmosphere, ice cores, sclerosponges and corals. The advantage of using foraminifera is that they are ubiquitous in the world ocean, and therefore abundant in ocean sediments world-wide.

A handful of studies have investigated the Suess effect in surface waters by either comparing $\delta^{13}\text{C}$ values in modern day planktonic foraminifera collected in sediment traps with those in core tops (*Beveridge and Shackleton*, 1994; *King and Howard*, 2004), or using $\delta^{13}\text{C}$ downcore records in high-resolution sediment cores (*Al-Rousan et al.*, 2004; *Xu et al.*, 2014; *Black et al.*, 2011). *Al-Rousan et al.* (2004) investigated the invasion

of anthropogenic CO₂ in the Gulf of Aqaba and showed a decline in $\delta^{13}\text{C}$ recorded on *Globigerinoides sacculifer* of roughly -0.63‰ since 1750 AD. *Xu et al.* (2014) measured $\delta^{13}\text{C}$ on *Globigerinoides ruber* from six coastal sediment cores in the northern South China Sea. Three downcore records showed a decrease in $\delta^{13}\text{C}$ at rates between -0.006‰ and -0.009‰ per year, while three others had no decrease (*Xu et al.*, 2014). *Xu et al.* (2014) explained the lack of ^{13}C Suess effect in the latter three cores by balanced vertical mixing and the biological pump. An enhanced biological pump would increase photosynthetic fractionation of DIC, leaving surface waters enriched in ^{13}C , hence dampening the Suess effect. *Bauch et al.* (2000) compared $\delta^{13}\text{C}$ values in *Neogloboquadrina pachyderma* from the water column and core top sediment, in which they found a Suess effect of $-0.9\text{‰} \pm (0.2\text{‰})$ in Arctic halocline waters, and -0.6‰ in the Atlantic derived waters of the Nansen basin. They interpreted spatial differences in the ^{13}C Suess effect to be caused by different ventilation times of shelf vs. basin waters. They inferred the vital effect of *N. pachyderma* in Arctic waters to be approximately -2‰ (*Bauch et al.*, 2000). *Black et al.* (2011) published a high resolution *G. ruber* $\delta^{13}\text{C}$ record from the Caribbean Sea that spanned the last 300 years. They found the ^{13}C Suess effect to be -0.75‰ from preindustrial values, with the most rapid change occurring since 1950 (Figure 2.4), coincident with the atmospheric rise in CO₂ (*Black et al.*, 2011).

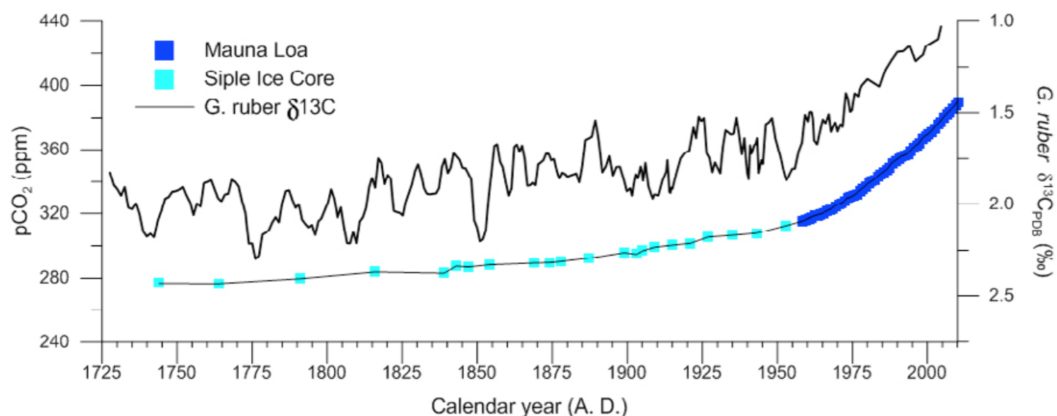


Figure 2.4: Record of planktonic foraminifera $\delta^{13}\text{C}$ from the Caribbean Sea since 1725 (heavy black line) compared to Siple ice core (light blue square) and Mauna Loa atmospheric CO₂ records (dark blue squares). Figure retrieved from *Black et al.* (2011) with permission from John Wiley and Sons.

Although the $\delta^{13}\text{C}$ in planktonic and benthic foraminifera are widely used to reconstruct changes in past $\delta^{13}\text{C}_{\text{DIC}}$, foraminiferal calcite may be in slight isotopic disequilibrium with DIC (*Ravelo and Hillaire-Marcel, 2007*). This disequilibrium may be attributed to the following species-specific vital effects (*King and Howard, 2004; Ravelo and Hillaire-Marcel, 2007*):

1. calcification temperature (*Bemis et al., 2000; King and Howard, 2004*)
2. the pH and carbonate ion concentration of seawater (*Spero et al., 1997; Bemis et al., 2000; Bauch et al., 2002*)
3. the shell size of foraminifera (*Curry and Matthews, 1981; Oppo and Fairbanks, 1989; Ravelo and Fairbanks, 1995; Spero and Lea, 1996*)
4. photosynthesis and respiration by algal symbionts affecting the internal carbon pool of foraminifera (*Zeebe et al., 1999; Bemis et al., 2000*)
5. the isotopic composition of the foraminiferal diet (*Spero and Lea, 1996; Kohfeld et al., 1996*)
6. habitat migration during the life cycle (*Hemleben and Bijma, 1994; Lohmann, 1995*)
7. genotype variation, ie. *Neogloboquadrina pachyderma* (Npd) vs. *Neogloboquadrina incompta* (Nps) (*Ravelo and Hillaire-Marcel, 2007; Bauch et al., 2003*)

Various laboratory experiments with living foraminifera, and coretop studies give insight into environmental conditions that affect carbon isotope variability. Temperature has been shown to have a negative correlation with $\delta^{13}\text{C}$ of some planktic foraminifera. *Bemis et al. (2000)* found that the $\delta^{13}\text{C}$ of cultured *Globigerina bulloides* decreases by 0.11 ‰ per °C increase over a temperature range of 15-25°C. They explain this as the result of incorporating more respired CO_2 into the shell at higher metabolic rates (*Bemis et al., 2000*). *King and Howard (2004)*, found a similar temperature dependency of planktic foraminifera in the Southern Ocean. Planktic foraminifera cultured under increased carbonate ion concentration ($[\text{CO}_3^{2-}]$) were isotopically depleted compared to those cultured in lower $[\text{CO}_3^{2-}]$ conditions (*Spero et al., 1997; Bemis et al., 2000*). This is an

important vital effect to consider in this study because as CO₂ concentrations increase in surface waters, [CO₃²⁻] should decrease. A coretop study in the tropical Atlantic found that foraminifera with algal symbionts typically have a greater $\delta^{13}\text{C}$ size dependence, such that $\delta^{13}\text{C}$ increases with shell size (*Ravelo and Fairbanks, 1995*). The effect of diet is typically small. Feeding experiments with *G. bulloides* showed that 8-15% of the $\delta^{13}\text{C}$ chamber signal is due to incorporation of metabolic CO₂, after consuming prey of different $\delta^{13}\text{C}$ values (*Spero and Lea, 1996*). It is important to consider all of these vital effects when interpreting a $\delta^{13}\text{C}$ record of foraminiferal calcite.

2.3 Oceanographic Conditions in the Northwest Atlantic

The study area spans the continental shelf of the northwest Atlantic Ocean from the Gulf of Maine to the south of the Grand Banks, including the Gulf of St. Lawrence and Scotian Shelf (Figure 2.5). The shelf widths and depths are typically 100-200 km and 100-200 m respectively, however there are regional variations associated with basins, banks, and gulfs (*Loder et al., 1998*). The shelf-slope waters in this region are strongly influenced by the Labrador Current, which is the western boundary current of the North Atlantic subpolar gyre. The Gulf Stream lies south and offshore of the study area.

The cold, low-salinity water that makes up the Labrador Current (LC) is a combination of a branch of the East-West Greenland Current system flowing westward along the northern Labrador Sea, the Baffin Island Current flowing south through the western Davis Strait, and outflow from the Hudson Strait (*Loder et al., 1998*). The majority of the LC flows onto the northeastern Newfoundland shelf and southwards to the Grand Banks region (*Colbourne et al., 1997*). At 47°N, it splits into a low-transport inshore branch flowing onto the southern Newfoundland shelf, and a high-transport shelf-break branch flowing south toward the tail of the bank (*Loder et al., 1998*). A schematic of the major current systems of the northwest Atlantic ocean is shown in Figure 2.5.

The seasonal mean circulation on the Scotian shelf consists of two southwestward currents, one coastally trapped and moving along the inshore trench that connects deeper basins (ie. west of Laurentian channel to Emerald basin), known as the Nova Scotia Current (NSC), and the other moving alongslope at the shelf break (*Dever et al., 2016; Loder et al., 1998; Han and Loder, 2003*). The NSC is mainly a continuation of the Cabot Strait outflow from the GSL, and the shelf break current includes contributions

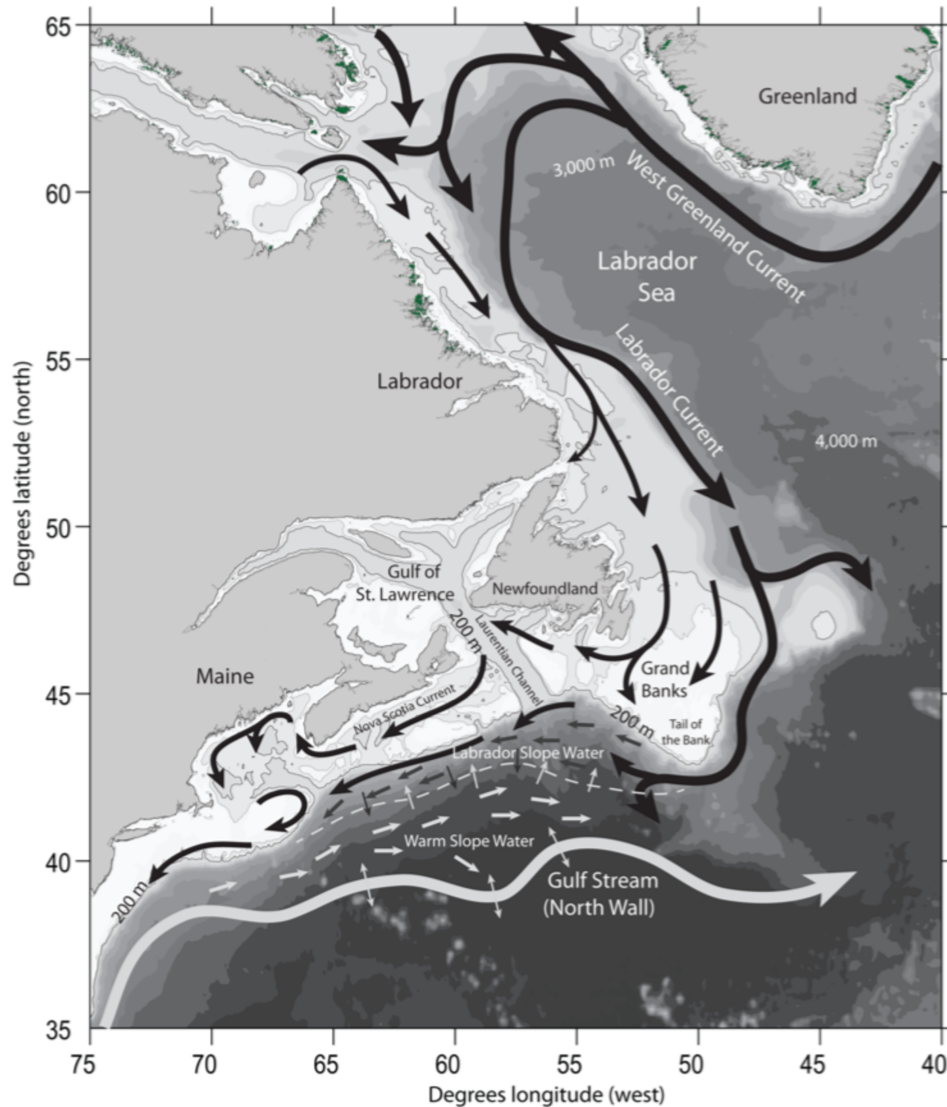


Figure 2.5: Bathymetric map and major current systems of the northwest Atlantic. Warmer currents are coloured grey and colder currents black. The dashed line separates the two types of slope water, Warm Slope Water and Labrador Slope Water, of which the small arrows denote presumed flow directions. Reprinted with permission from *Townsend et al.* (2015).

from the GSL, LC extension, and the northern branch of the cyclonic Slope Water gyre (*Han and Loder, 2003*). The topography of the shelf also influences smaller scale features, such as cyclonic flow around basins and anticyclonic flow around banks (*Han et al., 1997*).

Water from the NSC flows southwestward into the GoM. Here it combines with the

GoM Coastal Current and generally flows cyclonically around the GoM. In the eastern GoM, there are linked cyclonic gyres around the Jordan Basin and Georges Bank (Pettigrew *et al.*, 2005). Warm, relatively salty slope water flows in at depth through the Northeast Channel, compensated by outflow of surface and intermediate waters through both the Northeast Channel and Great South Channel on either end of Georges Bank (Pettigrew *et al.*, 2005). Temperatures in the GoM are seasonally and interannually variable, influenced by the North Atlantic Oscillation (NAO). The NAO index is the difference in winter sea level atmospheric pressures between the Azores High and Icelandic Low, which fluctuate in strength and position over time. The larger the NAO index value, the larger the atmospheric pressure gradient, and consequently stronger westerly winds prevail over the northern North Atlantic (Hebert *et al.*, 2014). A negative (positive) NAO index corresponds to warm, salty (cold, fresh) conditions on the Newfoundland-Labrador shelf, eastern Scotian Shelf, and in the Gulf of St. Lawrence, while an opposite response is observed in the western Scotian Shelf and GoM (Petrie, 2007)

High seasonal temperature variability is characteristic of the northwest Atlantic Ocean. The seasonal changes in water column stratification are fairly similar in each shelf region. In the winter, the Scotian shelf generally consists of two layers: an upper cold, fresh and well-mixed layer above a relatively warmer and saltier layer from offshore slope waters, which enters the shelf through deep channels and gullies (Drinkwater *et al.*, 2003). In the summer, a third solar heated layer forms above the cold, fresh layer (Drinkwater *et al.*, 2003). The Gulf of St. Lawrence consists of three distinct layers in the summer: a warm surface layer, the cold intermediate layer, and warmer deep layer (Galbraith *et al.*, 2013). Surface temperatures peak in mid-July to mid-August after which the waters start cooling. The wind driven mixing in the fall leads to a deeper and cooler mixed layer, eventually encompassing the cold intermediate layer. The new surface layer forms in the spring from surface warming, sea-ice melt waters, and continental runoff (Galbraith *et al.*, 2013).

CHAPTER 3

METHODS

3.1 Core Collection

Sediment samples were collected from multicores (MC), a box core (BC), and a gravity core (GC) at five locations. Table 3.1 shows the core IDs, locations, depths, and core lengths. OCE400 44MC was collected from Jordan Basin in August 2010, onboard R/V Knorr (*Keigwin and Pilskalns, 2015*). OCE326 29MC was collected from Emerald Basin onboard R/V Oceanus, in July 1998 (*Keigwin et al., 2003*). The KNR158 cores were collected on the Laurentian slope in June 1998 on the R/V Knorr (Marchitto and De Menocal, unpublished). The MSM46 cores were collected in the Gulf of St. Lawrence in August 2015, onboard the German R/V Maria S. Merian. All core locations are displayed in Figure 3.1 and Table 3.1.

Table 3.1: Locations of the cores investigated in my thesis. Note KNR158 13GGC and KNR158 11BC are from the same location, and data will be provided as a spliced record (See Subsection 4.2.1)

Core ID	Location	Latitude	Longitude	Depth (m)	Core Length (cm)
OCE400 44MC	Jordan Basin	43°29' N	67°53' W	287	53
OCE326 29MC	Emerald Basin	43°53' N	62°48' W	250	50
KNR158-4 13GGC	Laurentian Fan	45°01' N	55°11' W	1035	300
KNR158-4 11BC	Laurentian Fan	45°01' N	55°12' W	1072	59
MSM46 2MC	Gulf of St. Lawrence	47°50' N	60°05' W	500	38
MSM46 4MC	Gulf of St. Lawrence	49°17' N	63°59' W	381	30

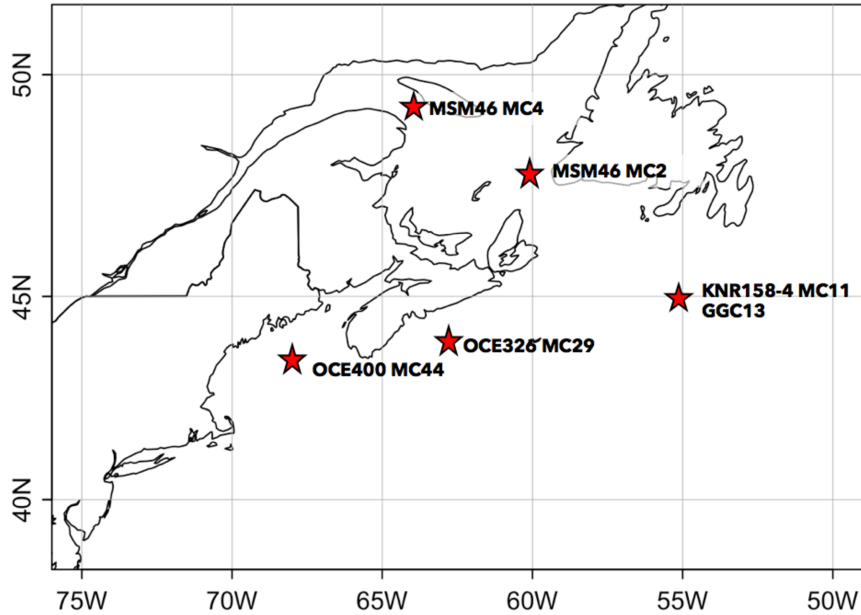


Figure 3.1: Map of core sites from this study on the northwestern shelf of the North Atlantic.

3.2 Laboratory Analysis

The cores were sampled at the intervals indicated in Table 3.2. In preparation for identifying and picking foraminifera, the sediment samples were washed with tap water through 63 μm sieves. They were then dried in an oven at 60°C. Except where $\delta^{13}\text{C}$ data were already available from published and unpublished sources, I picked planktic and benthic foraminifera according to the size fractions indicated in Table 3.3. Planktic species include *N. pachyderma*, *G. bulloides*, and *N. incompta*, and the epibenthic species *C. lobatulus*.

Stable carbon and oxygen isotopes were analyzed on all specified foraminifera samples from each of the sediment cores discussed above. All of the delta values are expressed relative to the international standard, VPDB (Vienna PeeDee Belemnite) (See Eq. 2.1). Details on the instruments used for each core are given below:

- Samples of the MSM46 cores were measured for $\delta^{18}\text{O}$ and $\delta^{13}\text{C}$ isotopes on a ThermoScientific Kiel IV carbonate device interfaced to a ThermoScientific MAT-253 dual-inlet isotope ratio mass spectrometer (IRMS) at the University of Santa Cruz Stable Isotope Facility. Analytical precision is $\pm 0.05\text{‰}$ for $\delta^{13}\text{C}$, and $\pm 0.08\text{‰}$

Table 3.2: Approximate sampling intervals of each core investigated in this study.

Core ID	Sampling Intervals
OCE400 44MC	1 cm
OCE326 29MC	1 cm
KNR158-4 13GGC	~2 cm
KNR158-4 11BC	1 cm
MSM46 2MC	1 cm
MSM46 4MC	1 cm (0.5-10.5), 5 cm (10.5-25.5)

Table 3.3: Foraminifera species and grain sizes picked from each core in this study.

Core ID	Foraminifera Species	Number of Specimens	Grain Size μm
OCE400 44MC	<i>N. incompta</i>	8-20	150-250
OCE326 29MC	<i>N. pachyderma</i>	15	150-250
	<i>C. lobatulus</i>	1	>250
KNR158-4 13GGC	<i>G. bulloides</i>	8-10	250-300
KNR158-4 11BC	<i>G. bulloides</i>	8-10	250-300
MSM46 2MC	<i>N. pachyderma</i>	20-30	125-250
	<i>N. incompta</i>	limited	125-250
	<i>G. bulloides</i>	limited	125-250
MSM46 4MC	<i>N. pachyderma</i>	20-30	125-250
	<i>C. lobatulus</i>	2-10	>250

for $\delta^{18}\text{O}$ (this study).

- KNR158 stable isotope measurements were run on a Micromass Optima mass spectrometer. The analytical precision for this instrument, reported on another stable isotope ($\delta^{18}\text{O}$), is $\pm 0.06\text{‰}$ (1s) (Marchitto and DeMenocal, 2003).
- OCE400 MC44 stable isotope measurements were made on a VG Prism instrument at the National Ocean Sciences Accelerator Mass Spectrometry facility at Woods Hole Oceanographic Institution. The analytical precision is approximately $\pm 0.05\text{‰}$ for both $\delta^{13}\text{C}$ and $\delta^{18}\text{O}$ (Keigwin and Pilskalns, 2015).
- OCE326 MC29-D stable isotopes were measured on a partially automated VG 903 mass spectrometer with a high sensitivity source (Keigwin et al., 2003).

Additionally, I collected samples from MSM46 MC2 and MC4 for percent organic carbon ($\%C_{org}$) and $\delta^{13}C$ of organic matter ($\delta^{13}C_{org}$). I measured these parameters to compare the Suess effect magnitude between foraminiferal calcite and the organic carbon pool. Analysis was done on acidified samples (saturated with 10% HCl, dried at 50°C, and transferred to silver capsules) with a microCube-Isoprime 100 by Claire Normandeau at Dalhousie University. The analytical error on $\delta^{13}C_{org}$ of a blind standard was 0.11‰ (1 standard deviation). $\%C_{org}$ was determined on the same acidified samples using an elemental analyzer coupled to the microCube-Isoprime 100.

The method and associated laboratory techniques for applying ages to the sediment records are discussed in Chapter 4.

3.3 Statistical Analysis

To constrain the Time of Emergence (ToE), magnitude, and rate of change of any carbon isotope excursion (CIE), I fit a broken-line model to each of the $\delta^{13}C$ records. A broken-line model fits two or more piecewise linear regressions connected at unknown values called change points (*Muggeo, 2003*). The change point is determined iteratively by finding the point along the x-axis that best reduces the residuals of the linear segments. To apply this piecewise regression to my data, the R package ‘segmented’ was used.

For each $\delta^{13}C$ record, a two-piece regression was fit with time as the predictor variable, and $\delta^{13}C$ as the response. In cases where there seemed to be two clear change points over the long-term trend, a three-piece regression was fit instead. If the most recent segment had a negative slope (or the two most recent segments), it was considered a CIE and the $\delta^{13}C$ decrease rate was defined by the slope of that segment. The magnitude of the CIE was determined using the $\delta^{13}C$ decrease rate from the change point to the most recent sample age. In one case where the change point did not seem to represent the pre-industrial $\delta^{13}C$ value, it was determined by averaging the $\delta^{13}C$ values of all the samples that were located before the CIE. This case is discussed in further detail in Section 5.2.1. In order to compare magnitudes of the CIE between cores, the CIEs were normalized by extrapolating to year 2013 using the model. Year 2013 was chosen because it was the most recent age sampled by any of the cores (MSM46 MC2, 0.5 cm).

The uncertainties reported include only the piecewise linear regression error, which

are displayed as both 95% confidence and prediction intervals. Confidence intervals inform us about how well we know the mean– the true CIE value, while prediction intervals tell us the distribution of 95% of the sampled data points. In addition, I estimated uncertainty in the timing of the change point by applying the piecewise regression to $\delta^{13}\text{C}$ records with depth (instead of time) on the x-axis, and then converted the depth change point to age in Bacon, a Bayesian age-depth modeling software. Bacon output the associated age and uncertainty for each given change point depth.

To calculate the average Suess effect for the region, I took the mean CIE magnitude of all records, except the record that did not display a CIE. For the average $\delta^{13}\text{C}$ decrease rate, I only included the records with age model uncertainty around the change point of 15 years or less. For the ToE determination, I calculated the weighted average of all the change points using a weighting system relative to the 1σ uncertainties of the age-depth and broken line models.

CHAPTER 4

AGE MODELS

4.1 Age Model Methods

Since I am interested in exploring the $\delta^{13}\text{C}$ record through time rather than depth in a sediment core, it is necessary to develop models that convert from depth to age. Most age-depth models are made by determining average sedimentation rates or absolute dates at selected depths throughout the core using different radioisotopes. Radiocarbon (^{14}C) and ^{210}Pb are the most effective isotopes for investigating sediment age in the late Holocene, and will be discussed in Sections 4.1.1 and 4.1.2, respectively.

Keeping the wise words of E.P. Box in mind “all models are wrong, but some are useful”, the goal is to best represent reality using the resources we have, while staying aware of the uncertainties that are inherent of converting from space to time. The basic assumption behind age-depth modeling is that sediments were deposited forward in time from the bottom of a core towards the top. This assumption can only be disrupted by significant biological mixing (bioturbation) or physical reworking (such as a landslide), where evidence of the latter would be detectable in the core and could be corrected for accordingly. Classical age models use only one dating method, such as determining radiocarbon dates at discrete intervals and linearly interpolate between age points, or perhaps determining a constant sedimentation rate based on a ^{210}Pb profile. The caveat with linear interpolation between age points is that it causes the model to change sedimentation rate at every dated depth, despite there being no physical justification for it. Also, a simple linear interpolation makes it difficult to estimate uncertainties of the intervals between dated samples.

Bayesian age modeling is a more sophisticated method for creating age models that

combines sample data with other information about the site, called “prior” information, to arrive at inferences of posterior distributions. Bayesian models have become increasingly common because they can accommodate the non-normal distribution of radiocarbon dates, combine multiple dating techniques, and handle outliers during analysis rather than discard them *a priori* (Blaauw and Christen, 2011). For this study, Bacon, a Bayesian accumulation software, was used to construct age-depth models (Blaauw and Christen, 2011). It works by dividing the core into many thin sections and then uses millions of Markov Chain Monte Carlo (MCMC) iterations to estimate accumulation rates of each section. The software interface runs on R (R Development Core Team, 2013).

Since age estimates from Bayesian methods are strongly influenced by both new information (the data) and priors, it is important to input priors that are well supported (Goring *et al.*, 2012). The accumulation rate prior is a powerful setting in Bacon because it allows us to tell the model that accumulation rates should always be positive, following an asymmetric gamma distribution (Figure 4.1a). This is a safe assumption, as sediments do not accumulate backwards in time. The default mean accumulation rate prior that Bacon uses is 0.05 cm/yr (input as a sedimentation time of 20 yr per cm) (Goring *et al.*, 2012), but Bacon can assess the input age information to adjust the prior accumulation rate to better match the individual core location.

Memory defines how much the sedimentation rate at a particular depth depends on the sedimentation rates at neighbouring depths. If memory is high, then accumulation rates are relatively stable over time, while if memory is low, accumulation rates fluctuate more over time. The values for memory range between 0 and 1, with Bacon’s default mean value at 0.7 that follows a beta distribution (Figure 4.1b). The input prior information and Bacon outputs for each core in this study are discussed in Section 4.2.

The types of data input to Bacon for each core in this study were chosen based on sample and data availability (See Table 4.1. Age model inputs included a mix of fixed ^{14}C dates, and ages derived from Pb-210 and mercury (Hg) measurements. The age model outputs from Bacon are presented and discussed in Section 4.2.

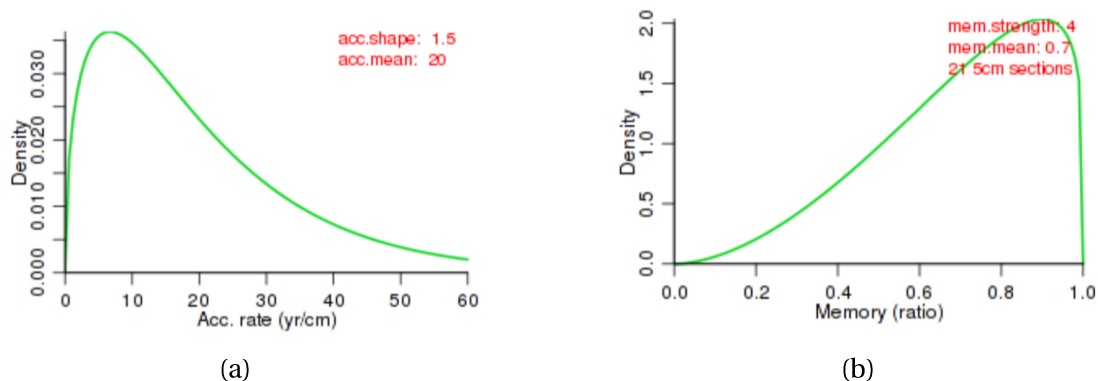


Figure 4.1: (a) Bacon default accumulation rate prior, which follows a gamma distribution. The default mean is 20 yr/cm and shape is 1.5, where higher values give more peaked shapes. (b) Bacon default memory prior, which follows a beta distribution. The default mean is 0.7 and strength is 4, where higher values give more peaked shapes (Blaauw and Christen, 2011).

Core	Dating Methods Applied
MSM46 MC2	Hg
MSM46 MC4	Hg
KNR158	^{14}C
OCE326 MC29	^{14}C , ^{210}Pb
OCE400 MC44	^{14}C , ^{210}Pb

Table 4.1: Types of dating methods applied to each sediment core from this study. Method selection was based on sample and data availability.

4.1.1 ^{210}Pb

The natural radionuclide ^{210}Pb is a useful tool for determining sedimentation rates at the seafloor (Appleby, 2002). It is part of the ^{238}U decay series, has a half-life of 22.26 years and can be used for dating sediments up to five half lives or approximately 110 years (Sorgente *et al.*, 1999). This time frame makes ^{210}Pb a great dating tool for investigating histories of anthropogenic activities, including the Suess effect, in marine environments.

The ^{210}Pb activity within the sediment is made up of two components from different sources. The first is the *supported* ^{210}Pb , which is produced via radioactive decay of ^{222}Rn . The second is the *unsupported* ^{210}Pb that derives from ^{222}Rn decaying to ^{210}Pb in the atmosphere and is subsequently deposited at the seafloor through rainfall and

dry fallout (*Ghaleb*, 2009). An idealized activity profile of total ^{210}Pb in a sediment core starts with a maximum at the top and exponentially decreases with depth until it stabilizes at the supported ^{210}Pb background value. Age-depth models are established by quantifying and analyzing the unsupported ^{210}Pb (total minus supported). The derivation of unsupported ^{210}Pb is illustrated using data from OCE400 MC44 (Ed Boyle, unpublished) in Figures 4.2(a) and (b).

We measured total ^{210}Pb indirectly via alpha emissions of granddaughter species ^{210}Po . This method assumes that ^{210}Po is in secular equilibrium with ^{210}Pb after two years (*Sorgente et al.*, 1999). The supported background ^{210}Pb activity was determined using gamma spectrometry to measure ^{226}Ra , which is assumed to be in isotopic equilibrium with daughter species ^{214}Pb (*Ghaleb*, 2009).

To establish the age-depth model with ^{210}Pb , I used the Constant Flux-Constant Supply model (CF-CS). It assumes that each sediment layer would have the same initial unsupported ^{210}Pb concentration (*Appleby*, 2002), independent of sediment flux. The alternative model, called Constant Rate of Supply (CRS), allows for concentration or dilution of ^{210}Pb within the sinking particles, but requires continuous ^{210}Pb measurements throughout the core and accumulated dry weight of the samples (*Appleby and Oldfield*, 1978). These necessary data were not available from the cores in this study, therefore the CF-CS model was chosen. Within this model the exponential decay of ^{210}Pb follows Equation 4.1.

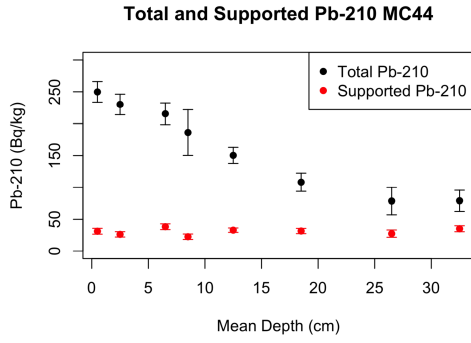
$$A_z = A_0 e^{\lambda t} \quad (4.1)$$

where A_0 is the initial activity measured at the core top, A_z is the activity at depth z , λ is the ^{210}Pb decay constant (Equation 4.2), and t is the time elapsed since the deposition of sediment at depth z . This can be rearranged to solve for time elapsed, according to Equation 4.3 (*Sorgente et al.*, 1999).

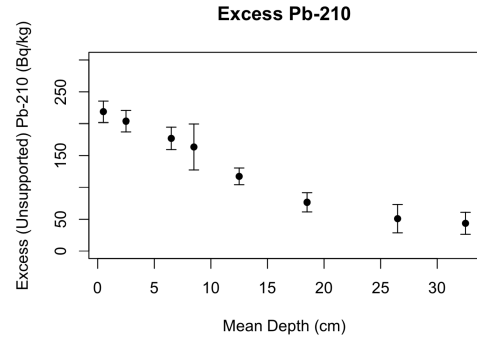
$$\lambda = \frac{\ln(2)}{t_{1/2}} = \frac{\ln(2)}{22.26} = 0.03114 \text{ yr}^{-1} \quad (4.2)$$

$$t = \frac{-1}{\lambda} \ln\left(\frac{A_z}{A_0}\right) \quad (4.3)$$

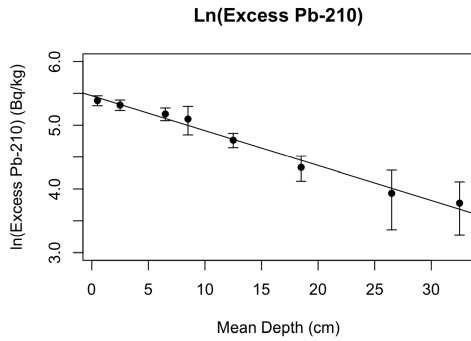
Following the method outlined by *Ghaleb* (2009), the sedimentation rate is obtained



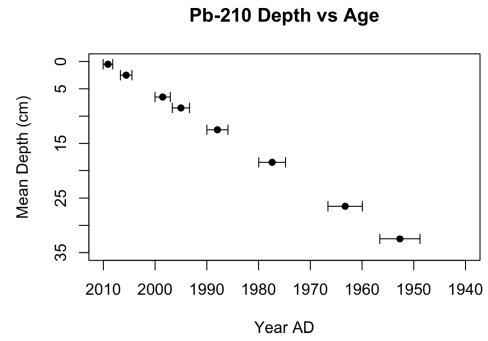
(a) Total and supported ^{210}Pb activity



(b) Unsupported ^{210}Pb activity



(c) Natural logarithm of unsupported ^{210}Pb activity and linear regression



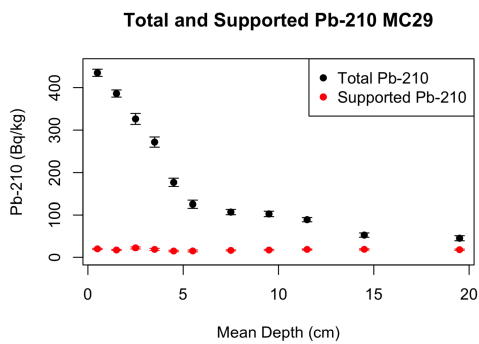
(d) ^{210}Pb age-depth model

Figure 4.2: ^{210}Pb activity profiles of core OCE400 MC44. Error bars in (d) represent ± 1 SD on the slope of the linear regression line from (c) combined with measurement error (Boyle, unpublished).

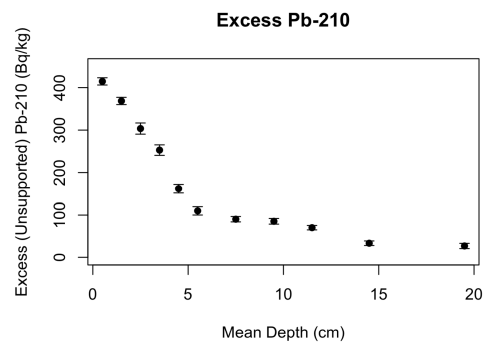
by fitting a line to the natural logarithm of unsupported ^{210}Pb vs depth (Figure 4.2c). The slope of this line, M , is calculated using Equation 4.4 and related to the sedimentation rate, S , according to Equation 4.5. The sedimentation rate is then used to determine the ^{210}Pb age model displayed in Figure 4.2d. The error bars are calculated by a combination of the total ^{210}Pb measurement error and the 1 SD uncertainty from the linear regression.

$$M = \frac{\ln A_z - \ln A_0}{Z} \quad (4.4)$$

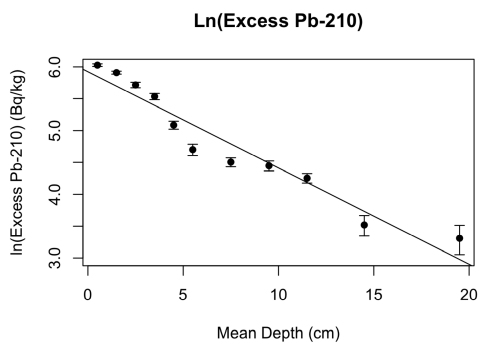
$$S = -\frac{\lambda}{M} \quad (4.5)$$



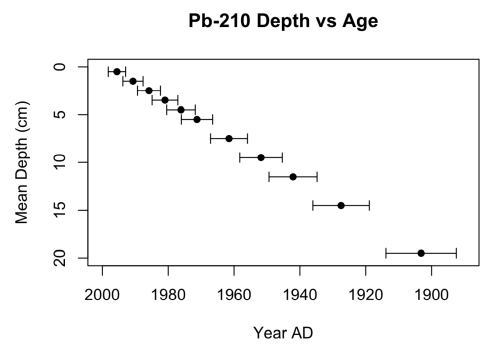
(a) Total and supported ^{210}Pb activity



(b) Unsupported ^{210}Pb activity



(c) Natural logarithm of unsupported ^{210}Pb activity and linear regression



(d) ^{210}Pb age-depth model

Figure 4.3: ^{210}Pb activity profiles of core OCE326 MC29 . Error bars in (d) represent ± 1 SD on the slope of the linear regression line from (c) combined with measurement error (Keigwin *et al.*, 2003).

Note that this model assumes a constant sedimentation rate and therefore cannot be applied if the ^{210}Pb profile deviates significantly from the idealized exponential decrease. These deviations may include 1) vertical ^{210}Pb activity in the core surface from mixing in surface sediments, 2) an activity peak slightly below core top, potentially caused by steep redox gradients, 3) rapid change in sedimentation rate, and 4) the deepest sections analyzed may still be above the supported ^{210}Pb , hence it would be an incomplete profile. The data imply relatively constant sedimentation rates, therefore these other factors appear not to be significant. The results of the described method in this section are also presented for OCE326 MC29 in Figure 4.3a through 4.3d (*Keigwin et al.*, 2003).

4.1.2 ^{14}C

Radiocarbon dating is one of the most common methods of dating sediment cores in paleoceanography. However, the construction of an age-depth model from radiocarbon dates is not as trivial as linearly interpolating between absolute dates. The radiocarbon dates need to be calibrated and the resulting probability distributions are non-Gaussian (multi-modal), adding another layer of complexity (*Bennett*, 1994; *Telford et al.*, 2004).

^{14}C is a cosmogenic nuclide produced by cosmic rays colliding with ^{14}N in the upper atmosphere, which rapidly oxidizes to form CO_2 (*Liebetrau* 2011). It is a radioactive isotope and is the least abundant of the three natural carbon isotopes. The stable forms ^{12}C and ^{13}C make up 98.98% and 1.11% respectively, while ^{14}C only makes up $1.176 \times 10^{-10-12}$ atoms per ^{12}C atom (*Liebetrau*, 2011). When organisms use CO_2 in metabolic processes, the carbon incorporated into their tissue is in isotopic equilibrium with the $^{14}\text{C}/^{12}\text{C}$ of the carbon source, ie. the atmosphere or ocean. When the organism dies, the carbon ceases to maintain isotopic equilibrium with the carbon source. This is essentially time zero of the radiocarbon clock. At this point, the ^{14}C decays exponentially with a half-life of 5,730 years.

By measuring the $^{14}\text{C}/^{12}\text{C}$ ratio of an organic carbon or CaCO_3 sample, the conventional radiocarbon age can be determined. Converting the radiocarbon date to calendar age is not trivial because the atmospheric $^{14}\text{C}/^{12}\text{C}$ ratio fluctuates over time, and the apparent age of a specific reservoir may be very different than the atmospheric $^{14}\text{C}/^{12}\text{C}$ ratio at that time. The atmospheric ^{14}C concentration fluctuates because of changes in the upper atmospheric production rate and the carbon cycle over time (*Reimer et al.*,

2013).

The equilibration of ^{14}C between the atmosphere and other reservoirs is delayed, therefore the ^{14}C age offset for a given reservoir is defined as its ‘reservoir age’. Consideration of the reservoir age is especially important in the ocean, because the apparent age of a CaCO_3 sample in the present day ocean is, on average, 400 radiocarbon years older than the atmosphere. In other words, the amount of ^{14}C in a sample at time zero of the radiocarbon clock has noteworthy uncertainty around it, and must be calibrated using more specific information about the location of the sample. Bacon uses the Marine13 calibration curve (*Reimer et al.*, 2013) and reservoir ages were selected based on *Marchitto and DeMenocal* (2003), *Keigwin et al.* (2003), and *Keigwin and Pilskałn* (2015). The conventional radiocarbon dates for cores OCE326 MC29, KNR148 11BC/13GGC, and OCE400 MC44 are presented in Tables 4.2 through 4.4.

Depth Interval	Depth	Species	Accession #	Conventional ^{14}C age	Error, 1σ
0-1	0.50	mixed BF	OS-20560	375	30
12-13	12.5	mixed PF	OS-27370	255	60
14-15	14.5	mixed PF	OS-27369	375	60
16-17	16.5	mixed PF	OS-27393	505	120
29-30	29.5	mixed PF	OS-27372	960	70
49-50	49.5	mixed PF	OS-25803	2040	60

Table 4.2: Radiocarbon ages on foraminifera from OCE326 MC-29D, Emerald Basin (published in *Keigwin et al.* (2003)). PF= planktonic foraminifera; BF= benthic foraminifera.

Composite Depth (cm)	CAMS #	Core	Depth (cm)	Conventional 14C age	Error 1 σ
17.25	110218	11BC	17	730	80
27.25	101346	13GGC	10	845	40
39.25	110219	11BC	39	1200	90
46.25	110220	11BC	46	1160	90
47.25	109803	13GGC	30	1335	40
67.25	104795	13GGC	50	1965	40
87.25	104796	13GGC	70	2440	35
119.25	104797	13GGC	102	2950	40
149.25	104798	13GGC	132	4980	35
167.25	101347	13GGC	150	3800	35

Table 4.3: Radiocarbon ages on planktonic foraminifera (*G. bulloides*) from KNR158-4-11BC and KNR158-13GGC (unpublished Marchitto and deMenocal).

Depth	Species	Mass (mg)	Accession #	Conventional 14C age	Error, 1 σ
3.5	Mixed PF	3.60	OS-66198	>Mod	
50	Mixed PF	1.40	OS-66977	580	85

Table 4.4: Radiocarbon ages on planktonic foraminifera from OCE400 MC44 (*Keigwin and Pilskałn, 2015*).

4.2 Results from Bacon Age Models

4.2.1 KNR158

For KNR158, both a box core (11BC) and gravity core (13GGC) were collected from the same location and combined to give a more complete $\delta^{13}\text{C}$ that preserves both the most recent sediments and three meters of core material. The two cores were spliced together using percent lithics and percent *N. pachyderma*, which was justified since they were collected from the same location. The age-depth model for spliced KNR158 11BC/13GGC was constructed using the conventional radiocarbon dates in Table 4.3. These radiocarbon dates were input to bacon along with priors of 0.05 cm/yr and 0.07 for accumulation rate and memory, respectively. The dates were calibrated using Marine13 and an assumed reservoir age of 492 ± 27 , based on *Marchitto and DeMenocal (2003)*. The output age-depth model is presented in Figure 4.4, with the best model marked by the red stippled line. The sedimentation rate varies between 0.030 and 0.058 cm/yr.

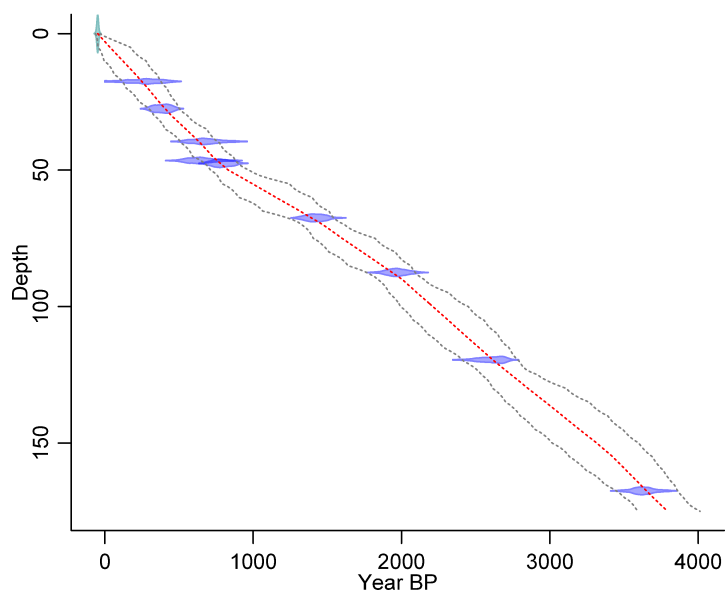


Figure 4.4: Calibrated radiocarbon dates (purple) and corresponding age-depth model for KNR158 11BC/13GGC, where the darker grays represent more likely calendar ages. Ages are displayed as years before present (BP, Present: 1950). The red curves represent the best model from the weighted mean age at each depth and gray stippled lines represent the 95% confidence intervals. This age-depth model was constructed using Bacon (Blaauw and Christen, 2011).

4.2.2 OCE326 MC29D and OCE400 MC44

OCE326 MC29D and OCE400 MC44 were dated with both ^{210}Pb and ^{14}C . The ^{210}Pb derived age points are displayed in Figures 4.3d and 4.2d, and the conventional radiocarbon dates displayed in Table 4.2 and 4.4, respectively. For each core, both dating methods were combined into single age-depth models using Bacon. The radiocarbon dates were calibrated with the Marine13 calibration curve and both cores assumed a 400 year reservoir age, based on Keigwin *et al.* (2003); Keigwin and Pilskalns (2015). The ^{210}Pb derived age points from the CF-CS model were input to Bacon at each depth of which there was a ^{210}Pb measurement. Bacon combined these two dating methods with millions of Markov Chain Monte Carlo iterations, giving the output models in Figure 4.5a and 4.5b. The best age-depth model for each core is displayed with a red stippled line.

For OCE326 MC29, the sedimentation rate increased by an order of magnitude at approximately 25 cm (~1800 AD) from 0.020 to 0.210 cm/yr. Similarly in OCE400 MC44, the sedimentation rate suddenly increased from 0.097 to 0.571 cm/yr at 35 cm (~1950

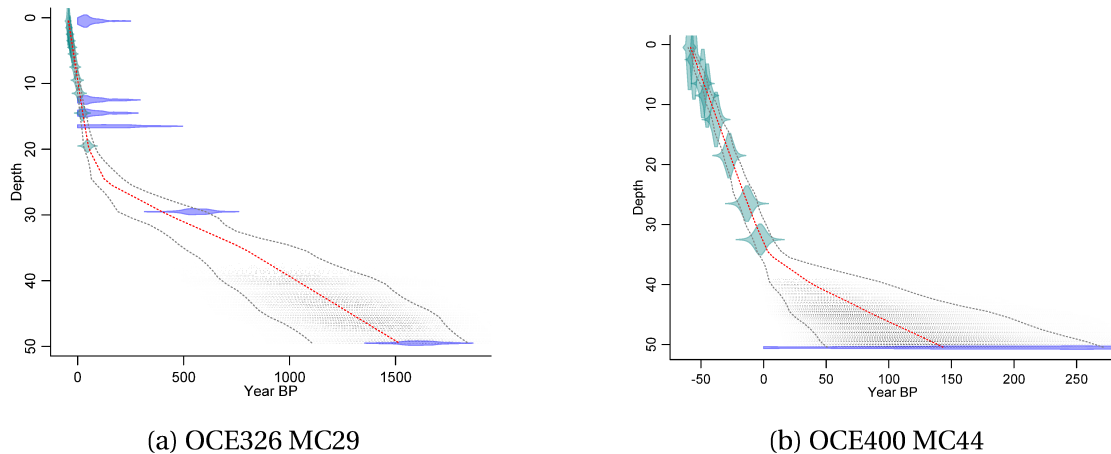


Figure 4.5: Radiocarbon dates (purple), Pb-210 derived age points (green) and corresponding age-depth models for both (a) OCE326 MC29 and (b) OCE400 MC44, where the darker grays represent more likely calendar ages. The red curves represent the best model from the weighted mean age at each depth and gray stippled lines represent the 95% confidence intervals. These age-depth models were constructed using *Bacon*, an R-based program (Blaauw and Christen, 2011)

AD). These drastic changes in sedimentation rate occur between the ^{210}Pb dated and the deeper segments of both cores. This indicates that high uncertainty in the deeper segments, which only have ^{14}C dates, may be responsible for the sedimentation rate change rather than a natural phenomenon. These large uncertainties in the deeper segments will be considered when interpreting proxy data.

4.2.3 Hg analysis and MSM46 Cores

Although Mercury (Hg) is not conventionally used in constructing age models, its contamination from chlor-alkali plants and other anthropogenic activities over the 20th century make it a valuable stratigraphic marker of modern sediments. For two sediment cores where there were no samples available for radioisotope dating, Hg profiles were used to compare with sedimentation rates published by other studies within the region (Louchouart *et al.*, 1997; Jennane, 1993; Smith and Schafer, 1999). For MSM46 MC2, near the Cabot Strait, previous studies published sedimentation rates of 0.008-0.01 (Louchouart *et al.*, 1997) and 0.04 cm/yr (Smith and Schafer, 1999). Assuming the age of the core top was equivalent to the date of core collection (2015), these sedimentation rates were used to construct three potential age models. The Hg data are plotted with each age model in Figure 4.6a.

Since Hg concentrations in sediments are influenced by anthropogenic pollution over the 20th century (*Engstrom and Swain, 1997*), all of these sedimentation rates result in age models that make the Hg profile too old to be consistent with anthropogenic origin. Therefore, instead of using published sedimentation rates from this location, I developed an age model based on the Hg profile and knowledge of local chlor-alkali plant operations and Hg emissions from the United States. The local Hg concentration increase began in the 1950s when the chlor-alkali plant in Saguenay fjord started operations (Figure 4.7a; *Smith and Schafer (1999)*). However, other Hg pollution sources around the United States started in the earlier 20th century (1900-1940, see Figure 4.7b; (*Engstrom and Swain, 1997*)) and could potentially influence the Hg profiles in our study region. Based on both Figure 4.7a and 4.7b, Hg emissions increasingly steepened in the 1960s, so I chose this as a more reliable second age point, about halfway up the profile. I input this age point and a core top year of 2015 to Bacon to arrive at a sedimentation rate of 0.226 cm/yr. The Hg data were plotted with this sedimentation rate in Figure 4.6b.

For core MSM46 MC4 in the inner Gulf of St. Lawrence, a previous study published sedimentation rates from nearby cores of 0.1-0.13 (*Jennane, 1993*). I also constructed an age model with the same method outlined for MSM46 MC2, above. This gave a sedimentation rate of 0.18 cm/yr, which is very similar to published values. For comparison, these three sedimentation rates were plotted with the MC4 Hg profile in Figure 4.8.

The age models constructed in Bacon for these two cores are displayed in Figure 4.9a and 4.9b.

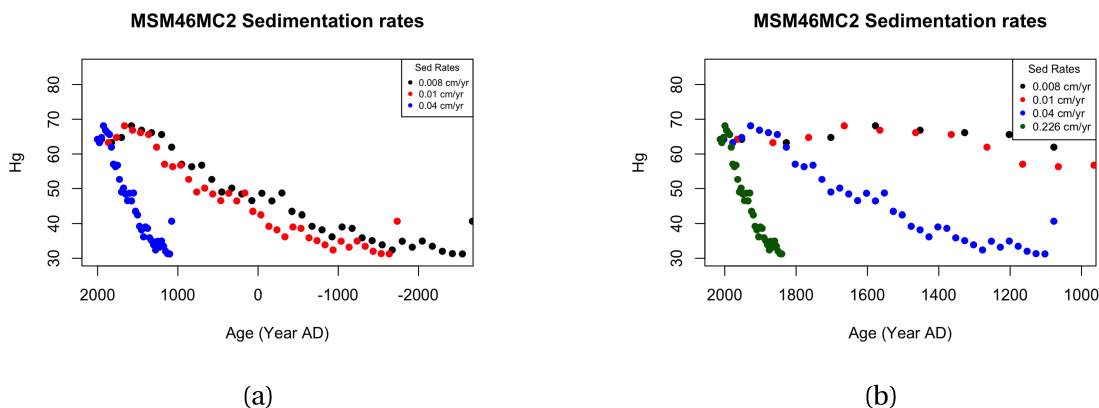


Figure 4.6: The Hg profile from MSM46MC2 plotted with different age models. In (a), the Hg is plotted with published sedimentation rates from nearby core sites in *Louchouart et al.* (1997) (black and red) and *Smith and Schafer* (1999) (blue). In (b) Hg is also plotted with the constructed age model (green) described in the text. The x-axis is zoomed in to cover the last 1000 years.

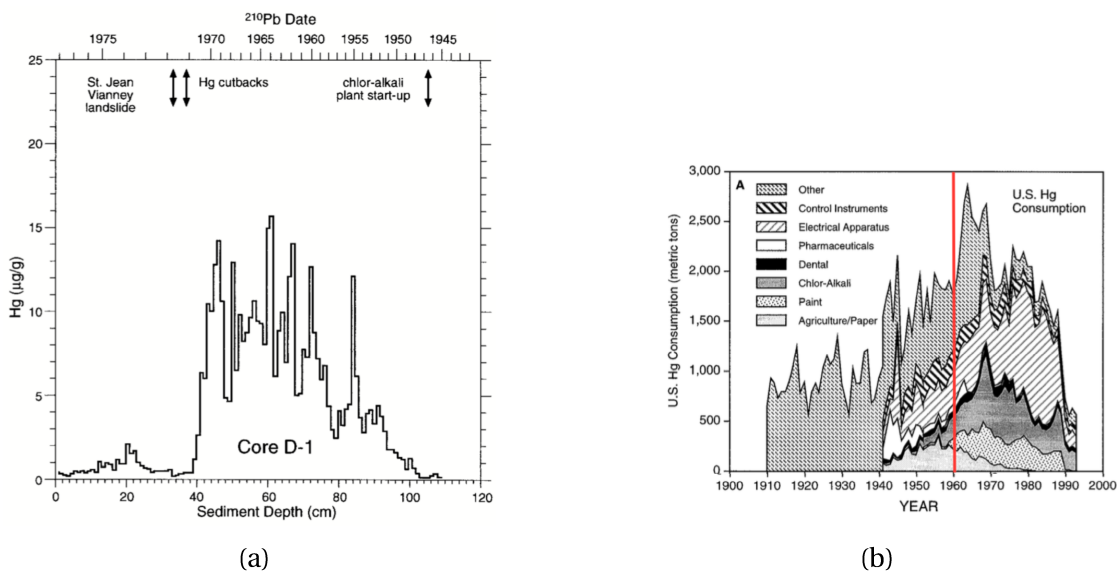


Figure 4.7: (a) Hg ($\mu\text{g/g}$) vs. sediment depth (bottom axis) and ^{210}Pb date (top axis) of a non-bioturbated core from the Saguenay Fjord. The chlor-alkali plant on this Fjord released Hg emissions from 1947 until 1970, as reflected in the Hg profile (Retrieved from *Smith and Schafer* (1999) with permission from John Wiley and Sons). (b) Time series of industrial Hg consumption in the United States from 1910 to 1993. Red line marks 1960, the point chosen as an age marker for cores MSM46 MC2 and MC4. Adapted with permission from *Engstrom and Swain* (1997). Copyright (2018) American Chemical Society.

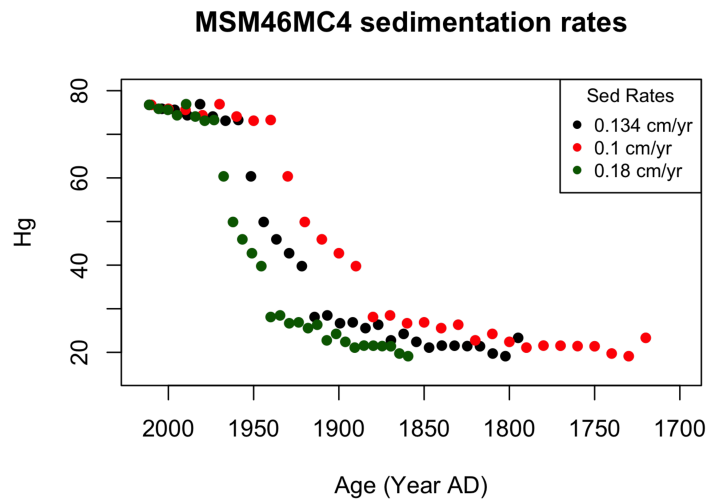


Figure 4.8: Hg profile of core MSM46 MC4 plotted with published sedimentation rates from nearby core sites in (*Jennane, 1993*) (red and black) and the constructed age model described in the text (green).

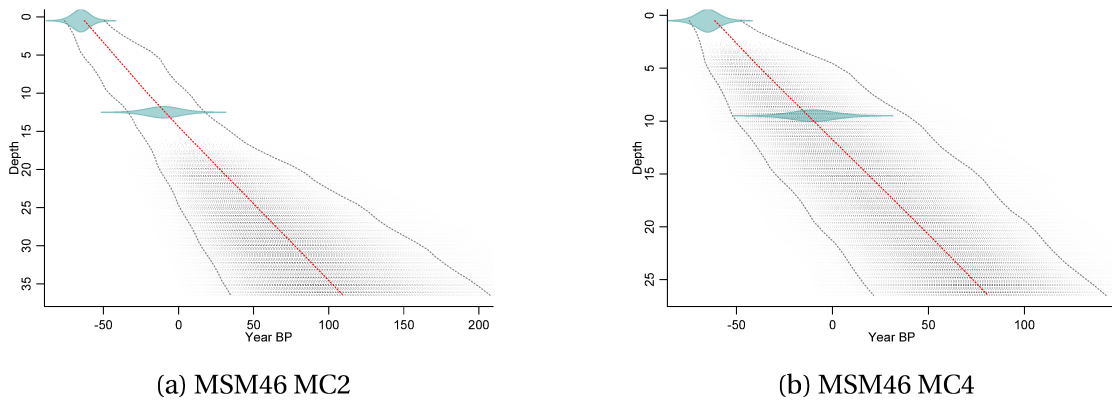


Figure 4.9: Age markers (green) and corresponding age-depth models for both (a) MSM46 MC2 and (b) MSM46 MC4, where the darker grays represent more likely calendar ages. The red curves represent the best model from the weighted mean age at each depth and gray stippled lines represent the 95% confidence intervals. These age-depth models were constructed using *bacon*, an R-based program (*Blaauw and Christen, 2011*)

CHAPTER 5

RESULTS

5.1 Carbon Isotopes

5.1.1 Foraminiferal Records

The carbon isotope ($\delta^{13}\text{C}$) results on foraminiferal calcite for all downcore records are presented in Figure 5.1. The planktic records are displayed in blue and benthic in red. The main observation that can be made is the negative carbon isotope excursions (CIE) evident in the modern sections of the cores are unprecedented over the core lengths. The Time of Emergence (ToE) of the CIEs were investigated by applying the age-depth models discussed in Chapter 4, and Figure 5.2 displays the $\delta^{13}\text{C}$ records vs. age over the period of 1800 to 2015. These time series reveal that the ToE is within the most recent 50 to 150 years.

For better visual comparison of the ToE of CIEs between all records, they were plotted on one shared axis in Figure 5.3. This visualization of the data better demonstrates the coherence between the CIEs, despite age model error and background $\delta^{13}\text{C}$ values being offset by up to 1.5‰. Magnitude, $\delta^{13}\text{C}$ rate of change, the ToE of the CIEs, and corresponding uncertainties are quantified and discussed in Section 5.2.

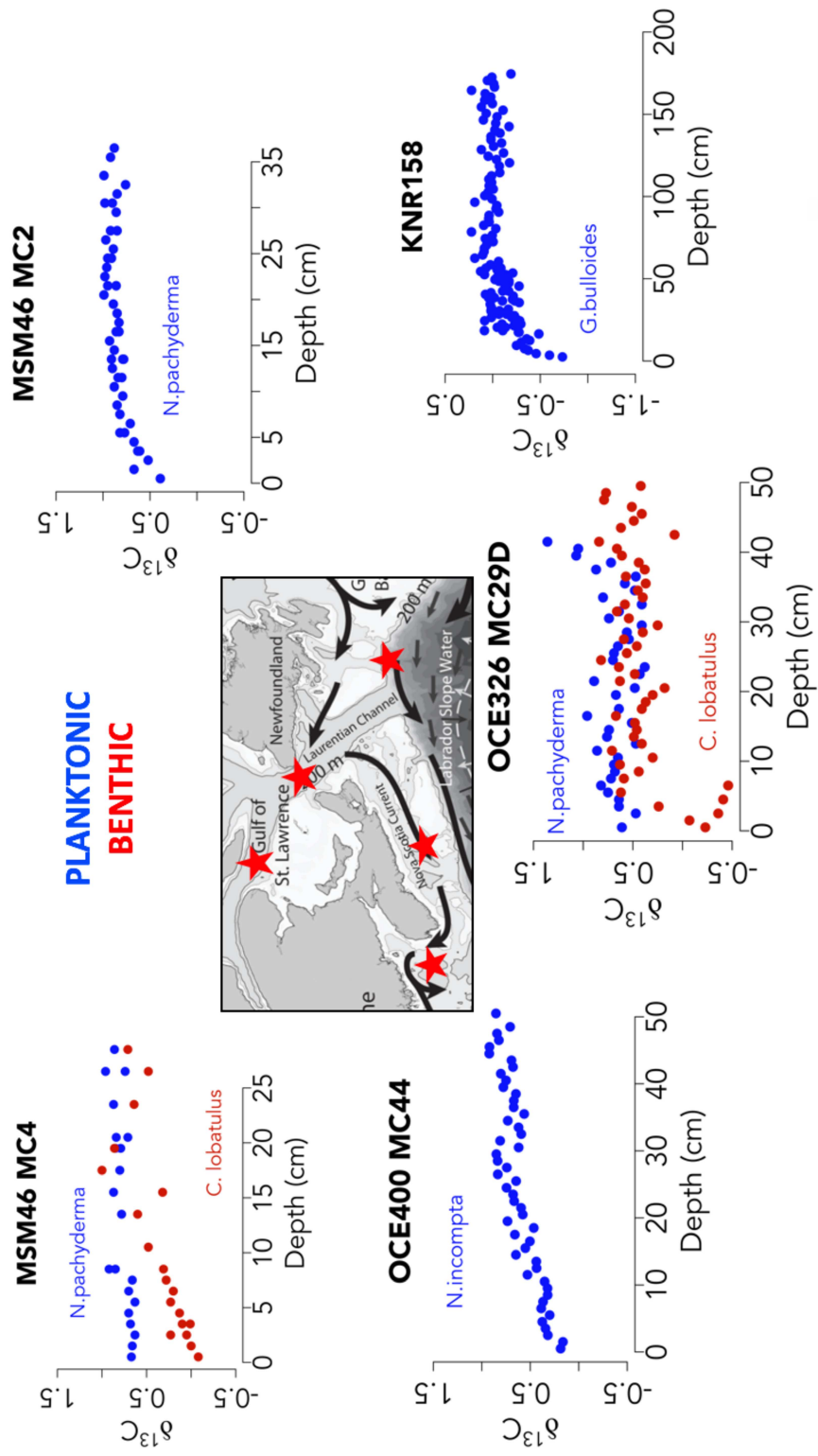


Figure 5.1: Results of all foraminiferal $\delta^{13}C$ downcore records from the eastern Canadian continental margin (Blue= Planktic foraminifera; Red= Benthic foraminifera).

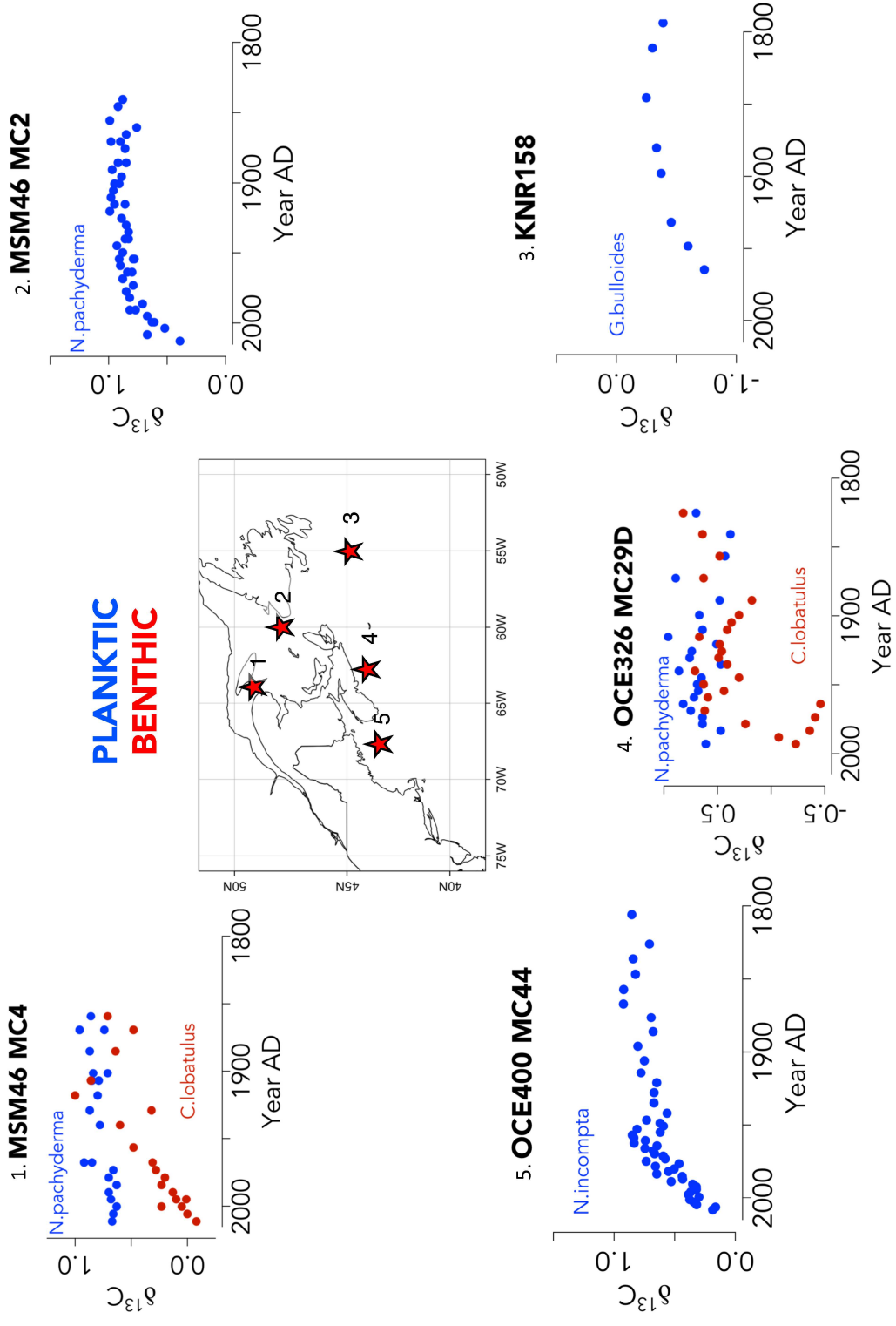


Figure 5.2: Results of all foraminiferal $\delta^{13}\text{C}$ time series records from the eastern Canadian continental margin. All cores are plotted on a time range from 1800 to 2015 AD (Blue= Planktic foraminifera; Red= Benthic foraminifera).

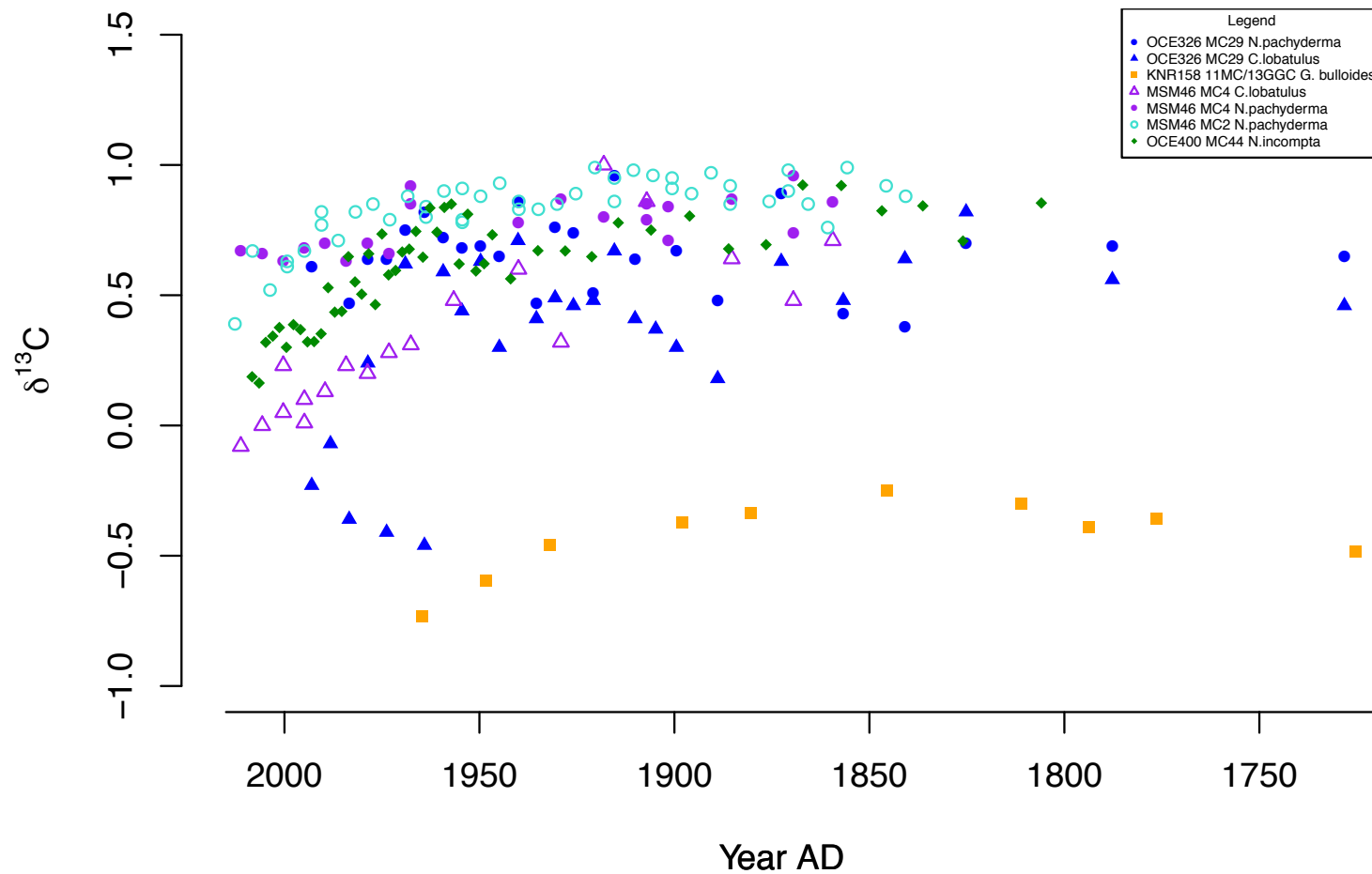


Figure 5.3: All $\delta^{13}\text{C}$ core records plotted versus age from 1700-2015 AD. $\delta^{13}\text{C}$ records from the same core are plotted with the same colour, while those of the same species are plotted with the same shape (See legend).

5.1.2 Organic Matter

Results of $\delta^{13}\text{C}_{org}$ and $\%C_{org}$ from the cores in the Gulf of St. Lawrence (MSM46 MC2 and MC4) are presented in Figures 5.4a and 5.4b. There appears to be a negative $\delta^{13}\text{C}_{org}$ CIE in MSM46 MC2 of similar magnitude to the foraminiferal CIE from the same core (Figure 5.5a). MSM46 MC4 $\delta^{13}\text{C}_{org}$ does not show a distinct CIE and has more scatter. The $\%C_{org}$ of both cores remains relatively constant throughout the record, with a slight increase in MC4.

There is more scatter in $\delta^{13}\text{C}$ of organic matter compared to the *N. pachyderma* records, but in general the CIEs begin at similar depths and have similar magnitudes.

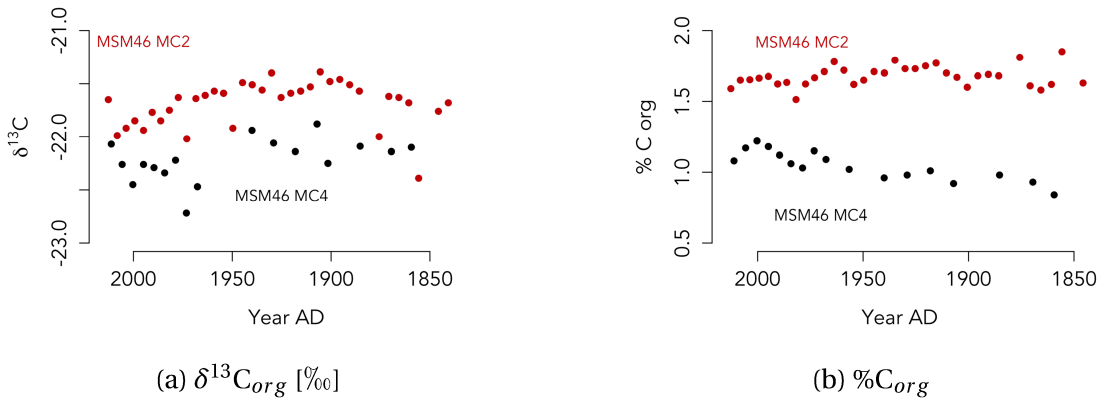


Figure 5.4: Time series results of (a) $\delta^{13}C_{org}$ and (b) %C_{org} of the MSM46 cores in the Gulf of St. Lawrence (MSM46 MC2= Red; MSM46 MC4= Black).

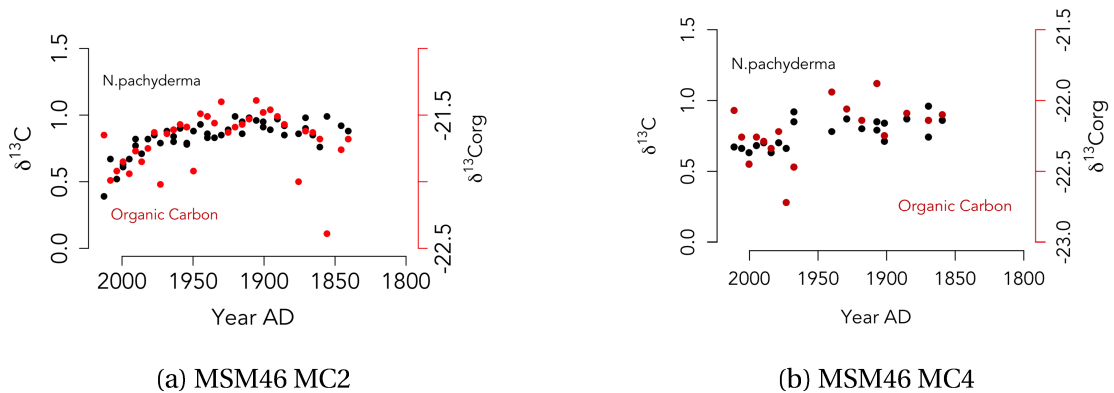


Figure 5.5: $\delta^{13}C$ of organic carbon (red) and *N. pachyderma* (black) time series results of cores (a) MSM46 MC2 and (b) MSM46 MC4.

5.2 Results of Piecewise Regressions

Results from the broken-line models are presented throughout this section for each $\delta^{13}\text{C}$ record. The resulting models were assessed for goodness of fit visually and statistically. The results are summarized in Section 5.3, and organized into Tables 5.2 and 5.1.

5.2.1 MSM46 MC4

Results of the piecewise linear regression for $\delta^{13}\text{C}$ *N. pachyderma* and *C. lobatulus* MSM46 MC4 records are presented in Figure 5.6a and 5.6b, respectively. The change point determined by the two-piece regression appears to be a good fit. The planktic record (*N. pachyderma*) exhibits a small CIE of $-0.172 \pm 0.133\text{‰}$ from 1968 to 2011. The $\delta^{13}\text{C}$ rate of change is $-0.0039 \pm 0.0009\text{‰/yr}$. This rate of change was used to extrapolate the CIE to 2013, for the purpose of normalizing with the other records (see Section 3.3). The magnitude of the extrapolated CIE is $-0.180 \pm 0.138\text{‰}$. Even though the piecewise linear regression determined a change point of 1968 ± 21 years, the age model at the depth equivalent of the change point (8.5 cm) has a 95% confidence interval range between 2004 and 1920.

The results from the piecewise regression of the benthic record (*C. lobatulus*) show large model uncertainty in the earlier section of the core due to fewer samples and fewer *C. lobatulus* per sample, compared to the later half of the core. Because of this large scatter, the change point does not seem to represent the pre-industrial $\delta^{13}\text{C}$ value well. Instead of using the change point $\delta^{13}\text{C}$ value, I therefore used an average of all the samples up until the scattering diminished significantly at 1940. The resulting average pre-industrial $\delta^{13}\text{C}$ value and corresponding uncertainty are denoted by the solid and dashed red lines, respectively, in Figure 5.6b. Calculating the CIE between this value and the most recent model value (2011) reveals a relatively large negative CIE of $-0.697 \pm 0.256\text{‰}$. The $\delta^{13}\text{C}$ rate of change was -0.00848 ± 0.00046 . The magnitude of the 2013-extrapolated CIE was $-0.712 \pm 0.258\text{‰}$.

Since the piecewise linear regression does not take into account error in the x-axis, the large uncertainty in the age model of this core causes more error in the $\delta^{13}\text{C}$ rate of change and extrapolated CIE value than the reported uncertainty values. This unreported uncertainty was considered in any further interpretation of these parameters throughout this thesis. Despite these large uncertainties, it can still be said with confidence that the CIE is larger and starts earlier in the *C. lobatulus* compared to the *N.*

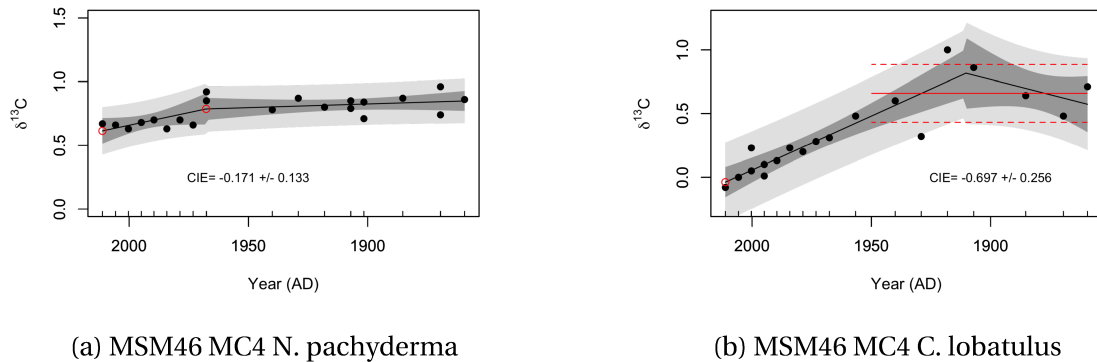


Figure 5.6: Piecewise linear regression results on foraminiferal $\delta^{13}\text{C}$ records from MSM46 MC4. The model average is represented by the black solid line with 95% confidence intervals and prediction intervals displayed in dark grey and light grey, respectively. (a) Planktic foraminiferal reconstruction (*N. pachyderma*) with associated CIE calculated between the core top and change point (two red circles). (b) Epibenthic foraminiferal reconstruction (*C. lobatulus*) with associated CIE calculated between core top (red circle) and Pre-industrial $\delta^{13}\text{C}$ (red line) of $0.659 \pm 0.227\text{‰}$ (red dashed line). These analyses were performed with the segmented package in R.

pachyderma $\delta^{13}\text{C}$ record, and both signals have a ToE in the 20th century.

5.2.2 MSM46 MC2

Results of the piecewise linear regression for $\delta^{13}\text{C}$ *N. pachyderma* of MSM46 MC2 are presented in Figure 5.7a. The first observation from this preliminary analysis is that a three piece regression may be a better fit. It appears that the decrease in $\delta^{13}\text{C}$ starts earlier than the determined change point from the segmented package, and it looks like the rate of change increases after this initial onset of the CIE.

The three piece linear regression was performed *post hoc* since it appears to better represent the relationship between $\delta^{13}\text{C}$ and age/depth. The result of this regression is presented in Figure 5.7b. The initial onset of the negative CIE occurs at 1910 AD \pm 14 years with a slope of $-0.0020 \pm 0.0006 \text{‰/year}$, which increase to $0.0143 \pm 0.0028 \text{‰/year}$ ($R^2=.857$) at 1990 (± 3). The total magnitude of the negative CIE is $0.482 \pm 0.105 \text{‰}$ between 1910 and 2013. Since all other core records were adjusted to the most recent data point of MSM46 MC2, no extrapolation was necessary for normalization.

As discussed in the previous section, the actual slopes reported here are subject to large error in the dependent variable (time), and therefore should be interpreted with

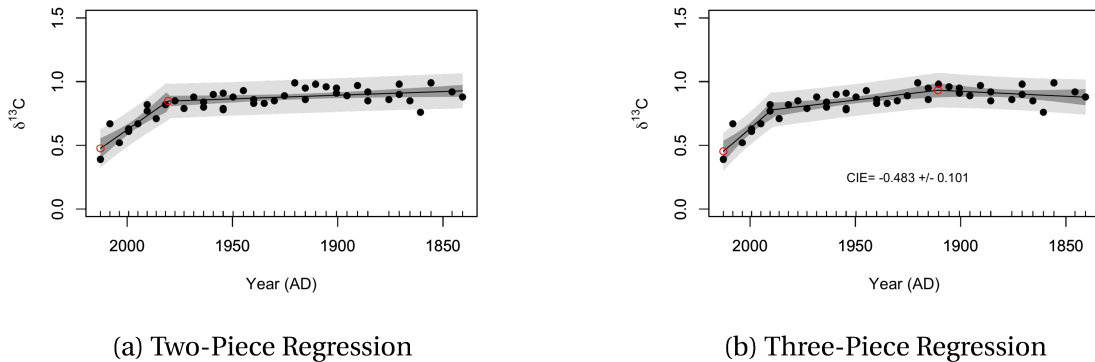


Figure 5.7: The MSM46 MC2 (a) two-piece and (b) three-piece linear regression results on $\delta^{13}\text{C}$ of planktic foraminifera, *N. pachyderma*. The three-piece regression also displays the 95% CI and PI in dark grey and light grey respectively. The associated CIE was calculated between the first change point and core top (red circles). These analyses were performed with the segmented package in R.

caution. However, the magnitude of the CIE from onset to present day is reliable, as the calculation is performed independent of the time axis.

5.2.3 KNR15 11BC/13GGC

Results of the piecewise linear regression for $\delta^{13}\text{C}$ *G. bulloides* of KNR158 are presented in Figure 5.8a. It is evident that the light $\delta^{13}\text{C}$ values of the modern samples are unprecedented. However, the first observation from this preliminary analysis is that the change point at 1514 AD (1412 to 1626 AD) happens much earlier than the time range of interest. It also appears that the model is not picking up the full magnitude of the CIE at the top of the core. Therefore I explored the piecewise regressions at both the full range (Figure 5.8a) and from 1500-1964 AD (Figure 5.8b).

The magnitude of the CIE from the full record was $0.455 \pm 0.099\text{‰}$. The slope after the change point was $-0.0010 \pm 0.0001\text{‰/year}$. This model seems to be a good fit to the long term $\delta^{13}\text{C}$ trends, but there appears to be some high-resolution variability not represented well by a linear relationship. The 2013 CIE was determined through extrapolation, resulting in a CIE of $0.504 \pm 0.112\text{‰}$.

The CIE magnitude from the 1500-1964 AD record was $0.343 \pm 0.253\text{‰}$. Starting at a change point of $1924 \text{ AD} \pm 20$ years, the $\delta^{13}\text{C}$ rate of change was $-0.0084 \pm 0.0051\text{‰/year}$. This relationship was extrapolated to give the 2013-adjusted CIE of $0.743 \pm 0.701\text{‰}$. The confidence interval range increased significantly because of the lower sample size

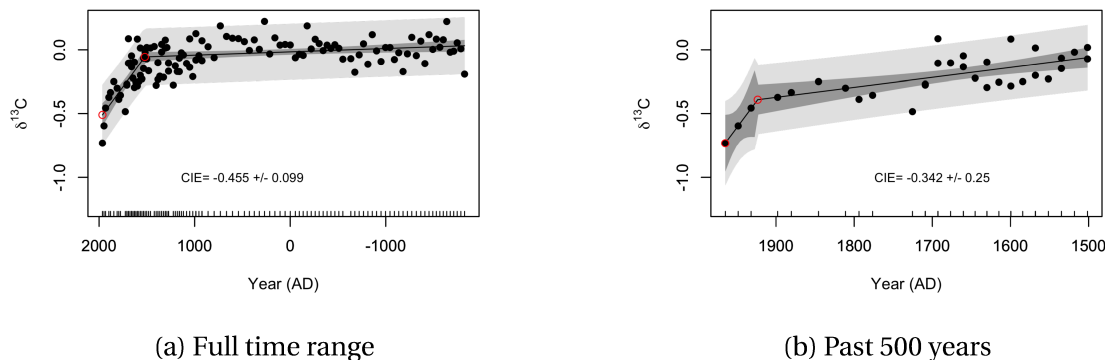


Figure 5.8: The KNR158 11BC/13GGC piecewise linear regression results on $\delta^{13}\text{C}$ of planktic foraminifera, *G. bulloides*. The model average is represented by the black solid line with 95% confidence intervals and prediction intervals displayed in dark grey and light grey, respectively. The regression in (a) covers the entire record from 2000 BC to 1964 AD, while (b) includes only 1500 to 1964 AD. The associated CIE of both records is calculated between the change point and core top (red circles). These analyses were performed with the segmented package in R.

compared to the full record. The earlier section of this record reveals a lot of systematic variability that is not best represented by a linear model. Future analysis may require a different modelling technique for KNR158.

The relatively large uncertainty in the age model of this core is due to the fact that only radiocarbon dates were used. Additional ^{210}Pb dates would be an asset for determining the onset of the CIE, but there is no sample material left from the modern portion of this core.

5.2.4 OCE326 MC29

Results of the piecewise linear regression for $\delta^{13}\text{C}$ of *N. pachyderma* and *C. lobatulus* OCE326 MC29D records are presented in Figure 5.9a and 5.9b, respectively. The *N. pachyderma* record shows no negative CIE in the top section of the core. There does appear to be a significant decrease in the $\delta^{13}\text{C}$ at the beginning of the record from approximately 800 to 1000 AD. The cause of this decrease will not be investigated in this thesis.

The piecewise linear regression of the *C. lobatulus* record reveals a large negative CIE starting at $1950 \text{ AD} \pm 9 \text{ years}$ with a slope of $-0.0179 \pm 0.0050\text{‰}$ per year. The magnitude of the CIE was $-0.779 \pm 0.292\text{‰}$ (from 1950 to 1993). The extrapolated 2013 CIE was

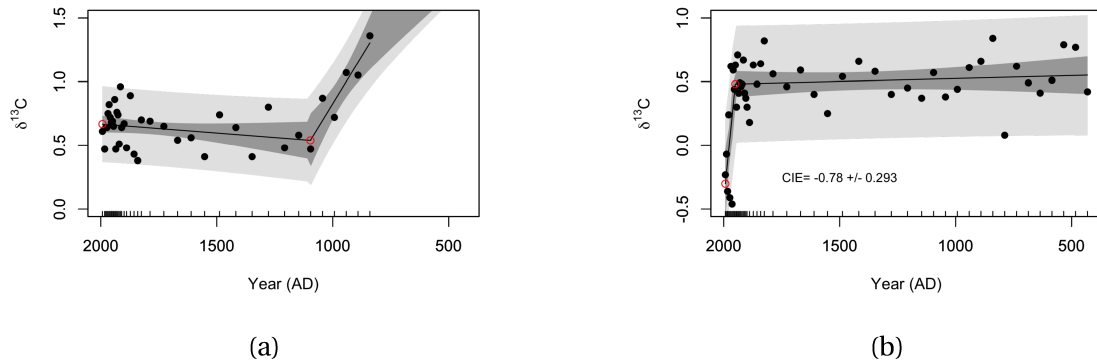


Figure 5.9: Piecewise linear regression results on foraminiferal $\delta^{13}\text{C}$ records from OCE326 MC29D. The model average is represented by the black solid line with 95% confidence intervals and prediction intervals displayed in dark grey and light grey, respectively. (a) Planktonic foraminiferal reconstruction (*N. pachyderma*) with no evident CIE in top of the core. (b) Epibenthic foraminiferal reconstruction (*C. lobatulus*) with associated CIE calculated between change point and core top (red circles). These analyses were performed with the segmented package in R.

$-1.144 \pm 0.503\text{‰}$. The age model in this core has significantly less uncertainty than the previous three cores. This low uncertainty implies that the timing of CIE onset and $\delta^{13}\text{C}$ rate of change values are reliable and can hence be compared with and interpreted relative to other well-dated processes, such as the atmospheric Suess effect.

5.2.5 OCE400 MC44

Results of the piecewise linear regression for $\delta^{13}\text{C}$ *N. incompta* of OCE400 MC44 are presented in Figure 5.10. The resulting model appears to be a very good fit to the data, therefore no post hoc adjustments to the analysis were necessary. The ToE of the CIE was $1967 \text{ AD} \pm 4$ years with a slope of $-0.01147 \pm 0.00142\text{‰}$. The magnitude of the CIE was $-0.478 \pm 0.083\text{‰}$ from 1967 to 2008, and the extrapolated 2013 CIE magnitude was $-0.532 \pm 0.093\text{‰}$. It should be noted that the $\delta^{13}\text{C}$ may have begun to decrease earlier than the change point, as the first segment of this piecewise regression has a small negative slope of $-0.00084 \pm 0.00034\text{‰}$. This will not significantly impact the magnitude of the calculated CIE, but it may affect the interpretation of ToE of the Suess effect relative to the atmosphere.

The age model for this core has relatively low uncertainty. This low uncertainty implies that the ToE and $\delta^{13}\text{C}$ rate of change values are reliable and can hence be

compared with and interpreted relative to other well dated processes.

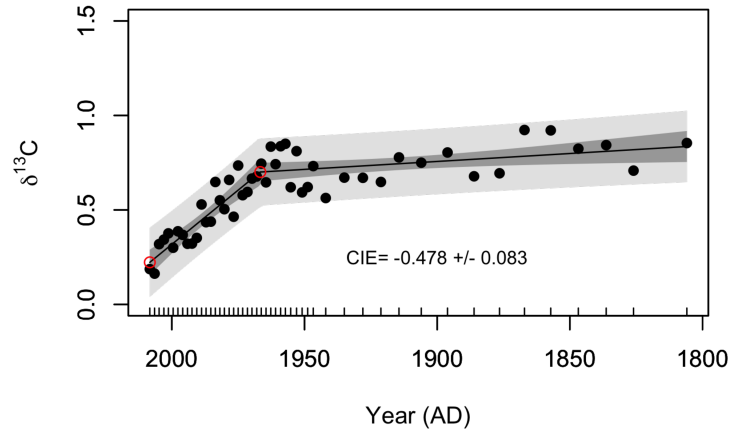


Figure 5.10: OCE400 MC44 piecewise linear regression results on $\delta^{13}\text{C}$ of planktic foraminifera, *N. incompta*. The model average is represented by the black solid line with 95% confidence intervals and prediction intervals displayed in dark grey and light grey, respectively. The associated CIE was calculated between the change point and core top (red circles). This analysis was performed with the segmented package in R.

5.2.6 MSM46 Organic Carbon

The results of CIE analysis for organic matter of MSM46 MC2 and MC4 are presented in Figures 5.11(a) and (b). The piecewise linear regression of $\delta^{13}\text{C}_{org}$ MSM46 MC2 revealed a CIE of $-0.426 \pm 0.193\text{‰}$ and a $\delta^{13}\text{C}$ decrease rate of $-0.004 \pm 0.001\text{‰/yr}$. The broken-line model was not a good choice for MSM46 MC4, so instead a CIE was estimated by the difference between mean pre-industrial and modern $\delta^{13}\text{C}_{org}$ values (denoted by red line in Figure). This analysis revealed a smaller CIE of $-0.276 \pm 0.222\text{‰}$.

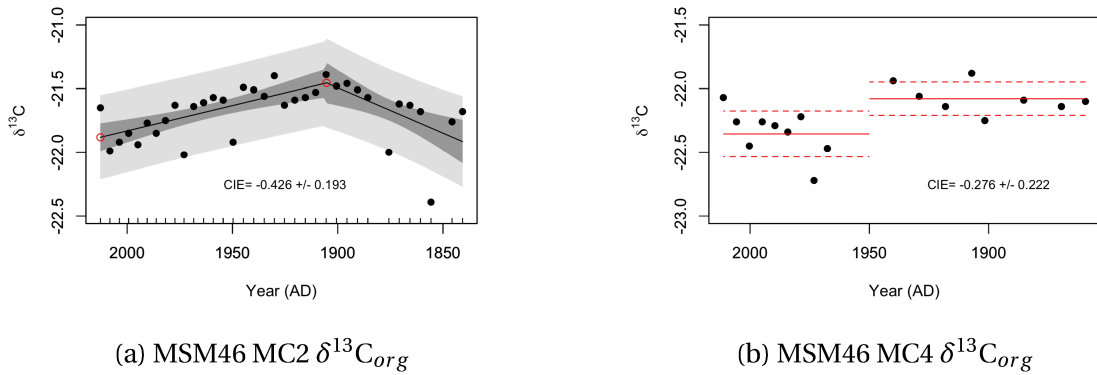


Figure 5.11: Statistical analysis of CIEs on $\delta^{13}C_{org}$ of a) MSM46 MC2 using a broken-line model and b) MSM46 MC4 using the difference between pre-industrial and modern day $\delta^{13}C$ values. These analyses were performed with the segmented package in R.

5.2.7 Time of Emergence of CIEs

A summary of the change points determined from the broken line models (excluding OCE326 MC29 *N. pachyderma* and KNR158– full depth range) are presented in Table 5.1. There were two types of uncertainty that were quantified about the change point year 1) the 1σ uncertainty of the change point determination from the piecewise model and 2) the age model uncertainty around the change point depth. These two types of error are also presented in Table 5.1. The ToE of the CIEs was determined from the weighted mean of the change point year, of which the weights were assigned according to the cumulative uncertainties. The weighted mean resulted in a ToE of 1959 AD \pm 10 years.

Core	Species	Change Point (Year AD)	Age Model 1σ	Change Point 1σ	Cumulative 1σ
MSM46_MC4	<i>N.pachyderma</i>	1968	36	20	56
MSM46_MC4	<i>C.lobatulus</i>	1911	51	11	62
MSM46_MC2	<i>N.pachyderma</i>	1910	93	14	107
KNR158 zoom	<i>G.bulloides</i>	1924	46	20	66
OCE326_MC29D	<i>C.lobatulus</i>	1950	10	9	19
OCE400_MC44	<i>N.incompta</i>	1967	8	4	12

Table 5.1: Change point year (AD) of each foraminifera record and corresponding 1σ uncertainties in the age-depth and broken line models, respectively. The reported cumulative uncertainties were used in the weighted average to determine the ToE of the CIEs.

5.3 Summary of Results

In summary, the benthic $\delta^{13}\text{C}$ records revealed larger CIEs than the planktic. The 2013-adjusted *C. lobatulus* CIEs from OCE326 MC29D and MSM46 MC4 were $-1.144\pm 0.503\text{‰}$ and $0.712\pm 0.258\text{‰}$, respectively. The next largest CIE occurred in the KNR158 11BC/13GGC record from 1500 to 1964 AD of planktic *G. bulloides*, of which the extrapolated value was $0.743\pm 0.701\text{‰}$ (full record 2013 CIE was $-0.504\pm 0.112\text{‰}$). Planktic records from OCE400 MC44 and MSM46 MC2 revealed similar magnitude CIEs of $0.532\pm 0.093\text{‰}$ and $0.486\pm 0.080\text{‰}$, respectively. The planktic record at MSM46 MC4 had the smallest CIE, with a magnitude $0.180\pm 0.138\text{‰}$, and the planktic record at OCE326 MC29D displayed no CIE at all. All CIE and $\delta^{13}\text{C}$ rate of change estimates are presented in Table 5.2.

Since $\delta^{18}\text{O}$ was measured simultaneously with $\delta^{13}\text{C}$ of calcite, the results of $\delta^{18}\text{O}$ for each foram record are presented in Figure 5.12 (See Figure 5.13 for comparison with $\delta^{13}\text{C}$). Results of $\delta^{13}\text{C}_{org}$ show similar timing, magnitude, and $\delta^{13}\text{C}$ rate of change compared planktic species, *N. pachyderma*, in MSM46 cores.

Core	Species	Change Point	CP Error	R ²	Slope	Error	CIE	Error	2013-Adj. CIE	Error
MSM46 MC4	<i>N. pachyderma</i>	1968	21	0.46	-0.00058 -0.00397	0.00061 0.00211	0.17	0.13	0.18	0.14
MSM46 MC4	<i>C. lobatulus</i>	1910	12	0.81	0.00476 -0.00847	0.00373 0.00125	0.70	0.26	0.71	0.26
MSM46 MC2	<i>N. pachyderma</i>	1911 1990	14 4	0.77	0.00078 -0.00195 -0.01429	0.00072 0.00063 0.00283	0.48	0.10	0.49	0.10
KNR158 11BC/13GGC	<i>G. bulloides</i>	1521	41	0.53	-0.00003 -0.00102	0.00001 0.00016	0.46	0.10	0.50	0.11
KNR158 ZOOM	<i>G. bulloides</i>	1924	20	0.61	-0.00078 -0.00835	0.00020 0.00511	0.34	0.25	0.74	0.70
OCE326MC29	<i>N. pachyderma</i>	1096	41	0.51	-0.00298 0.00014	0.00067 0.00010	-0.13	0.22	-0.13	0.22
OCE326 MC29	<i>C. lobatulus</i>	1950	9	0.44	-0.00005 -0.01818	0.00007 0.00595	0.78	0.29	1.14	0.50
OCE400 MC44	<i>N. incompta</i>	1967	4	0.82	-0.00084 -0.01148	0.00034 0.00142	0.48	0.08	0.53	0.09

Table 5.2: Summary table of the piecewise linear regressions for each core, including carbon isotope excursions. The change point (CP) error does not take into account uncertainty in the age model, only uncertainty in the placement of the change point in the piecewise regression. The 95% confidence intervals of the change point ages for each core are displayed in Table 5.1.

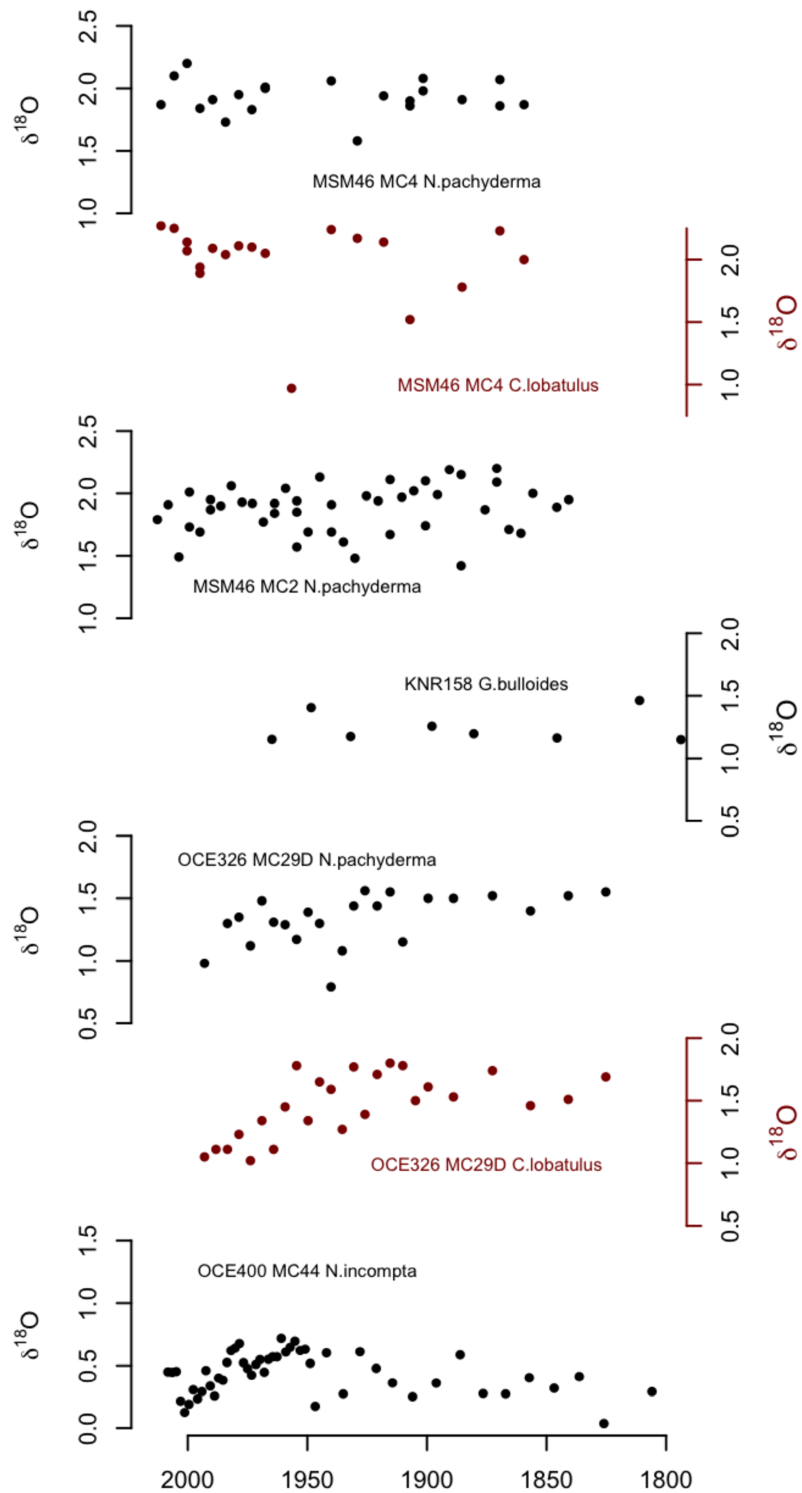


Figure 5.12: Compilation of foraminiferal $\delta^{18}\text{O}$ records from all core sites in the study region. Core sites and species names are labelled on each subplot. Planktonic foraminifera records are displayed in black and epibenthic in red.

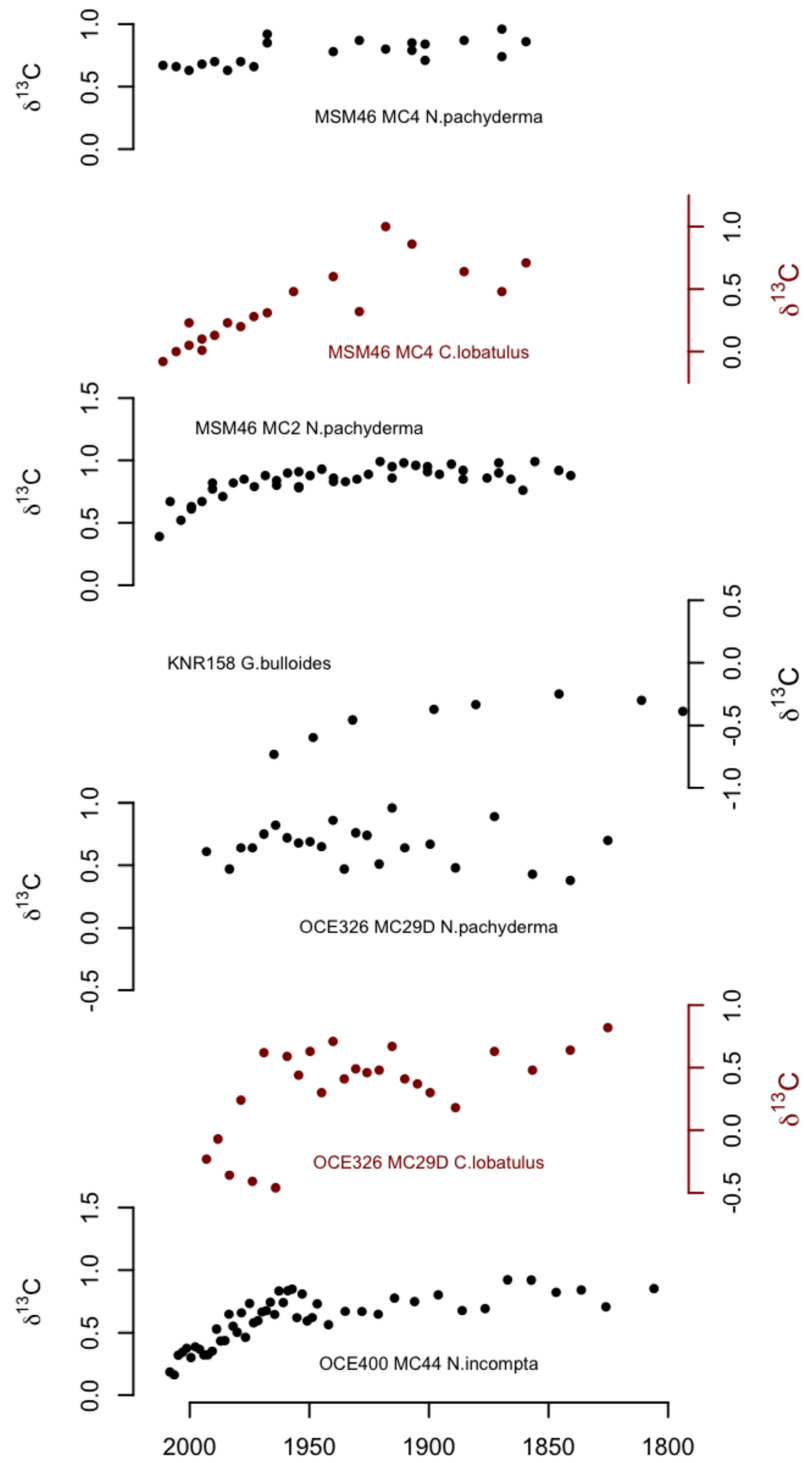


Figure 5.13: Compilation of foraminiferal $\delta^{13}\text{C}$ records from all core sites in the study region. Core sites and species names are labelled on each subplot. Planktonic foraminifera records are displayed in black and epibenthic in red.

CHAPTER 6

DISCUSSION

Despite very different oceanographic settings, negative $\delta^{13}\text{C}$ excursions (CIEs) are seen in the top sections of the cores at all five core locations. The magnitude of 2013-adjusted CIEs range from $-0.180 \pm 0.138\text{‰}$ to $-1.144 \pm 0.503\text{‰}$. Both observed and 2013-adjusted CIEs are depicted in Figure 6.1. The high uncertainty in the benthic records may be due to the fact that fewer foraminifera individuals were used per sample compared to the planktic records. The consequence of fewer individuals per sample is that each data point is more sensitive to microhabitats and vertical mixing in the sediment column (bioturbation) of individual foraminifera tests, adding more noise to the signal.

However, even taking into account the large uncertainty in the benthic CIEs, the 2013-adjusted magnitude was larger than planktic CIEs at sites where both planktic and benthic foraminifera were analyzed. This result does not match with the prediction of the relative Suess effect between surface and bottom waters. In theory, the magnitude of the Suess effect recorded in foraminifera should depend on the age of the water when it reaches the core site and the degree of equilibration during air-sea gas exchange. An older water parcel (usually deeper) will record the Suess effect of the atmosphere at the time that it last equilibrated with the atmosphere, hence we expect deeper waters to have a lower magnitude Suess effect than surface waters. The amount of time that the water parcel was in contact with the atmosphere would also have a significant impact because it takes approximately 10 years for the $\delta^{13}\text{C}$ of the DIC pool to fully equilibrate with atmosphere (*Broecker and Peng, 1974*).

To explain this discrepancy between the expected and observed CIEs, other environmental controls affecting $\delta^{13}\text{C}$ of DIC and of foraminifera, respectively, must be considered. These environmental controls are outlined and discussed in context of the

observed negative CIEs in the next two subsections (6.1 and 6.2).

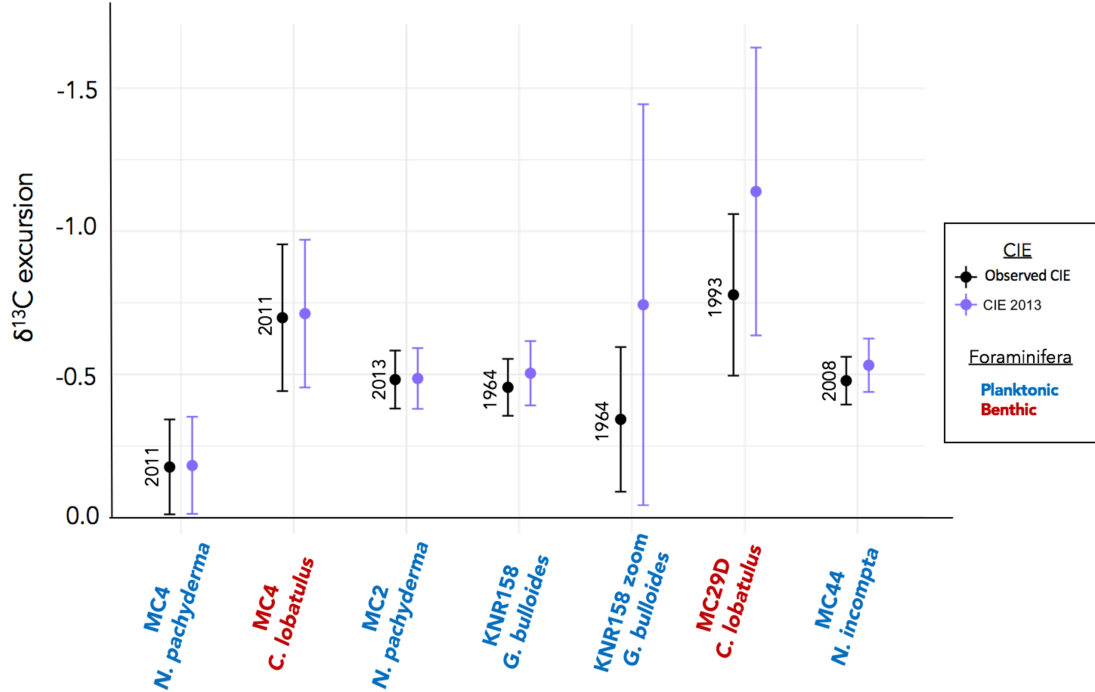


Figure 6.1: Observed (black) and 2013-adjusted (purple) $\delta^{13}C$ excursions for all foraminiferal records. Error bars denote the uncertainty to 1σ .

6.1 Effects on $\delta^{13}C$ of DIC

The processes that control the distribution of $\delta^{13}C$ of DIC in the modern and preindustrial ocean were investigated in a study by (Schmittner *et al.*, 2013). They analyzed observations and sensitivity experiments using a three dimensional global model of stable carbon isotope cycling. They found the dominant controlling factor to be biological production, followed by thermodynamic effects during air-sea gas exchange. The effects of calcium carbonate cycling, pH dependency of fractionation during air-sea gas exchange, and kinetic fractionation were minor, and will therefore be ignored in this study. The two major controlling factors on $\delta^{13}C$ distribution, thermodynamic effects during air-sea gas exchange and biological effects, will be discussed in context of the observed CIEs.

The first environmental parameter that can impact the $\delta^{13}C$ of DIC is thermodynamic fractionation during air-sea gas exchange. Colder waters have higher $\delta^{13}C_{DIC}$

than warmer waters at air-sea isotopic equilibrium (*Mook et al.*, 1974; *Eide et al.*, 2017b). For every 1°C warming, $\delta^{13}\text{C}_{DIC}$ depletes by about 0.1‰ (*Broecker and Maier-Reimer*, 1992). Therefore, a 5-10°C warming at all source water formation sites would be necessary to account for a 0.5-1.0‰ negative CIE. No warming this large has been observed over the time period investigated in this study.

It should be noted that full equilibrium is rarely achieved as the air-sea equilibration time scale for $\delta^{13}\text{C}$ is around 10 years (*Broecker and Peng*, 1974). Without knowing the detailed history of the water parcels present in the study area ie. exactly where they came from, when they formed and how long each water parcel was in contact with the atmosphere, there is no way of determining the exact contribution of the thermodynamic effect to the negative CIE observed in the foraminifera record. It is quite possible this effect is contributing slightly to the $\delta^{13}\text{C}$ change in some of the cores, but likely not significantly, since most of the temperature change recorded in the study area was in bottom waters (*Gilbert et al.*, 2005), while we see the negative CIE in both the surface and bottom. The recent warming seen in the bottom waters of the study region has been attributed to changing water mass proportions (*Gilbert et al.*, 2005), which will be discussed further in the next subsection. No correction for thermodynamic effects were applied to the CIEs.

Since photosynthesizing organisms fractionate carbon when forming organic matter (*O'Leary*, 1981), biological production is another major environmental control of $\delta^{13}\text{C}_{DIC}$, particularly the amount of primary production and organic matter export. Increasing (decreasing) amounts of primary productivity in the surface ocean increases (decreases) the $\delta^{13}\text{C}_{DIC}$ of surface waters. Since the degree of fractionation for marine organisms is approximately -20 to -22‰, an increased proportion of carbon in organic matter would result in the remaining DIC to be isotopically enriched (*Thibodeau et al.*, 2006). Likewise, an increased (decreased) organic matter flux to deep waters would enhance remineralization of isotopically light organic carbon, hence decreasing (increasing) the $\delta^{13}\text{C}_{DIC}$ of bottom waters. Even if the amount of increased production could be determined with another proxy, quantifying the exact impact of biological production on the observed $\delta^{13}\text{C}_{foram}$ record would be difficult. Therefore, I can only comment qualitatively regarding the influence of biological production on the $\delta^{13}\text{C}_{foram}$.

If all of the observed $\delta^{13}\text{C}$ changes were due to biological production, there would need to be significant reduction of primary productivity in the surface ocean and coincident increase in organic matter flux to bottom water to account for the high magnitude $\delta^{13}\text{C}$ decrease. Since there is no simple mechanism to explain both a decrease in primary production and increase in organic matter flux, biological effects could not account for the full observed negative isotope excursions seen at all of the core sites, both in surface and bottom waters. However, evidence from dinocyst assemblages, $\%C_{org}$, and abundance of benthic foraminifera suggests both primary productivity and organic matter flux increased since the 1960's in the LSLE (Thibodeau *et al.*, 2006). Although there is no quantitative correction for this effect, it is likely this increased productivity affected both the *N. pachyderma* and *C. lobatulus* records at MSM46 MC4. Heavier $\delta^{13}\text{C}_{DIC}$ in surface waters may be dampening the CIE of *N. pachyderma*, while lighter $\delta^{13}\text{C}_{DIC}$ of bottom water may be enhancing the CIE of *C. lobatulus*.

6.2 Disequilibrium effects between $\delta^{13}\text{C}$ DIC and carbonate

Foraminiferal calcite is often in slight disequilibrium with surrounding $\delta^{13}\text{C}_{DIC}$. The vital effects that are understood to contribute to this offset include calcification temperature, pH and carbonate ion concentration of seawater, foraminiferal diet, shell size, genotype variation, habitat migration during life cycle and photosynthesis of algal symbionts (King and Howard, 2004). In considering the impacts of these vital effects on the foraminiferal $\delta^{13}\text{C}$ records of this study, we can rule out shell size, genotype variation, habitat migration during the life cycle and photosynthesis of algal symbionts. Foraminiferal shells are picked at a constant size range throughout the core, hence preventing any consistent offsets due to the shell size effect. Genotype variation should not have an influence because the genotype was kept consistent for each $\delta^{13}\text{C}$ record. The species analyzed in this study have no algal symbionts and there is no reason to expect that habitat migration during the life cycle changed systematically over the core length. Therefore, only effects of temperature, pH, and foraminiferal diet are considered.

6.2.1 Calcification Temperature

A *G. bulloides* culturing study investigating the impact of calcification temperature on $\delta^{13}\text{C}_{\text{foram}}$ found a 0.11‰ decrease per °C increase over the 15-25°C temperature range (Bemis *et al.*, 2000). This pattern likely results from the incorporation of more isotopically light, respired CO_2 into the shell at higher metabolic rates. The temperature dependence of foraminiferal $\delta^{13}\text{C}$ has been observed in other planktic species, like *N. pachyderma*, but has not been quantified (King and Howard, 2004). For benthic species, the published studies are in disagreement as to whether temperature has an effect on foraminiferal $\delta^{13}\text{C}$. A modelling study of *C. wuellerstorfi* found an opposite effect to planktonic foraminifera, such that the $\delta^{13}\text{C}$ increased by 0.05‰ per °C increase (Hesse *et al.*, 2014). The mechanisms included in this model were the temperature dependent shifts in chemical speciation between the different carbonate species and temperature related calcite formation fractionation factors. This model did not include the impact of higher respiration rates at higher temperatures, which may completely offset this modelled temperature relationship. A global compilation of core top $\delta^{13}\text{C}_{\text{foram}}$ of epibenthic Cibicides species and preindustrial $\delta^{13}\text{C}_{\text{DIC}}$ of bottom water found no temperature effect (Schmittner *et al.*, 2017).

Temperature changes in the Northwest Atlantic have been observed over the time period of our foraminiferal $\delta^{13}\text{C}$ records. Instrumental measurements and $\delta^{18}\text{O}$ proxy records show a 1.65-1.95°C increase in bottom waters of the Gulf of St. Lawrence (GoSL) since the 1930s (Gilbert *et al.*, 2005; Thibodeau *et al.*, 2010). Gilbert *et al.* (2005) hypothesize that this warming was caused by changing proportions of the major water masses entering the GoSL through the Cabot Strait, which include North Atlantic Central Water (NACW) and Labrador Current Water (LCW). The NACW is a warm, salty, nutrient-rich, oxygen-depleted water mass that is transported Northeast through the Gulf Stream (Townsend *et al.*, 2015). The LCW is a cold, fresh, nutrient-replete, oxygen-rich water mass that moves southwards around the slope of the Grand Banks in the off-shore branch of the Labrador Current. These two water masses mix just south of the "Tail of the Banks" (Figure 2.5) before entering the GoSL through the Cabot Strait.

Using temperature and salinity as tracers, (Gilbert *et al.*, 2005) estimated that the proportion of NACW to LCW entering the Lower St. Lawrence Estuary (LSLE) and GoSL increased from 28:72% to 48:52% between 1930 and 2003. Thibodeau *et al.* (2010)

present supporting evidence of the changed water mass proportions in the $\delta^{18}\text{O}$ records of benthic foraminifera, *Globobulimina auriculata*, from three cores in the LSLE and GoSL (Figure 6.2). They assumed that the $\delta^{18}\text{O}$ values of -0.5‰ (LCW) and $+0.5\text{‰}$ (NACW) remained constant over time for both water masses, and hence the changing proportions of water masses reaching St. Lawrence Bottom Water would have increased the $\delta^{18}\text{O}$ by approximately 0.2‰ . Using this increase, they calculated the $\delta^{18}\text{O}$ -derived temperature anomaly record from LSLE core MD99-2220. The *Thibodeau et al.* (2010) results support the $\sim 1.65^\circ\text{C}$ bottom water increase recorded by *Gilbert et al.* (2005). A study in the Emerald Basin reported a larger warming in the bottom waters of up to 6°C over the last century, recorded by $\delta^{18}\text{O}$ and Mg/Ca in benthic foraminifera (*Keigwin et al.*, 2003). A more recent study compiled a collection of foraminiferal based temperature proxies that record subsurface temperatures on the Northwest Atlantic slope (*Thornalley et al.*, 2018). These reconstructions, displayed in Figure 6.3, show a warming of approximately $1.5\text{-}2^\circ\text{C}$ after 1830, which is unprecedented over the 1600-year record. They attribute this warming to an anomalously weak Atlantic Meridional Overturning Circulation (AMOC) over the past 150 years. This weakened AMOC may be responsible for the reduced portion of LCW entering the GoSL.

Since previous studies are in disagreement regarding the influence of temperature on epibenthic foraminiferal $\delta^{13}\text{C}$, no correction was applied to the CIE for the benthic species that experienced a 1.65 to potentially 6°C warming over the 20th century. The $1.5\text{-}2^\circ\text{C}$ warming in the subsurface may have an influence on planktic foraminifera that spend part of their life cycle in the thermocline. If they experienced the full warming, the maximum effect on $\delta^{13}\text{C}$ would be $-0.165\text{-}0.22\text{‰}$, which does not account for the full observed CIE. We assume the species in this study spend the majority of their lives in the surface layer, and therefore no corrections were applied to account for the subsurface warming. However, I acknowledge that this assumption may account for some uncertainty in the planktic Suess effects.

If we assume that changing mixing proportions of water masses are influencing the $\delta^{18}\text{O}$ of waters in the GoSL, we must also consider how these mixing ratios would affect the $\delta^{13}\text{C}$ of DIC. The $\delta^{13}\text{C}$ of these water masses differ by approximately 0.5‰ (*Wanying Ji 2018*, personal communication; *Lin Cheng 2018*, personal communication) with NACW at 0‰ and LCW at 0.5‰ . Using the previously discussed increased mixing

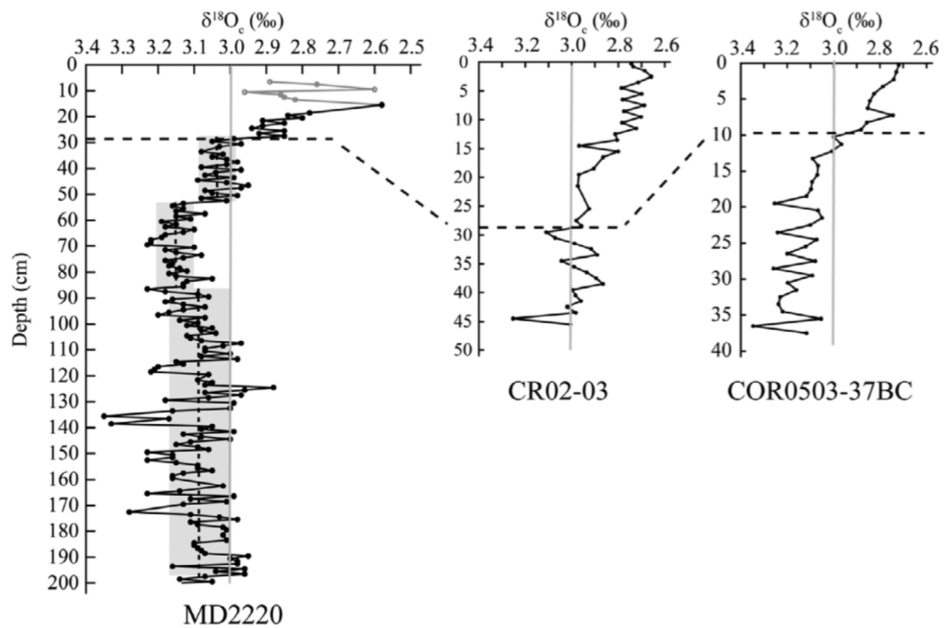


Figure 6.2: $\delta^{18}\text{O}$ *G. auriculata* downcore records from cores MD99-2220, CR02-23, and COR0503-37BC (Retrieved from *Thibodeau et al.* (2010) with permission by John Wiley and Sons).

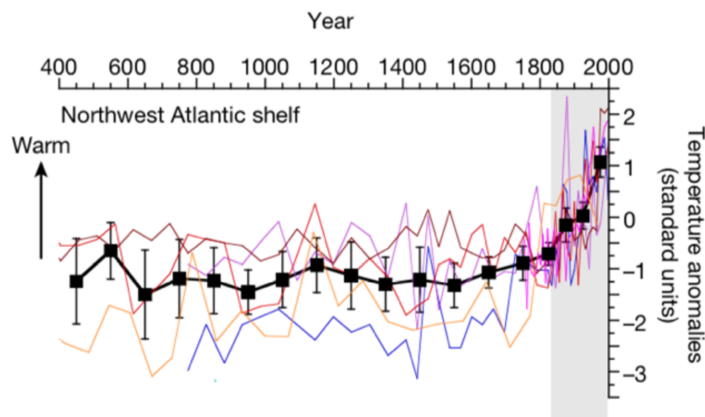


Figure 6.3: A compilation of foraminiferal based temperature proxies from three cores on the Northwest Atlantic Slope (Emerald Basin, Gulf of St. Lawrence, and Laurentian Fan). The composite stack is in black, while individual records are coloured. The grey bar denotes the industrial era, beginning in 1830 AD. Reprinted from *Thornalley et al.* (2018) by permission of Springer Nature.

ratios of NACW:LCW from 28:72% to 48:52%, the $\delta^{13}\text{C}_{DIC}$ would have undergone a small decrease of 0.15‰ since 1930. Therefore a correction of +0.15 was applied to the

negative *C. lobatulus* CIE at site MSM46 MC4 to account for water mass mixing.

6.2.2 Carbonate Ion Effect

The carbonate ion concentration [CO_3^{2-}] of seawater and pH were found to have a negative correlation with foraminiferal calcite $\delta^{13}\text{C}$ (*Spero et al.*, 1997; *Hesse et al.*, 2014). *Spero et al.* (1997) conducted a culturing study of *G. bulloides* and revealed an enrichment in $\delta^{13}\text{C}$ by 1.3‰ per 100 mol/kg decrease in [CO_3^{2-}]. A modelling study found the effect of pH on $\delta^{13}\text{C}$ of epibenthic *Cibicides wuellerstorfi* to be +0.1‰ per 0.1 unit decrease (*Hesse et al.*, 2014). It is still unknown whether pH or [CO_3^{2-}] change is driving the $\delta^{13}\text{C}$ change, but this detail is inconsequential because in the real ocean, pH and [CO_3^{2-}] covary linearly over the relevant pH range (*Bijma et al.*, 1999). A time series in the LSLE suggests that pH has decreased over the last 75 years by up to 0.2 units in waters deeper than 170 m (*Mucci et al.*, 2011). If we assume the modelled pH- $\delta^{13}\text{C}$ relationship for *C. wuellerstorfi* to hold true for *C. lobatulus*, a 0.2 decrease in pH would cause an increase in $\delta^{13}\text{C}$ of 0.2‰. Since MSM46 MC4 is located in the region of observed pH change, a correction of -0.2‰ was applied to the CIE of the *C. lobatulus* record.

No pH changes have been observed in the surface ocean of the study region over the time spanned by the $\delta^{13}\text{C}$ records, however the observations are too limited to rule out the possibility of this vital effect. As a precaution, I estimated the potential decrease in [CO_3^{2-}] since pre-industrial times by assuming the global average for change in pCO₂ and pH of +100pm and -0.1, respectively (*Doney et al.*, 2009). Inputting these values along with local annual averages for SST (10°) and SSS (32 psu) to CO2SYS (*Pierrot and Wallace*, 2006), I determined a 35 $\mu\text{mol/kg}$ decrease in [CO_3^{2-}]. If the *Spero et al.* (1997) relationship holds true for both *N. incompta* and *N. pachyderma*, then the full Suess effect may be masked by up to 0.45‰ for the planktic $\delta^{13}\text{C}$ records. This could potentially explain the discrepancy between planktic and benthic records. However, this carbonate ion effect should be interpreted as a maximum scenario only, as the global averages used for pCO₂ and pH may not apply to this region. This effect should be noted as a possible mechanism for the lower observed Suess effect from this study relative to direct measurements of $\delta^{13}\text{C}$ on DIC and atmospheric CO₂, which are discussed in Section 6.3.

The data from $\delta^{13}\text{C}$ of organic matter suggest the carbonate ion effect may not be

significantly impacting the planktonic records in this region. The organic matter CIE of MSM46 MC2 has practically the same magnitude as the corresponding *N. pachyderma* record ($-0.43 \pm 0.19\text{‰}$ vs. $0.486 \pm 0.10\text{‰}$). If the carbonate ion effect was significantly impacting the observed Suess effect in the *N. pachyderma* record, then we should see a larger Suess effect in the $\delta^{13}\text{C}$ of organic carbon. Changes in primary productivity or proportions of terrestrial and marine sourced organic matter may also impact the $\delta^{13}\text{C}$ of organic carbon, but there is no evidence for changes in these parameters. Therefore, I refrain from applying a correction for the carbonate ion effect to the planktonic $\delta^{13}\text{C}_{\text{foram}}$ records, but still consider it as a potential source of error.

6.2.3 Foraminiferal Diet

Since some of the carbon used by foraminifera during calcification is from their internal respired carbon pool, a change in the $\delta^{13}\text{C}$ of the food source has the potential to affect the shell $\delta^{13}\text{C}$. However, even with large food change, the $\delta^{13}\text{C}$ change is quite small (*Spero and Lea, 1996*). Figure 6.4 shows the results of a *G. bulloides* culture experiment where foraminifera were fed different food sources with $\delta^{13}\text{C}$ of -15.1 and -21.9‰ . Even though the food $\delta^{13}\text{C}$ varied by 4.7‰ , the maximum chamber $\delta^{13}\text{C}$ difference was only 0.6‰ . A study modelling effects of different environmental parameters on benthic foraminifera found $\delta^{13}\text{C}_{\text{foram}}$ changed by 3.5% of a given food source $\delta^{13}\text{C}$ change (*Hesse et al., 2014*). Assuming that this relationship would not be drastically different for other foraminifera species, these results indicate that changing food sources could not significantly impact $\delta^{13}\text{C}$ nor account for the observed negative CIE. Since the impact is small and there is no evidence for diet change, no correction is applied to the CIEs.

In summary, none of the environmental controls on $\delta^{13}\text{C}$ could account for the observed negative CIEs at all of the core sites, confirming that anthropogenic CO_2 penetration is likely the predominant cause. A net correction of -0.05 was applied to the MSM46 MC4 *C. lobatulus* CIE to account for observed changes in pH (-0.2) and water mass mixing ($+0.15$) over the study period in the bottom waters of the Gulf of St. Lawrence. Effects of increased biological production since the 1960s likely had a significant impact on both the *N. pachyderma* and *C. lobatulus* records of MSM46 MC4, but it is not possible to quantify this impact with the available data. I attribute increased biological production to be the key controlling factor for larger benthic CIEs compared to planktic's at sites where both are present. The carbonate ion effect in the surface

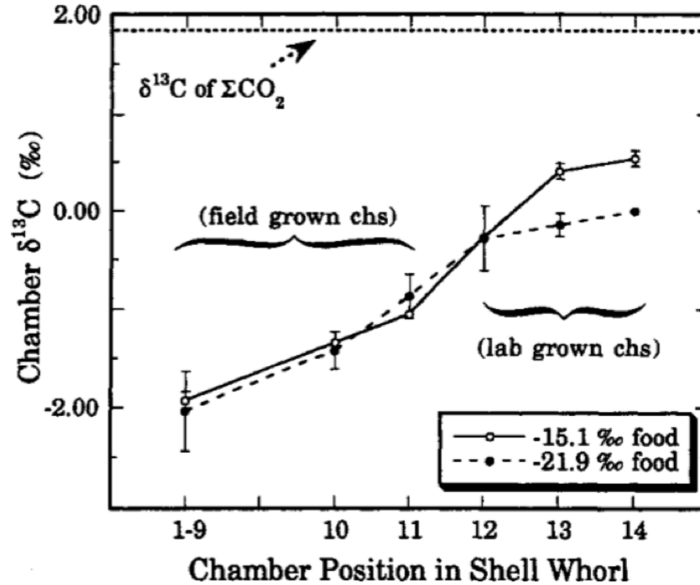


Figure 6.4: Effect of different $\delta^{13}\text{C}$ food sources on chamber $\delta^{13}\text{C}$ of *G. bulloides*. The dotted horizontal line denotes the $\delta^{13}\text{C}$ of ΣCO_2 (Retrieved from *Spero and Lea* (1996)).

ocean may also play a role in CIE differences between depths, but the $\delta^{13}\text{C}$ of organic matter do not support this hypothesis.

6.3 The northwestern North Atlantic Suess effect

The CIEs corrected for the other controlling factors on $\delta^{13}\text{C}_{\text{DIC}}$ and the disequilibrium of $\delta^{13}\text{C}_{\text{foram}}$ are presented in Figure 6.5. I postulate the remaining CIEs are attributable to anthropogenic CO_2 penetration into the surface ocean, and will refer to the CIEs as the surface ocean Suess effect, henceforth. The observed Suess effect for the northwestern North Atlantic shelf ranged from $-0.17 \pm 0.13\text{‰}$ to $-0.78 \pm 0.29 \text{‰}$, with a mean of $0.49 \pm 0.22\text{‰}$. The 2013-adjusted values ranged from $-0.18 \pm 0.14\text{‰}$ to $-1.14 \pm 0.50 \text{‰}$, with a mean of $0.64 \pm 0.32\text{‰}$. Independent of large uncertainties in some of the age-depth models, I can conclude that the ToE of this climate signal occurred in the mid-twentieth century, as the weighted mean of the change points was $1959 \text{ AD} \pm 10$ years.

The atmospheric $\delta^{13}\text{C}_{\text{CO}_2}$ Suess effect is the main controlling factor on the $\delta^{13}\text{C}_{\text{DIC}}$ Suess effect (*Quay et al.*, 1992; *Körtzinger et al.*, 2003). To make the comparison between the two reservoirs, an equivalent analysis using a three-piece linear regression was applied to a historical $\delta^{13}\text{C}_{\text{CO}_2}$ record of *Graven et al.* (2017). This analysis results

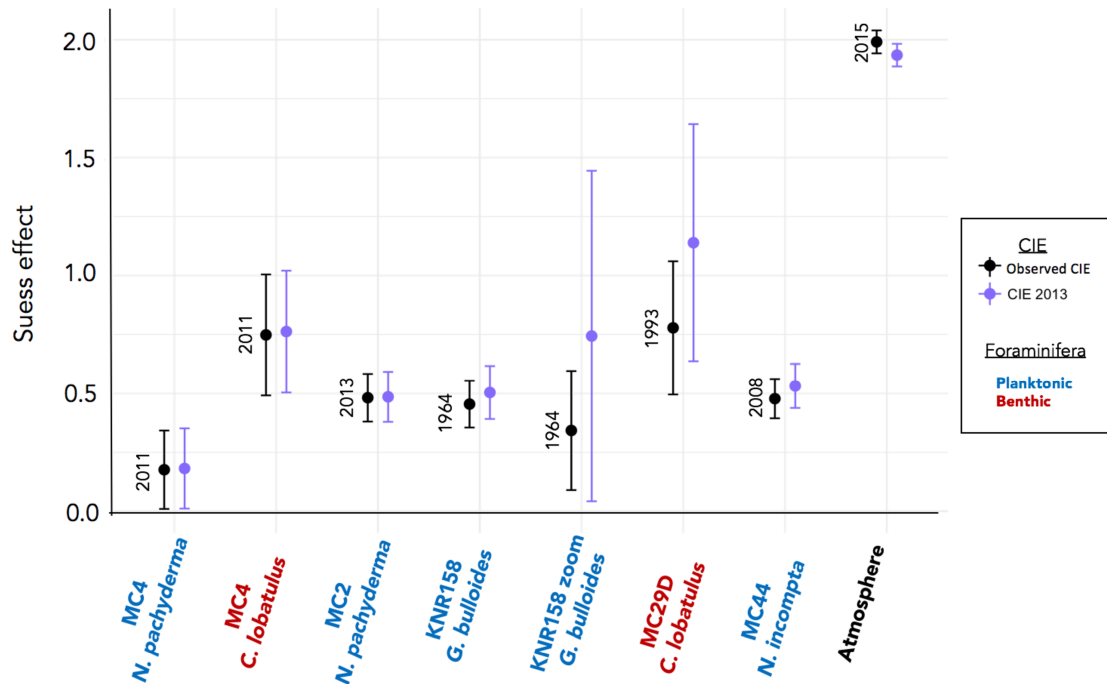


Figure 6.5: Observed (black) and 2013-adjusted (purple) Suess effect magnitudes for the atmosphere and all foraminiferal records. Error bars denote the uncertainty to 1σ .

in a $1.93 \pm 0.05\text{‰}$ atmospheric Suess effect for 2013 (Figure 6.6), which implies that the northwestern North Atlantic Suess effect accounts for between $9 \pm 7\%$ to $59 \pm 26\%$, averaging $33 \pm 16\%$, of the full atmospheric Suess effect (Figure 6.5).

After the onset of the industrial revolution in the early 1800s, the $\delta^{13}\text{C}$ of the atmosphere decreased at a rate of $-0.0037 \pm 0.0001\text{‰ yr}^{-1}$ and steepened to $-0.0246 \pm 0.0002\text{‰ yr}^{-1}$ in 1958. The timing of the steepening is indistinguishable from the ToE of the Suess effect in the foraminifera records ($1959 \text{ AD} \pm 10 \text{ years}$). Yet, the average of the two best dated $\delta^{13}\text{C}_{\text{foram}}$ records (MC29 and MC44) reveals a slower $\delta^{13}\text{C}$ decrease rate of $-0.014 \pm 0.005\text{‰ yr}^{-1}$, compared to the atmosphere. This lower rate and overall Suess effect may be due to the isotopic disequilibrium between the surface ocean and atmosphere. It takes approximately 10 years for $\delta^{13}\text{C}$ to equilibrate between atmospheric CO_2 and surface ocean DIC, hence the full atmospheric Suess effect is not expected to be reflected instantaneously in the surface ocean (Broecker and Peng, 1974). However, this may not be the full story.

Compared to estimates of open ocean $\delta^{13}\text{C}$ decrease rates for the North Atlantic, our foraminiferal $\delta^{13}\text{C}$ decrease rates are consistently lower. Direct $\delta^{13}\text{C}_{\text{DIC}}$ measurements

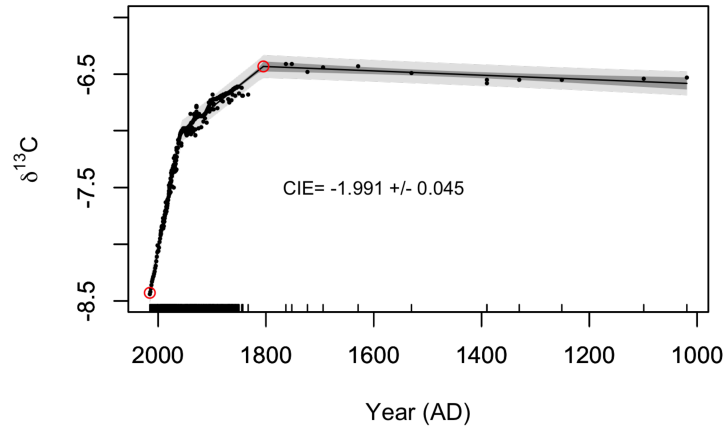


Figure 6.6: A high resolution $\delta^{13}\text{C}_{\text{CO}_2}$ record compiled from ice core, firn, and direct atmospheric CO_2 samples that cover 1000 to 2015 AD (Graven *et al.*, 2017). The average model output from the piecewise regression is represented by the black line, with confidence and prediction intervals denoted by the dark grey and light grey shading, respectively.

from transects taken in 1981 and 2003 in the subtropical northwest (20-40°N) show a $\delta^{13}\text{C}$ decrease rate of $-0.025 \pm 0.002\text{‰ yr}^{-1}$ (Quay *et al.*, 2007), with lower rates in the tropics ($-0.011 \pm 0.003\text{‰ yr}^{-1}$) and subpolar region ($-0.017 \pm 0.005\text{‰ yr}^{-1}$). The $\delta^{13}\text{C}$ decrease rate for northwestern shelf of the North Atlantic is more comparable to the reported global (-0.015 to -0.018‰ yr^{-1}) (Sonnerup *et al.*, 1999; Gruber *et al.*, 1999) and tropical mean (-0.01‰ yr^{-1}) (Swart *et al.*, 2010). The likely mechanism for these lower $\delta^{13}\text{C}$ decrease rates recorded in foraminifera compared to other North Atlantic estimates is the post-depositional process of bioturbation.

6.4 Impact of Bioturbation

A planktonic foraminifera (*G. ruber*) record from a high-resolution, laminated sediment core in the Cariaco Basin exhibited a similar $\delta^{13}\text{C}$ rate of change to the atmosphere (Black *et al.*, 2011). The study reports a near tripling of the $\delta^{13}\text{C}$ decrease rate from -0.01‰ yr^{-1} before 1950 to -0.025‰ yr^{-1} at 2008. The magnitude of the Suess effect from this foraminifera record was -0.75‰ , which is similar to, but potentially slightly higher than the mean value reported in our study of $-0.64 \pm 0.32\text{‰}$. The laminated

sediments of the Cariaco Basin may explain why the $\delta^{13}\text{C}_{\text{foram}}$ record in *Black et al.* (2011) exhibits a higher Suess effect magnitude and rate of change compared to the $\delta^{13}\text{C}_{\text{foram}}$ record from this study. Laminated sediments are more easily dated and are not subject to bioturbation.

In theory, high bioturbation could mix forams with light $\delta^{13}\text{C}$ deeper into the core, hence elongating the signal, slowing the apparent $\delta^{13}\text{C}$ decrease rate, and decreasing the observed CIE magnitude. The degree of signal attenuation depends on the mixing rate, mixing depth, sedimentation rate, and duration of event (*Anderson, 2001; Charbit et al., 2002*). Higher mixing rates, deeper mixing depths, lower sedimentation rates and shorter event durations all increase the degree of signal attenuation. The short event duration of the Suess effect (50-100 years) has a high susceptibility to bioturbation, but the high sedimentation rates at our core sites (20-60 cm/kyr) should limit this impact (*Charbit et al., 2002*). Knowledge of mixing rates and mixing depths would be necessary to more accurately quantify the impact of bioturbation on the $\delta^{13}\text{C}$ rates of change for each foraminifera record.

Signal attenuation may also be impacted by changing foraminifera abundance throughout the record (*Löwemark et al., 2008*), which has been observed as a decrease in % *N. pachyderma* in OCE326 MC29 (*Keigwin et al., 2003*). If abundance decreased towards the top of the core, then the signal may be elongated or dampened from bioturbation, perhaps accounting for the lack of observed Suess effect in this $\delta^{13}\text{C}$ record. Researchers counting foraminifera in the Lower St. Lawrence Estuary and Gulf of St. Lawrence observed decreased foraminiferal abundance due to modern day carbonate dissolution (*Al Mucci, personal communication, 2018*). This may be another potential mechanism to explain the small $\delta^{13}\text{C}$ decrease rate of *N. pachyderma* at site MSM46 MC4.

6.5 Estimates of Anthropogenic CO₂ Uptake

An approximate estimate of the anthropogenic CO₂ uptake rate (ΔC_t) can be made using the theoretical relationship between $\delta^{13}\text{C}$ and CO₂ uptake ($\Delta\delta^{13}\text{C}/\Delta C_t = \Delta\text{RC}$). Since the air-sea equilibration time of $\delta^{13}\text{C}$ is 10 years longer than DIC, the regional degree of air-sea $\delta^{13}\text{C}$ equilibration has an impact on ΔRC . For the North Atlantic, *Eide et al.* (2017) used gridded data to determine a mean ΔRC of $-0.015 \pm 0.006\text{‰} (\mu\text{mol/kg})^{-1}$.

They note that this relationship is subject to large uncertainty due to uncertainties in DIC trends. For other regions of the ocean, studies have reported a range of values from $-0.007 \text{ ‰} (\mu\text{mol/kg})^{-1}$ in the South Atlantic to $-0.021 \text{ ‰} (\mu\text{mol/kg})^{-1}$ in the North Pacific (Heimann and Maier-Reimer, 1996; Keir *et al.*, 1998; McNeil *et al.*, 2001; Körtzinger *et al.*, 1998), highlighting the regional dependence of this relationship.

Using the North Atlantic ΔRC from Eide *et al.* (2017a) and a $\delta^{13}\text{C}$ decrease rate of -0.014 ‰ yr^{-1} , I determined an anthropogenic CO_2 uptake rate of $1.07 \mu\text{mol/kg yr}^{-1}$. This is slightly smaller than the previously observed ΔC_t in the North Atlantic of $1.21 \pm 0.07 \mu\text{mol/kg yr}^{-1}$ by Körtzinger *et al.* (2003). However, given the highly regional dependence of ΔRC , my calculation of anthropogenic CO_2 uptake rate should be interpreted with caution. Further research exploring the relationship between $\delta^{13}\text{C}$ and CO_2 uptake rates at higher spatial and temporal resolution in the study area is necessary to get a better estimate of ΔC_t from our $\delta^{13}\text{C}_{\text{foram}}$ records.

CHAPTER 7

CONCLUSION

The role of coastal oceans in fossil fuel derived CO₂ uptake from the atmosphere is still a point of contention in the oceanographic and climate change community. Resolving whether these regions act as net CO₂ sinks or sources is mainly limited by the lack of time series measurements on parameters of the carbonate system and their limited spatial representation. My thesis presented the first long-term time series of $\delta^{13}\text{C}$, a proxy measure of anthropogenic CO₂ invasion into the ocean, for the northwestern shelf region of the North Atlantic. I analyzed $\delta^{13}\text{C}$ on both planktic and benthic foraminifera from five core sites spanning the Gulf of St. Lawrence, Scotian Shelf, and Gulf of Maine. Over the entire 150-4000 years sampled by these cores, the carbon isotope excursion observed in the top of the cores is unprecedented. I conclude that isotopically light anthropogenic CO₂ penetration (namely the Suess effect) must be responsible for such strikingly similar CIEs in each core, despite them having such different oceanographic settings.

In summary, I was able to detect and unambiguously identify the Suess effect in the $\delta^{13}\text{C}_{\text{foram}}$ records. The CIEs were coherent and unprecedented throughout the time period sampled by the cores, therefore I posit such a signal could only be explained by anthropogenic CO₂ penetration into the surface ocean. The Suess effect became apparent in northwestern shelf waters of the North Atlantic in 1959 AD \pm 10 years with an average $\delta^{13}\text{C}$ decrease rate of $-0.014 \pm 0.005\text{‰ yr}^{-1}$ and magnitude of $-0.64 \pm 0.32\text{‰}$. I did not observe any distinct spatial variation throughout the study region, but I acknowledge that the uncertainties in the $\delta^{13}\text{C}_{\text{foram}}$ CIEs were large enough to limit identifying any spatial variation. Using the $\delta^{13}\text{C}$ decrease rate and the ΔRC from *Eide et al.* (2017a), I determined an approximate anthropogenic CO₂ uptake rate of $1\text{ }\mu\text{mol/kg}$

yr⁻¹ for the study region since 1959.

In comparison to the atmosphere, the magnitude was less than 40% of the atmospheric Suess effect (-1.9‰) over the same time period and the decrease rate was 58% slower. This difference is partly explained by the 10 year equilibration time for $\delta^{13}\text{C}$ between the atmosphere and ocean. If water masses did not fully equilibrate with the atmosphere before sinking, then the Suess effect of the ocean could lag by more than 10 years. The timing of the Suess effect detected in the $\delta^{13}\text{C}_{\text{foram}}$ records was indistinguishable from the year in which the atmospheric $\delta^{13}\text{C}$ decrease rate steepened from $-0.0037 \pm 0.0001\text{‰ yr}^{-1}$ to $-0.0246 \pm 0.0002\text{‰ yr}^{-1}$ (Graven *et al.*, 2017). Given that foraminifera are sensitive to some signal dampening by bioturbation, it is not surprising that the $\delta^{13}\text{C}_{\text{foram}}$ displays more clear evidence of the Suess effect since the steepening of the $\delta^{13}\text{C}$ rate of change.

Bioturbation is the other important process that may contribute to discrepancies between the Suess effect recorded in fossil foraminifera and other archives like the atmosphere, ice cores, or dissolved inorganic carbon pool. Future work to determine the relationship between bioturbation, vis-à-vis mixing rates and mixing depths, and the Suess effect would be valuable for two reasons – first, we could account for the impact of bioturbation on the foraminiferal $\delta^{13}\text{C}$ records to improve the estimate of the surface water Suess effect in the study region, and second, we could explore the potential of using the Suess effect as a proxy for bioturbation in marine sedimentary sequences. The latter has implications for paleoclimate reconstructions, as measuring the foraminiferal Suess effect could provide a fairly simple correction for signal attenuation or distortion of other climate proxies.

The outcome of this study adds to the growing collection of evidence that human activity is perturbing the Earth's natural climate cycles. Without mitigation, the threat of ocean acidification will continue to increase, and with it will come impacts on marine ecosystems and global economies.

BIBLIOGRAPHY

- Al-Rousan, S., J. Patzold, S. Al-Moghrabi, and G. Wefer, Invasion of anthropogenic CO₂ recorded in planktonic foraminifera from the northern Gulf of Aqaba, *Int J Earth Sci*, 93, 1066–1076, 2004.
- Anderson, D. M., Attenuation of millennial-scale events by bioturbation in marine sediments, *Paleoceanography and Paleoclimatology*, 16, 352–357, 2001.
- Appleby, P., Chronostratigraphic techniques in recent sediments, in *Tracking environmental change using lake sediments*, pp. 171–203, Springer, 2002.
- Appleby, P., and F. Oldfield, The calculation of lead-210 dates assuming a constant rate of supply of unsupported 210pb to the sediment, *Catena*, 5, 1–8, 1978.
- Bauch, D., J. Carstens, G. Wefer, and J. Thiede, The imprint of anthropogenic CO₂ in the Arctic Ocean: Evidence from planktic delta13C data from watercolumn and sediment surfaces, *Deep-Sea Research Part II: Topical Studies in Oceanography*, 47, 1791–1808, 2000.
- Bauch, D., H. Erlenkeuser, G. Winckler, G. Pavlova, and J. Thiede, Carbon isotopes and habitat of polar planktic foraminifera in the Okhotsk Sea: the ‘carbonate ion effect’ under natural conditions, 45, 83–99, 2002.
- Bauch, D., K. Darling, J. Simstich, H. A. Bauch, and H. Erlenkeuser, Palaeoceanographic implications of genetic variation in living North Atlantic *Neogloboquadrina pachyderma*, *Nature*, 424, 11–14, 2003.
- Bemis, B. E., H. J. Spero, D. W. Lea, and J. Bijma, Temperature influence on the carbon isotopic composition of *Globigerina bulloides* and *Orbulina universa* (planktonic foraminifera), *Marine Micropaleontology*, 38, 213–228, 2000.
- Bennett, K., Confidence intervals for age estimates and deposition times in late-quaternary sediment sequences, *The Holocene*, 4, 337–348, 1994.
- Beveridge, N. A. S., and N. J. Shackleton, Carbon isotopes in recent planktonic foraminifera: A record of anthropogenic CO₂ invasion of the surface ocean, *Earth and Planetary Science Letters*, 126, 259–273, 1994.
- Bijma, J., H. Spero, and D. Lea, Reassessing foraminiferal stable isotope geochemistry: Impact of the oceanic carbonate system (experimental results), in *Use of proxies in paleoceanography*, pp. 489–512, Springer, 1999.
- Blaauw, M., and J. A. Christen, Flexible paleoclimate age-depth models using an autoregressive gamma process, *Bayesian Analysis*, 6, 457–474, 2011.

- Black, D., R. Thunell, K. Wejnert, and Y. Astor, Carbon isotope composition of Caribbean Sea surface waters: Response to the uptake of anthropogenic CO₂, *Geophysical Research Letters*, 38, 1–5, 2011.
- Böhm, F., E. L. Sevier, M. M. Joachimski, H. Lehnert, G. Morgenroth, W. Kretschmer, J. Vacelet, and W. Dullo, Carbon isotope records from extant Caribbean and South Pacific sponges: Evolution of delta¹³C in surface water DIC, *Earth and Planetary Science Letters*, 139, 291–303, 1996.
- Böhm, F., M. I. M. J. Joachimski, W. O. L. F. H. D. Ullo, A. N. E. Isenhauer, and H. E. L. Ehnert, Oxygen isotope fractionation in marine aragonite of coralline sponges, *Geochimica et Cosmochimica Acta*, 64, 1695–1703, 2000.
- Broecker, W. S., and E. Maier-Reimer, The influence of air and sea exchange on the carbon isotope distribution in the sea, *Global Biogeochemical Cycles*, 6, 315–320, 1992.
- Broecker, W. S., and T.-H. Peng, Gas exchange rates between air and sea, *Tellus*, 26, 21–35, 1974.
- Caldeira, K., and M. E. Wickett, Oceanography: Anthropogenic carbon and ocean pH, *Nature*, 425, 365, 2003.
- Charbit, S., C. Rabouille, and G. Siani, Effects of benthic transport processes on abrupt climatic changes recorded in deep-sea sediments: A time-dependent modeling approach, *Journal of Geophysical Research: Oceans*, 107, 2002.
- Colbourne, E., S. Narayanan, and J. Helbig, Comparison of hydrography and circulation on the Newfoundland Shelf during 1990-1993 with the long-term mean, *Canadian Journal of Fisheries and Aquatic Sciences*, 54, 68–80, 1997.
- Craig, H., Isotopic standards for carbon and oxygen and correction factors for mass-spectrometric analysis of carbon dioxide, *Geochimica et Cosmochimica Acta*, 12, 133–149, 1957.
- Curry, W. B., and R. Matthews, Equilibrium ¹⁸O Fractionation in small size fraction planktic foraminifera: Evidence from recent indian ocean sediments, *Marine Micropaleontology*, 6, 327–337, 1981.
- Dever, M., D. Hebert, B. J. W. Greenan, J. Sheng, and P. C. Smith, Hydrography and Coastal Circulation along the Halifax Line and the Connections with the Gulf of St. Lawrence, *Atmosphere-Ocean*, 54, 199–217, 2016.
- Dlugokencky, E., and P. Tans, Trends in Atmospheric Carbon Dioxide, 2017.
- Doney, S. C., V. J. Fabry, R. A. Feely, and J. A. Kleypas, Ocean acidification: The other CO₂ problem, 2009.

- Drinkwater, K. F., B. Petrie, and P. C. Smith, Climate variability on the Scotian Shelf during the 1990s, *ICES Marine Science Symposia*, 219, 40–49, 2003.
- Druffel, E. R. M., and L. M. Benavides, Input of excess CO₂ to the surface ocean based on ¹³C/¹²C ratios in a banded Jamaican sclerosponge, *Nature*, 321, 58–61, 1986.
- Eide, M., A. Olsen, U. Ninnemann, and T. Eldevik, A global estimate of the full oceanic ¹³C Suess effect since the preindustrial, *Global Biogeochemical Cycles*, 31, 1–23, 2017a.
- Eide, M., A. Olsen, U. S. Ninnemann, and T. Johannessen, A global ocean climatology of preindustrial and modern ocean $\delta^{13}\text{C}$, *Global Biogeochemical Cycles*, 31, 515–534, 2017b.
- Engstrom, D. R., and E. B. Swain, Recent declines in atmospheric mercury deposition in the upper Midwest, *Environmental Science & Technology*, 31, 960–967, 1997.
- Farquhar, G. D., J. R. Ehleringer, and K. T. Hubick, Carbon isotope discrimination and photosynthesis, *Annual review of plant biology*, 40, 503–537, 1989.
- Francey, R. J., I. G. Enting, M. Leuenberger, R. L. Langenfelds, E. Michel, and L. P. Steele, A 1000-year high precision record of $\delta^{13}\text{C}$ in atmospheric CO₂, *Tellus*, 51B, 170–193, 1999.
- Friedli, H., H. Lotscher, H. Oeschger, U. Siegenthaler, and B. Stauffer, Ice core record of the ¹³C/¹²C ratio of atmospheric CO₂ in the past two centuries, *Nature*, 324, 1986.
- Galbraith, P. S., J. Chasse, P. Larouche, D. Gilbert, D. Brickman, L. Devine, and C. Lafleur, Physical Oceanographic Conditions in the Gulf of St. Lawrence in 2012, *Tech. rep.*, DFO Can. Sci. Advis. Sec. Res., Moncton, 2013.
- Ghaleb, B., Overview of the methods for the measurement and interpretation of short-lived radioisotopes and their limits, in *IOP conference series: Earth and environmental science*, vol. 5, p. 012007, IOP Publishing, 2009.
- Gilbert, D., B. Sundby, C. Gobeil, A. Mucci, and G.-H. Tremblay, A seventy-two-year record of diminishing deep-water oxygen in the St. Lawrence estuary: The northwest Atlantic connection, *Limnology and Oceanography*, 50, 1654–1666, 2005.
- Goring, S., J. Williams, J. Blois, S. Jackson, C. Paciorek, R. Booth, J. Marlon, M. Blaauw, and J. Christen, Deposition times in the northeastern United States during the Holocene: establishing valid priors for Bayesian age models, *Quaternary Science Reviews*, 48, 54–60, 2012.
- Graven, H., C. E. Allison, D. M. Etheridge, S. Hammer, R. F. Keeling, I. Levin, H. A. Meijer, M. Rubino, P. P. Tans, C. M. Trudinger, et al., Compiled records of carbon isotopes in atmospheric CO₂ for historical simulations in CMIP6, *Geoscientific Model Development*, 10, 4405–4417, 2017.

- Gruber, N., D. Keeling, R. B. Bacastow, P. R. Guenther, T. J. Lueker, M. Wahlen, H. a. J. Meijer, W. G. Mook, and T. F. Stocker, Spatiotemporal patterns of carbon-13 in the global surface oceans and the oceanic Suess effect, *Global Biogeochemical Cycles*, 13, 307–335, 1999.
- Han, G., and J. W. Loder, Three-dimensional seasonal-mean circulation and hydrography on the eastern Scotian Shelf, *Journal of Geophysical Research*, 108, 3136, 2003.
- Han, G., C. G. Hannah, J. W. Loder, and P. C. Smith, Seasonal variation of the three-dimensional mean circulation over the Scotian Shelf, *Journal of Geophysical Research*, 102, 1011–1025, 1997.
- Hebert, D., R. Pettipas, D. Brickman, and M. Dever, Meteorological , Sea Ice and Physical Oceanographic Conditions on the Scotian Shelf and in the Gulf of Maine during 2013, *Tech. Rep. November*, Bedford Institute of Oceanography, Dartmouth, 2014.
- Heimann, M., and E. Maier-Reimer, On the relations between the oceanic uptake of CO₂ and its carbon isotopes, *Global Biogeochemical Cycles*, 10, 89–110, 1996.
- Hemleben, C., and J. Bijma, Foraminiferal population dynamics and stable carbon isotopes, in *Carbon Cycling in the Glacial Ocean: Constraints on the Ocean's Role in Global Change*, edited by R. Zahn, pp. 145–166, Springer-Verlag, Berlin, Heidelberg, 1994.
- Hendriks, I. E., C. M. Duarte, and M. Álvarez, Vulnerability of marine biodiversity to ocean acidification: A meta-analysis, *Estuarine, Coastal and Shelf Science*, 86, 157–164, 2010.
- Hesse, T., D. Wolf-Gladrow, G. Lohmann, J. Bijma, A. Mackensen, and R. E. Zeebe, Modelling $\delta^{13}\text{C}$ in benthic foraminifera: Insights from model sensitivity experiments, *Marine Micropaleontology*, 112, 50–61, 2014.
- IPCC, Climate Change 2014 Synthesis Report Summary Chapter for Policymakers, *Ippc*, p. 31, 2014.
- Jennane, A., Application de la méthode du Plomb-210 dans l'Estuaire et le Golfe du St-Laurent. Taux de sédimentation, flux et modes d'ablation, *MSc Thesis*, 1993.
- Keeling, C. D., The Suess effect: ¹³Carbon-¹⁴Carbon interrelations, *Environment International*, 2, 229–300, 1979.
- Keeling, C. D., S. C. Piper, M. Bacastow, M. Wahlen, T. P. Whorf, M. Heimann, and H. A. Meijer, *Exchanges of atmospheric CO₂ and ¹³CO₂ with the terrestrial biosphere and oceans from 1978 to 2000.*, vol. 01-06, Scripps Institute of Oceanography, San Diego, 2001.
- Keigwin, L. D., and C. H. Pilskalns, Sediment flux and recent paleoclimate in Jordan Basin, Gulf of Maine, *Continental Shelf Research*, 96, 45–55, 2015.

- Keigwin, L. D., J. P. Sachs, and Y. Rosenthal, A 1600-year history of the Labrador Current off Nova Scotia, *Climate Dynamics*, *21*, 53–62, 2003.
- Keir, R., G. Rehder, E. Suess, and H. Erlenkeuser, The $\delta^{13}\text{C}$ anomaly in the northeastern Atlantic, *Global Biogeochemical Cycles*, *12*, 467–477, 1998.
- King, A. L., and W. R. Howard, Planktonic foraminiferal $\delta^{13}\text{C}$ records from Southern Ocean sediment traps: New estimates of the oceanic Suess effect, *Global Biogeochemical Cycles*, *18*, 1–16, 2004.
- Kohfeld, K. E., R. G. Fairbanks, S. L. Smith, and I. D. Walsh, Neogloboquadrina pachyderma (sinistral coiling) as paleoceanographic tracers in polar oceans: Evidence from Northeast Water Polynya plankton tows, sediment traps, and surface sediments, *Paleoceanography*, *11*, 679–699, 1996.
- Körtzinger, A., L. Mintrop, and J. C. Duinker, On the penetration of anthropogenic CO_2 into the north atlantic ocean, *Journal of Geophysical Research: Oceans*, *103*, 18681–18689, 1998.
- Körtzinger, A., P. D. Quay, and R. E. Sonnerup, Relationship between anthropogenic CO_2 and the $\delta^{13}\text{C}$ suess effect in the north atlantic ocean, *Global Biogeochemical Cycles*, *17*, 2003.
- Le Quéré, C., R. M. Andrew, J. G. Canadell, S. Sitch, J. Ivar Korsbakken, G. P. Peters, A. C. Manning, T. A. Boden, P. P. Tans, R. A. Houghton, R. F. Keeling, S. Alin, O. D. Andrews, P. Anthoni, L. Barbero, L. Bopp, F. Chevallier, L. P. Chini, P. Ciais, K. Currie, C. Delire, S. C. Doney, P. Friedlingstein, T. Gkritzalis, I. Harris, J. Hauck, V. Haverd, M. Hoppema, K. Klein Goldewijk, A. K. Jain, E. Kato, A. Körtzinger, P. Landschützer, N. Lefèvre, A. Lenton, S. Lienert, D. Lombardozzi, J. R. Melton, N. Metzl, F. Millero, P. M. Monteiro, D. R. Munro, J. E. Nabel, S. I. Nakaoka, K. O'Brien, A. Olsen, A. M. Omar, T. Ono, D. Pierrot, B. Poulter, C. Rödenbeck, J. Salisbury, U. Schuster, J. Schwinger, R. Séférian, I. Skjelvan, B. D. Stocker, A. J. Sutton, T. Takahashi, H. Tian, B. Tilbrook, I. T. Van Der Laan-Luijkx, G. R. Van Der Werf, N. Viovy, A. P. Walker, A. J. Wiltshire, and S. Zaehle, Global Carbon Budget 2016, *Earth System Science Data*, *8*, 605–649, 2016.
- Liebtrau, V., *Geochronology*, pp. 413–416, Springer Netherlands, Dordrecht, 2011.
- Loder, J. W., B. Petrie, and G. Gawarkiewicz, The coastal ocean off northeastern north america: A large-scale view, in *The Sea*, edited by A. R. Robinson and K. H. Brink, pp. 105–133, John Wiley & Sons, Inc, 1998.
- Lohmann, G. P., A model for variation in the chemistry of planktonic foraminifera due to secondary calcification and selective dissolution, *Paleoceanography*, *10*, 445–457, 1995.
- Louchouart, P., M. Lucotte, E. Duchemin, and A. De Vernal, Early diagenetic processes in recent sediments of the Gulf of St-Lawrence: phosphorus, carbon and iron burial rates, *Marine Geology*, *139*, 181–200, 1997.

- Löwemark, L., K. Konstantinou, and S. Steinke, Bias in foraminiferal multispecies reconstructions of paleohydrographic conditions caused by foraminiferal abundance variations and bioturbational mixing: A model approach, *Marine Geology*, 256, 101–106, 2008.
- Marchitto, T. M., and P. DeMenocal, Late Holocene variability of upper North Atlantic Deep Water temperature and salinity, *Geochemistry, Geophysics, Geosystems*, 4, 1–12, 2003.
- McNeil, B., R. Matear, and B. Tilbrook, Does carbon-13 track anthropogenic CO₂ in the Southern Ocean?, *Global biogeochemical cycles*, 15, 597–613, 2001.
- Mook, W., J. Bommerson, and W. Staverman, Carbon isotope fractionation between dissolved bicarbonate and gaseous carbon dioxide, *Earth and Planetary Science Letters*, 22, 169–176, 1974.
- Mucci, A., M. Starr, D. Gilbert, and B. Sundby, Acidification of lower St. Lawrence Estuary bottom waters, *Atmosphere-Ocean*, 49, 206–218, 2011.
- Muggeo, V. M., Estimating regression models with unknown break-points, *Statistics in medicine*, 22, 3055–3071, 2003.
- O’Leary, M. H., Carbon isotope fractionation in plants, *Phytochemistry*, 20, 553–567, 1981.
- Olsen, A., and U. Ninnemann, Large 13C Gradients in the Preindustrial North Atlantic Revealed, *Science*, 330, 658–659, 2010.
- Olsen, A., A. M. Omar, R. G. J. Bellerby, T. Johannessen, U. Ninnemann, K. R. Brown, K. A. Olsson, J. Olafsson, G. Nondal, C. Kivima, S. Kringstad, and C. Neill, Magnitude and origin of the anthropogenic CO₂ increase and Suess effect in the Nordic seas since 1981, *Global Biogeochemical Cycles*, 20, 1–12, 2006.
- Oppo, D. W., and R. G. Fairbanks, Carbon Isotopes composition of tropical surface water during the past 22,000 years, *Paleoceanography*, 4, 333–351, 1989.
- Petrie, B., Does the north Atlantic oscillation affect hydrographic properties on the Canadian Atlantic continental shelf?, *Atmosphere-Ocean*, 45, 141–151, 2007.
- Pettigrew, N. R., J. H. Churchill, C. D. Janzen, L. J. Mangum, R. P. Signell, A. C. Thomas, D. W. Townsend, J. P. Wallinga, and H. Xue, The kinematic and hydrographic structure of the Gulf of Maine Coastal Current, *Deep-Sea Research II*, 52, 2369–2391, 2005.
- Pierrot, D. L., and D. W. Wallace, MS Excel Program Developed for CO₂ System Calculations, 2006.
- Quay, P., R. Sonnerup, J. Stutsman, J. Maurer, A. Ko, X. A. Padin, and C. Robinson, Anthropogenic CO₂ accumulation rates in the North Atlantic Ocean from changes in the 13C/12C of dissolved inorganic carbon, *Global Biogeochemical Cycles*, 21, 1–15, 2007.

- Quay, P. D., B. Tilbrook, and C. S. Wong, Oceanic Uptake of Fossil Fuel CO₂: Carbon-13 Evidence, *Science*, 256, 74–79, 1992.
- Ravelo, A. C., and R. G. Fairbanks, Carbon isotopic fractionation in multiple species of planktonic foraminifera from core-tops in the tropical Atlantic, *Journal of Foraminiferal Research*, 25, 1995.
- Ravelo, A. C., and C. Hillaire-Marcel, The Use of Oxygen and Carbon Isotopes of Foraminifera in Paleoceanography, in *Proxies in the Late Cenezoic Paleoceanography*, edited by C. Hillaire-Marcel and A. De Vernal, vol. 1, chap. 18, pp. 735–764, Elsevier, Amsterdam, Oxford, 2007.
- Reimer, P. J., E. Bard, A. Bayliss, J. W. Beck, P. G. Blackwell, C. B. Ramsey, C. E. Buck, H. Cheng, R. L. Edwards, M. Friedrich, et al., IntCal13 and Marine13 radiocarbon age calibration curves 0–50,000 years cal BP, *Radiocarbon*, 55, 1869–1887, 2013.
- Rubino, M., D. M. Etheridge, C. M. Trudinger, C. E. Allison, M. O. Battle, R. L. Langenfelds, L. P. Steele, M. Curran, M. Bender, J. W. C. White, T. M. Jenk, T. Blunier, and R. J. Francey, A revised 1000 year atmospheric 13C-CO₂ record from Law Dome and South Pole, Antarctica, *Journal of Geophysical Research: Atmospheres*, 118, 8482–8499, 2013.
- Sabine, C. L., R. A. Feely, N. Gruber, R. M. Key, K. Lee, J. L. Bullister, R. Wanninkhof, C. S. Wong, D. Wallace, B. Tilbrook, F. J. Millero, T.-H. Peng, A. Kozyr, T. Ono, and A. F. Riod, The Oceanic Sink for Anthropogenic CO₂, *Science*, 305, 367–371, 2004.
- Schmittner, A., N. Gruber, A. Mix, R. Key, A. Tagliabue, and T. Westberry, Biology and air–sea gas exchange controls on the distribution of carbon isotope ratios ($\delta^{13}\text{C}$) in the ocean, *Biogeosciences*, 10, 5793–5816, 2013.
- Schmittner, A., H. C. Bostock, O. Cartapanis, W. B. Curry, H. L. Filipsson, E. D. Galbraith, J. Gottschalk, J. C. Herguera, B. Hoogakker, S. L. Jaccard, et al., Calibration of the carbon isotope composition ($\delta^{13}\text{C}$) of benthic foraminifera, *Paleoceanography*, 32, 512–530, 2017.
- Smith, J., and C. Schafer, Sedimentation, bioturbation, and Hg uptake in the sediments of the estuary and Gulf of St. Lawrence, *Limnology and Oceanography*, 44, 207–219, 1999.
- Sonnerup, R. E., P. D. Quay, A. P. McNichol, J. L. Bullister, T. A. Westby, and H. L. Anderson, Reconstructing the oceanic 13C Suess effect, *Global Biogeochemical Cycles*, 13, 857–872, 1999.
- Sonnerup, R. E., D. Quay, and A. P. McNichol, The Indian Ocean 13C Suess effect, *Global Biogeochemical Cycles*, 14, 903–916, 2000.
- Sorgente, D., M. Frignani, L. Langone, and M. Ravaioli, Chronology of marine sediments: Interpretation of activity-depth profiles of 210Pb and other radioactive tracers: PART I, 1999.

- Spero, H. J., and D. W. Lea, Experimental determination of stable isotope variability in *Globigerina bulloides*: implications for paleoceanographic reconstructions, *Marine Micropaleontology*, 28, 231–246, 1996.
- Spero, H. J., J. Bijma, D. W. Lea, and B. E. Bemis, Effect of seawater carbonate concentration on foraminiferal carbon and oxygen isotopes, *Nature*, 390, 497–500, 1997.
- Suess, H. E., Radiocarbon Concentration in Modern Wood, *Science*, 122, 415–417, 1955.
- Swart, P. K., R. E. Dodge, H. J. Hudson, and P. K. Swart, A 240-Year Stable Oxygen and Carbon Isotopic Record in a Coral from South Florida : Implications for the Prediction of Precipitation in Southern Florida, *PALAIOS*, 11, 362–375, 1996.
- Swart, P. K., L. Greer, B. E. Rosenheim, C. S. Moses, A. J. Waite, A. Winter, R. E. Dodge, and K. Helmle, The ^{13}C Suess effect in scleractinian corals mirror changes in the anthropogenic CO_2 inventory of the surface oceans, *Geophysical Research Letters*, 37, 1–6, 2010.
- Telford, R. J., E. Heegaard, and H. J. B. Birks, All age–depth models are wrong: but how badly?, *Quaternary science reviews*, 23, 1–5, 2004.
- Thibodeau, B., A. de Vernal, and A. Mucci, Recent eutrophication and consequent hypoxia in the bottom waters of the Lower St. Lawrence Estuary: Micropaleontological and geochemical evidence, *Marine Geology*, 231, 37–50, 2006.
- Thibodeau, B., A. De Vernal, C. Hillaire-Marcel, and A. Mucci, Twentieth century warming in deep waters of the Gulf of St. Lawrence: A unique feature of the last millennium, *Geophysical Research Letters*, 37, 2010.
- Thornalley, D. J., D. W. Oppo, P. Ortega, J. I. Robson, C. M. Brierley, R. Davis, I. R. Hall, P. Moffa-Sanchez, N. L. Rose, P. T. Spooner, et al., Anomalously weak Labrador Sea convection and Atlantic overturning during the past 150 years, *Nature*, 556, 227, 2018.
- Townsend, D. W., N. R. Pettigrew, M. A. Thomas, M. G. Neary, J. McGillicuddy, J. Dennis, and J. O’Donnell, Water masses and nutrient sources to the Gulf of Maine, *Journal of marine research*, 73, 93–122, 2015.
- Worheide, G., The Reef Cave Dwelling Ultraconservative Coralline Demosponge *As-trosclera willeyana* LISTER 1900 from the Indo-Pacific, *Facies*, 38, 1–88, 1998.
- Xu, S., G. Jia, W. Deng, G. Wei, and W. Chen, Carbon isotopic disequilibrium between seawater and air in the coastal Northern South China Sea over the past century, *Estuarine, Coastal and Shelf Science*, 149, 38–45, 2014.
- Zeebe, R. E., and D. A. Wolf-Gladrow, *CO₂ in seawater: equilibrium, kinetics, isotopes*, 65, Gulf Professional Publishing, 2001.
- Zeebe, R. E., J. Bijma, and D. A. Wolf-gladrow, A diffusion-reaction model of carbon isotope fractionation in foraminifera, *Marine Chemistry*, 64, 199–227, 1999.

APPENDIX A: DATA

The $\delta^{13}\text{C}$, $\delta^{13}\text{O}$, and Bacon age output data from cores MSM46 MC2 and MC4 are presented in Tables 1 and 2, respectively. The unpublished data provided by several collaborators are not included in this appendix. These data include $\delta^{13}\text{C}$ and $\delta^{13}\text{O}$ from Lloyd Keigwin (OCE326 MC29, OCE400 MC44), Tom Marchitto and Peter DeMenocal (KNR158), ^{210}Pb from Ed Boyle (OCE400 MC44), and Hg measurements from Matthias Moros (MSM46 MC2 and MC4).

Depth (cm)	MSM46 MC2 Species	$\delta^{13}\text{C}$	$\delta^{13}\text{O}$	Year BP -1σ	Year BP $+1\sigma$	Year BP (Median)	Year BP (Mean)	Year AD
0.5	<i>N. pachyderma</i>	0.39	1.79	-76	-49	-63	-63	2013
1.5	<i>N. pachyderma</i>	0.67	1.91	-72	-44	-58	-58	2008
2.5	<i>N. pachyderma</i>	0.52	1.49	-70	-36	-54	-54	2004
3.5	<i>N. pachyderma</i>	0.61	1.73	-68	-28	-50	-49	1999
3.5	<i>N. pachyderma</i>	0.63	2.01	-68	-28	-50	-49	1999
4.5	<i>N. pachyderma</i>	0.67	1.69	-66	-19	-46	-45	1995
5.5	<i>N. pachyderma</i>	0.77	1.87	-62	-12	-42	-41	1991
5.5	<i>N. pachyderma</i>	0.82	1.95	-62	-12	-42	-41	1991
6.5	<i>N. pachyderma</i>	0.71	1.90	-58	-9	-37	-36	1986
7.5	<i>N. pachyderma</i>	0.82	2.06	-54	-6	-33	-32	1982
8.5	<i>N. pachyderma</i>	0.85	1.93	-51	-2	-28	-27	1977
9.5	<i>N. pachyderma</i>	0.79	1.92	-49	4	-24	-23	1973
10.5	<i>N. pachyderma</i>	0.88	1.77	-44	9	-19	-18	1968
11.5	<i>N. pachyderma</i>	0.80	1.84	-38	13	-14	-14	1964
11.5	<i>N. pachyderma</i>	0.84	1.92	-38	13	-14	-14	1964
12.5	<i>N. pachyderma</i>	0.90	2.04	-34	18	-10	-9	1959
13.5	<i>N. pachyderma</i>	0.91	1.85	-30	24	-5	-4	1954
13.5	<i>N. pachyderma</i>	0.79	1.57	-30	24	-5	-4	1954
13.5	<i>N. pachyderma</i>	0.78	1.94	-30	24	-5	-4	1954
14.5	<i>N. pachyderma</i>	0.88	1.69	-28	31	-0	0	1950
15.5	<i>N. pachyderma</i>	0.93	2.13	-24	38	5	5	1945

16.5	<i>N. pachyderma</i>	0.86	1.91	-21	44	10	10	1940
16.5	<i>N. pachyderma</i>	0.83	1.69	-21	44	10	10	1940
17.5	<i>N. pachyderma</i>	0.83	1.61	-18	54	14	15	1935
18.5	<i>N. pachyderma</i>	0.85	1.48	-16	64	18	20	1930
19.5	<i>N. pachyderma</i>	0.89	1.98	-14	76	23	25	1925
20.5	<i>N. pachyderma</i>	0.99	1.94	-11	85	27	30	1920
21.5	<i>N. pachyderma</i>	0.95	2.11	-8	91	32	35	1915
21.5	<i>N. pachyderma</i>	0.86	1.67	-8	91	32	35	1915
22.5	<i>N. pachyderma</i>	0.98	1.97	-5	100	37	40	1910
23.5	<i>N. pachyderma</i>	0.96	2.02	-2	109	42	45	1905
24.5	<i>N. pachyderma</i>	0.95	2.10	-0	119	46	50	1900
24.5	<i>N. pachyderma</i>	0.91	1.74	-0	119	46	50	1900
25.5	<i>N. pachyderma</i>	0.89	1.99	2	126	51	55	1895
26.5	<i>N. pachyderma</i>	0.97	2.19	5	132	56	60	1890
27.5	<i>N. pachyderma</i>	0.85	1.42	9	139	61	65	1885
27.5	<i>N. pachyderma</i>	0.92	2.15	9	139	61	65	1885
29.5	<i>N. pachyderma</i>	0.86	1.87	14	158	70	75	1875
30.5	<i>N. pachyderma</i>	0.98	2.09	16	166	75	80	1870
30.5	<i>N. pachyderma</i>	0.90	2.20	16	166	75	80	1870
31.5	<i>N. pachyderma</i>	0.85	1.71	20	171	80	85	1865
32.5	<i>N. pachyderma</i>	0.76	1.68	23	178	85	90	1860
33.5	<i>N. pachyderma</i>	0.99	2.00	26	186	90	95	1855
35.5	<i>N. pachyderma</i>	0.92	1.89	32	201	99	105	1845
36.5	<i>N. pachyderma</i>	0.88	1.95	35	208	104	110	1840

Table 1: Foraminiferal $\delta^{13}\text{C}$, $\delta^{13}\text{O}$, and Bacon age output data from MSM46 MC2.

Depth (cm)	MSM46 MC4 Species	$\delta^{13}\text{C}$	$\delta^{13}\text{O}$	Year BP -1 σ	Year BP +1 σ	Year BP (Median)	Year BP (Mean)	Year AD
0.5	<i>N. pachyderma</i>	0.67	1.87	-74	-48	-62	-61	2011
1.5	<i>N. pachyderma</i>	0.66	2.10	-71	-39	-56	-56	2006
2.5	<i>N. pachyderma</i>	0.63	2.20	-68	-27	-52	-50	2000
3.5	<i>N. pachyderma</i>	0.68	1.84	-67	-14	-47	-45	1995

4.5	<i>N. pachyderma</i>	0.70	1.91	-65	1	-43	-40	1990
5.5	<i>N. pachyderma</i>	0.63	1.73	-62	10	-38	-34	1984
6.5	<i>N. pachyderma</i>	0.70	1.95	-58	16	-32	-29	1979
7.5	<i>N. pachyderma</i>	0.66	1.83	-55	22	-26	-23	1973
8.5	<i>N. pachyderma</i>	0.92	2.01	-53	30	-20	-18	1968
8.5	<i>N. pachyderma</i>	0.85	2.00	-53	30	-20	-18	1968
13.5	<i>N. pachyderma</i>	0.78	2.06	-35	64	8	10	1940
15.5	<i>N. pachyderma</i>	0.87	1.58	-28	78	18	21	1929
17.5	<i>N. pachyderma</i>	0.80	1.94	-17	87	30	32	1918
19.5	<i>N. pachyderma</i>	0.85	1.86	-10	100	41	43	1907
19.5	<i>N. pachyderma</i>	0.79	1.90	-10	100	41	43	1907
20.5	<i>N. pachyderma</i>	0.84	2.08	-5	106	47	48	1902
20.5	<i>N. pachyderma</i>	0.71	1.98	-5	106	47	48	1902
23.5	<i>N. pachyderma</i>	0.87	1.91	9	123	64	65	1885
26.5	<i>N. pachyderma</i>	0.74	1.86	20	143	79	80	1870
26.5	<i>N. pachyderma</i>	0.96	2.07	20	143	79	80	1870
28.5	<i>N. pachyderma</i>	0.86	1.87	27	159	89	91	1859
0.5	<i>C. lobatulus</i>	-0.08	2.27	-74	-48	-62	-61	2011
1.5	<i>C. lobatulus</i>	0.00	2.25	-71	-39	-56	-56	2006
2.5	<i>C. lobatulus</i>	0.05	2.07	-68	-27	-52	-50	2000
2.5	<i>C. lobatulus</i>	0.23	2.14	-68	-27	-52	-50	2000
3.5	<i>C. lobatulus</i>	0.01	1.89	-67	-14	-47	-45	1995
3.5	<i>C. lobatulus</i>	0.10	1.94	-67	-14	-47	-45	1995
4.5	<i>C. lobatulus</i>	0.13	2.09	-65	1	-43	-40	1990
5.5	<i>C. lobatulus</i>	0.23	2.04	-62	10	-38	-34	1984
6.5	<i>C. lobatulus</i>	0.20	2.11	-58	16	-32	-29	1979
7.5	<i>C. lobatulus</i>	0.28	2.10	-55	22	-26	-23	1973
8.5	<i>C. lobatulus</i>	0.31	2.05	-53	30	-20	-18	1968
10.5	<i>C. lobatulus</i>	0.48	0.97	-47	48	-9	-7	1957
13.5	<i>C. lobatulus</i>	0.60	2.24	-35	64	8	10	1940
15.5	<i>C. lobatulus</i>	0.32	2.17	-28	78	18	21	1929
17.5	<i>C. lobatulus</i>	1.00	2.14	-17	87	30	32	1918

19.5	<i>C. lobatulus</i>	0.86	1.52	-10	100	41	43	1907
23.5	<i>C. lobatulus</i>	0.64	1.78	9	123	64	65	1885
26.5	<i>C. lobatulus</i>	0.48	2.23	20	143	79	80	1870
28.5	<i>C. lobatulus</i>	0.71	2.00	27	159	89	91	1859

Table 2: Foraminiferal $\delta^{13}\text{C}$, $\delta^{13}\text{O}$, and Bacon age output data from MSM46 MC4.

APPENDIX B: COPYRIGHT LICENSES

**JOHN WILEY AND SONS LICENSE
TERMS AND CONDITIONS**

Oct 20, 2018

This Agreement between Miss. Stefanie Mellon ("You") and John Wiley and Sons ("John Wiley and Sons") consists of your license details and the terms and conditions provided by John Wiley and Sons and Copyright Clearance Center.

License Number	4445491120433
License date	Oct 10, 2018
Licensed Content Publisher	John Wiley and Sons
Licensed Content Publication	Geophysical Research Letters
Licensed Content Title	Carbon isotope composition of Caribbean Sea surface waters: Response to the uptake of anthropogenic CO ₂
Licensed Content Author	David Black, Robert Thunell, Kate Wejnert, et al
Licensed Content Date	Aug 30, 2011
Licensed Content Volume	38
Licensed Content Issue	16
Licensed Content Pages	5
Type of use	Dissertation/Thesis
Requestor type	University/Academic
Format	Print and electronic
Portion	Figure/table
Number of figures/tables	1
Original Wiley figure/table number(s)	Figure 2
Will you be translating?	No
Title of your thesis / dissertation	INVESTIGATING THE 13C SUESS EFFECT IN THE NORTHWESTERN NORTH ATLANTIC
Expected completion date	Oct 2018
Expected size (number of pages)	1
Requestor Location	Miss. Stefanie Mellon 1-6539 Chebucto Rd. Halifax, NS B3L1L6 Canada Attn: Miss. Stefanie Mellon
Publisher Tax ID	EU826007151
Total	0.00 CAD

[Terms and Conditions](#)

TERMS AND CONDITIONS

This copyrighted material is owned by or exclusively licensed to John Wiley & Sons, Inc. or one of its group companies (each a "Wiley Company") or handled on behalf of a society with which a Wiley Company has exclusive publishing rights in relation to a particular work (collectively "WILEY"). By clicking "accept" in connection with completing this licensing transaction, you agree that the following terms and conditions apply to this transaction (along with the billing and payment terms and conditions established by the Copyright Clearance Center Inc., ("CCC's Billing and Payment terms and conditions"), at the time that you opened your RightsLink account (these are available at any time at <http://myaccount.copyright.com>).

Terms and Conditions

- The materials you have requested permission to reproduce or reuse (the "Wiley Materials") are protected by copyright.
- You are hereby granted a personal, non-exclusive, non-sub licensable (on a stand-alone basis), non-transferable, worldwide, limited license to reproduce the Wiley Materials for the purpose specified in the licensing process. This license, **and any CONTENT (PDF or image file) purchased as part of your order**, is for a one-time use only and limited to any maximum distribution number specified in the license. The first instance of republication or reuse granted by this license must be completed within two years of the date of the grant of this license (although copies prepared before the end date may be distributed thereafter). The Wiley Materials shall not be used in any other manner or for any other purpose, beyond what is granted in the license. Permission is granted subject to an appropriate acknowledgement given to the author, title of the material/book/journal and the publisher. You shall also duplicate the copyright notice that appears in the Wiley publication in your use of the Wiley Material. Permission is also granted on the understanding that nowhere in the text is a previously published source acknowledged for all or part of this Wiley Material. Any third party content is expressly excluded from this permission.
- With respect to the Wiley Materials, all rights are reserved. Except as expressly granted by the terms of the license, no part of the Wiley Materials may be copied, modified, adapted (except for minor reformatting required by the new Publication), translated, reproduced, transferred or distributed, in any form or by any means, and no derivative works may be made based on the Wiley Materials without the prior permission of the respective copyright owner. **For STM Signatory Publishers clearing permission under the terms of the [STM Permissions Guidelines](#) only, the terms of the license are extended to include subsequent editions and for editions in other languages, provided such editions are for the work as a whole in situ and does not involve the separate exploitation of the permitted figures or extracts**, You may not alter, remove or suppress in any manner any copyright, trademark or other notices displayed by the Wiley Materials. You may not license, rent, sell, loan, lease, pledge, offer as security, transfer or assign the Wiley Materials on a stand-alone basis, or any of the rights granted to you hereunder to any other person.
- The Wiley Materials and all of the intellectual property rights therein shall at all times remain the exclusive property of John Wiley & Sons Inc, the Wiley Companies, or their respective licensors, and your interest therein is only that of having possession of and the right to reproduce the Wiley Materials pursuant to Section 2 herein during the continuance of this Agreement. You agree that you own no right, title or interest in or to the Wiley Materials or any of the intellectual property rights therein. You shall have no rights hereunder other than the license as provided for above in Section 2. No right, license or interest to any trademark, trade name, service mark or other branding ("Marks") of WILEY or its licensors is granted hereunder, and you agree that you shall not assert any such right, license or interest with respect thereto
- NEITHER WILEY NOR ITS LICENSORS MAKES ANY WARRANTY OR REPRESENTATION OF ANY KIND TO YOU OR ANY THIRD PARTY, EXPRESS, IMPLIED OR STATUTORY, WITH RESPECT TO THE MATERIALS OR THE ACCURACY OF ANY INFORMATION CONTAINED IN THE MATERIALS, INCLUDING, WITHOUT LIMITATION, ANY IMPLIED WARRANTY OF MERCHANTABILITY, ACCURACY, SATISFACTORY QUALITY, FITNESS FOR A PARTICULAR PURPOSE, USABILITY, INTEGRATION OR NON-INFRINGEMENT AND ALL SUCH WARRANTIES ARE HEREBY EXCLUDED BY WILEY AND ITS LICENSORS AND WAIVED BY YOU.
- WILEY shall have the right to terminate this Agreement immediately upon breach of this Agreement by you.

- You shall indemnify, defend and hold harmless WILEY, its Licensors and their respective directors, officers, agents and employees, from and against any actual or threatened claims, demands, causes of action or proceedings arising from any breach of this Agreement by you.
- IN NO EVENT SHALL WILEY OR ITS LICENSORS BE LIABLE TO YOU OR ANY OTHER PARTY OR ANY OTHER PERSON OR ENTITY FOR ANY SPECIAL, CONSEQUENTIAL, INCIDENTAL, INDIRECT, EXEMPLARY OR PUNITIVE DAMAGES, HOWEVER CAUSED, ARISING OUT OF OR IN CONNECTION WITH THE DOWNLOADING, PROVISIONING, VIEWING OR USE OF THE MATERIALS REGARDLESS OF THE FORM OF ACTION, WHETHER FOR BREACH OF CONTRACT, BREACH OF WARRANTY, TORT, NEGLIGENCE, INFRINGEMENT OR OTHERWISE (INCLUDING, WITHOUT LIMITATION, DAMAGES BASED ON LOSS OF PROFITS, DATA, FILES, USE, BUSINESS OPPORTUNITY OR CLAIMS OF THIRD PARTIES), AND WHETHER OR NOT THE PARTY HAS BEEN ADVISED OF THE POSSIBILITY OF SUCH DAMAGES. THIS LIMITATION SHALL APPLY NOTWITHSTANDING ANY FAILURE OF ESSENTIAL PURPOSE OF ANY LIMITED REMEDY PROVIDED HEREIN.
- Should any provision of this Agreement be held by a court of competent jurisdiction to be illegal, invalid, or unenforceable, that provision shall be deemed amended to achieve as nearly as possible the same economic effect as the original provision, and the legality, validity and enforceability of the remaining provisions of this Agreement shall not be affected or impaired thereby.
- The failure of either party to enforce any term or condition of this Agreement shall not constitute a waiver of either party's right to enforce each and every term and condition of this Agreement. No breach under this agreement shall be deemed waived or excused by either party unless such waiver or consent is in writing signed by the party granting such waiver or consent. The waiver by or consent of a party to a breach of any provision of this Agreement shall not operate or be construed as a waiver of or consent to any other or subsequent breach by such other party.
- This Agreement may not be assigned (including by operation of law or otherwise) by you without WILEY's prior written consent.
- Any fee required for this permission shall be non-refundable after thirty (30) days from receipt by the CCC.
- These terms and conditions together with CCC's Billing and Payment terms and conditions (which are incorporated herein) form the entire agreement between you and WILEY concerning this licensing transaction and (in the absence of fraud) supersedes all prior agreements and representations of the parties, oral or written. This Agreement may not be amended except in writing signed by both parties. This Agreement shall be binding upon and inure to the benefit of the parties' successors, legal representatives, and authorized assigns.
- In the event of any conflict between your obligations established by these terms and conditions and those established by CCC's Billing and Payment terms and conditions, these terms and conditions shall prevail.
- WILEY expressly reserves all rights not specifically granted in the combination of (i) the license details provided by you and accepted in the course of this licensing transaction, (ii) these terms and conditions and (iii) CCC's Billing and Payment terms and conditions.
- This Agreement will be void if the Type of Use, Format, Circulation, or Requestor Type was misrepresented during the licensing process.

- This Agreement shall be governed by and construed in accordance with the laws of the State of New York, USA, without regards to such state's conflict of law rules. Any legal action, suit or proceeding arising out of or relating to these Terms and Conditions or the breach thereof shall be instituted in a court of competent jurisdiction in New York County in the State of New York in the United States of America and each party hereby consents and submits to the personal jurisdiction of such court, waives any objection to venue in such court and consents to service of process by registered or certified mail, return receipt requested, at the last known address of such party.

WILEY OPEN ACCESS TERMS AND CONDITIONS

Wiley Publishes Open Access Articles in fully Open Access Journals and in Subscription journals offering Online Open. Although most of the fully Open Access journals publish open access articles under the terms of the Creative Commons Attribution (CC BY) License only, the subscription journals and a few of the Open Access Journals offer a choice of Creative Commons Licenses. The license type is clearly identified on the article.

The Creative Commons Attribution License

The [Creative Commons Attribution License \(CC-BY\)](#) allows users to copy, distribute and transmit an article, adapt the article and make commercial use of the article. The CC-BY license permits commercial and non-

Creative Commons Attribution Non-Commercial License

The [Creative Commons Attribution Non-Commercial \(CC-BY-NC\) License](#) permits use, distribution and reproduction in any medium, provided the original work is properly cited and is not used for commercial purposes.(see below)

Creative Commons Attribution-Non-Commercial-NoDerivs License

The [Creative Commons Attribution Non-Commercial-NoDerivs License](#) (CC-BY-NC-ND) permits use, distribution and reproduction in any medium, provided the original work is properly cited, is not used for commercial purposes and no modifications or adaptations are made. (see below)

Use by commercial "for-profit" organizations

Use of Wiley Open Access articles for commercial, promotional, or marketing purposes requires further explicit permission from Wiley and will be subject to a fee.

Further details can be found on Wiley Online Library

<http://olabout.wiley.com/WileyCDA/Section/id-410895.html>

Other Terms and Conditions:

v1.10 Last updated September 2015

Questions? customercare@copyright.com or +1-855-239-3415 (toll free in the US) or +1-978-646-2777.



RightsLink®

[Home](#)[Create Account](#)[Help](#)

Title: Recent Declines in Atmospheric Mercury Deposition in the Upper Midwest

Author: Daniel R. Engstrom, Edward B. Swain

Publication: Environmental Science & Technology

Publisher: American Chemical Society

Date: Apr 1, 1997

Copyright © 1997, American Chemical Society

LOGIN

If you're a **copyright.com user**, you can login to RightsLink using your copyright.com credentials.

Already a **RightsLink user** or want to [learn more?](#)

PERMISSION/LICENSE IS GRANTED FOR YOUR ORDER AT NO CHARGE

This type of permission/license, instead of the standard Terms & Conditions, is sent to you because no fee is being charged for your order. Please note the following:

- Permission is granted for your request in both print and electronic formats, and translations.
- If figures and/or tables were requested, they may be adapted or used in part.
- Please print this page for your records and send a copy of it to your publisher/graduate school.
- Appropriate credit for the requested material should be given as follows: "Reprinted (adapted) with permission from (COMPLETE REFERENCE CITATION). Copyright (YEAR) American Chemical Society." Insert appropriate information in place of the capitalized words.
- One-time permission is granted only for the use specified in your request. No additional uses are granted (such as derivative works or other editions). For any other uses, please submit a new request.

If credit is given to another source for the material you requested, permission must be obtained from that source.

[BACK](#)[CLOSE WINDOW](#)

Copyright © 2018 [Copyright Clearance Center, Inc.](#) All Rights Reserved. [Privacy statement.](#) [Terms and Conditions.](#) Comments? We would like to hear from you. E-mail us at customercare@copyright.com

**THE AMERICAN ASSOCIATION FOR THE ADVANCEMENT OF SCIENCE LICENSE
TERMS AND CONDITIONS**

Oct 20, 2018

This Agreement between Miss. Stefanie Mellon ("You") and The American Association for the Advancement of Science ("The American Association for the Advancement of Science") consists of your license details and the terms and conditions provided by The American Association for the Advancement of Science and Copyright Clearance Center.

License Number	4445451263738
License date	Oct 10, 2018
Licensed Content Publisher	The American Association for the Advancement of Science
Licensed Content Publication	Science
Licensed Content Title	The Oceanic Sink for Anthropogenic CO ₂
Licensed Content Author	Christopher L. Sabine, Richard A. Feely, Nicolas Gruber, Robert M. Key, Kitack Lee, John L. Bullister, Rik Wanninkhof, C. S. Wong, Douglas W. R. Wallace, Bronte Tilbrook, Frank J. Millero, Tsung-Hung Peng, Alexander Kozyr, Tsueno Ono, Aida F. Rios
Licensed Content Date	Jul 16, 2004
Licensed Content Volume	305
Licensed Content Issue	5682
Volume number	305
Issue number	5682
Type of Use	Thesis / Dissertation
Requestor type	Scientist/individual at a research institution
Format	Print and electronic
Portion	Figure
Number of figures/tables	1
Order reference number	
Title of your thesis / dissertation	INVESTIGATING THE 13C SUESS EFFECT IN THE NORTHWESTERN NORTH ATLANTIC
Expected completion date	Oct 2018
Estimated size(pages)	1
Requestor Location	Miss. Stefanie Mellon 1-6539 Chebucto Rd. Halifax, NS B3L1L6 Canada Attn: Miss. Stefanie Mellon
Billing Type	Invoice
Billing Address	Miss. Stefanie Mellon 1-6539 Chebucto Rd. Halifax, NS B3L1L6 Canada Attn: Miss. Stefanie Mellon
Total	0.00 CAD

Terms and Conditions

American Association for the Advancement of Science TERMS AND CONDITIONS
Regarding your request, we are pleased to grant you non-exclusive, non-transferable permission, to republish the AAAS material identified above in your work identified above,

subject to the terms and conditions herein. We must be contacted for permission for any uses other than those specifically identified in your request above.

The following credit line must be printed along with the AAAS material: "From [Full Reference Citation]. Reprinted with permission from AAAS."

All required credit lines and notices must be visible any time a user accesses any part of the AAAS material and must appear on any printed copies and authorized user might make. This permission does not apply to figures / photos / artwork or any other content or materials included in your work that are credited to non-AAAS sources. If the requested material is sourced to or references non-AAAS sources, you must obtain authorization from that source as well before using that material. You agree to hold harmless and indemnify AAAS against any claims arising from your use of any content in your work that is credited to non-AAAS sources.

If the AAAS material covered by this permission was published in Science during the years 1974 - 1994, you must also obtain permission from the author, who may grant or withhold permission, and who may or may not charge a fee if permission is granted. See original article for author's address. This condition does not apply to news articles.

The AAAS material may not be modified or altered except that figures and tables may be modified with permission from the author. Author permission for any such changes must be secured prior to your use.

Whenever possible, we ask that electronic uses of the AAAS material permitted herein include a hyperlink to the original work on AAAS's website (hyperlink may be embedded in the reference citation).

AAAS material reproduced in your work identified herein must not account for more than 30% of the total contents of that work.

AAAS must publish the full paper prior to use of any text.

AAAS material must not imply any endorsement by the American Association for the Advancement of Science.

This permission is not valid for the use of the AAAS and/or Science logos.

AAAS makes no representations or warranties as to the accuracy of any information contained in the AAAS material covered by this permission, including any warranties of merchantability or fitness for a particular purpose.

If permission fees for this use are waived, please note that AAAS reserves the right to charge for reproduction of this material in the future.

Permission is not valid unless payment is received within sixty (60) days of the issuance of this permission. If payment is not received within this time period then all rights granted herein shall be revoked and this permission will be considered null and void.

In the event of breach of any of the terms and conditions herein or any of CCC's Billing and Payment terms and conditions, all rights granted herein shall be revoked and this permission will be considered null and void.

AAAS reserves the right to terminate this permission and all rights granted herein at its discretion, for any purpose, at any time. In the event that AAAS elects to terminate this permission, you will have no further right to publish, publicly perform, publicly display, distribute or otherwise use any matter in which the AAAS content had been included, and all fees paid hereunder shall be fully refunded to you. Notification of termination will be sent to the contact information as supplied by you during the request process and termination shall be immediate upon sending the notice. Neither AAAS nor CCC shall be liable for any costs, expenses, or damages you may incur as a result of the termination of this permission, beyond the refund noted above.

This Permission may not be amended except by written document signed by both parties.

The terms above are applicable to all permissions granted for the use of AAAS material.

Below you will find additional conditions that apply to your particular type of use.

FOR A THESIS OR DISSERTATION

If you are using figure(s)/table(s), permission is granted for use in print and electronic versions of your dissertation or thesis. A full text article may be used in print versions only of a dissertation or thesis.

Permission covers the distribution of your dissertation or thesis on demand by ProQuest / UMI, provided the AAAS material covered by this permission remains in situ.

If you are an Original Author on the AAAS article being reproduced, please refer to your License to Publish for rules on reproducing your paper in a dissertation or thesis.

FOR JOURNALS:

Permission covers both print and electronic versions of your journal article, however the

AAAS material may not be used in any manner other than within the context of your article.

FOR BOOKS/TEXTBOOKS:

If this license is to reuse figures/tables, then permission is granted for non-exclusive world rights in all languages in both print and electronic formats (electronic formats are defined below).

If this license is to reuse a text excerpt or a full text article, then permission is granted for non-exclusive world rights in English only. You have the option of securing either print or electronic rights or both, but electronic rights are not automatically granted and do garner additional fees. Permission for translations of text excerpts or full text articles into other languages must be obtained separately.

Licenses granted for use of AAAS material in electronic format books/textbooks are valid only in cases where the electronic version is equivalent to or substitutes for the print version of the book/textbook. The AAAS material reproduced as permitted herein must remain in situ and must not be exploited separately (for example, if permission covers the use of a full text article, the article may not be offered for access or for purchase as a stand-alone unit), except in the case of permitted textbook companions as noted below.

You must include the following notice in any electronic versions, either adjacent to the reprinted AAAS material or in the terms and conditions for use of your electronic products: "Readers may view, browse, and/or download material for temporary copying purposes only, provided these uses are for noncommercial personal purposes. Except as provided by law, this material may not be further reproduced, distributed, transmitted, modified, adapted, performed, displayed, published, or sold in whole or in part, without prior written permission from the publisher."

If your book is an academic textbook, permission covers the following companions to your textbook, provided such companions are distributed only in conjunction with your textbook at no additional cost to the user:

- Password-protected website
- Instructor's image CD/DVD and/or PowerPoint resource
- Student CD/DVD

All companions must contain instructions to users that the AAAS material may be used for non-commercial, classroom purposes only. Any other uses require the prior written permission from AAAS.

If your license is for the use of AAAS Figures/Tables, then the electronic rights granted herein permit use of the Licensed Material in any Custom Databases that you distribute the electronic versions of your textbook through, so long as the Licensed Material remains within the context of a chapter of the title identified in your request and cannot be downloaded by a user as an independent image file.

Rights also extend to copies/files of your Work (as described above) that you are required to provide for use by the visually and/or print disabled in compliance with state and federal laws.

This permission only covers a single edition of your work as identified in your request.

FOR NEWSLETTERS:

Permission covers print and/or electronic versions, provided the AAAS material reproduced as permitted herein remains in situ and is not exploited separately (for example, if permission covers the use of a full text article, the article may not be offered for access or for purchase as a stand-alone unit)

FOR ANNUAL REPORTS:

Permission covers print and electronic versions provided the AAAS material reproduced as permitted herein remains in situ and is not exploited separately (for example, if permission covers the use of a full text article, the article may not be offered for access or for purchase as a stand-alone unit)

FOR PROMOTIONAL/MARKETING USES:

Permission covers the use of AAAS material in promotional or marketing pieces such as information packets, media kits, product slide kits, brochures, or flyers limited to a single print run. The AAAS Material may not be used in any manner which implies endorsement or promotion by the American Association for the Advancement of Science (AAAS) or Science of any product or service. AAAS does not permit the reproduction of its name, logo or text on promotional literature.

If permission to use a full text article is permitted, The Science article covered by this permission must not be altered in any way. No additional printing may be set onto an article

copy other than the copyright credit line required above. Any alterations must be approved in advance and in writing by AAAS. This includes, but is not limited to, the placement of sponsorship identifiers, trademarks, logos, rubber stamping or self-adhesive stickers onto the article copies.

Additionally, article copies must be a freestanding part of any information package (i.e. media kit) into which they are inserted. They may not be physically attached to anything, such as an advertising insert, or have anything attached to them, such as a sample product. Article copies must be easily removable from any kits or informational packages in which they are used. The only exception is that article copies may be inserted into three-ring binders.

FOR CORPORATE INTERNAL USE:

The AAAS material covered by this permission may not be altered in any way. No additional printing may be set onto an article copy other than the required credit line. Any alterations must be approved in advance and in writing by AAAS. This includes, but is not limited to the placement of sponsorship identifiers, trademarks, logos, rubber stamping or self-adhesive stickers onto article copies.

If you are making article copies, copies are restricted to the number indicated in your request and must be distributed only to internal employees for internal use.

If you are using AAAS Material in Presentation Slides, the required credit line must be visible on the slide where the AAAS material will be reprinted

If you are using AAAS Material on a CD, DVD, Flash Drive, or the World Wide Web, you must include the following notice in any electronic versions, either adjacent to the reprinted AAAS material or in the terms and conditions for use of your electronic products: "Readers may view, browse, and/or download material for temporary copying purposes only, provided these uses are for noncommercial personal purposes. Except as provided by law, this material may not be further reproduced, distributed, transmitted, modified, adapted, performed, displayed, published, or sold in whole or in part, without prior written permission from the publisher." Access to any such CD, DVD, Flash Drive or Web page must be restricted to your organization's employees only.

FOR CME COURSE and SCIENTIFIC SOCIETY MEETINGS:

Permission is restricted to the particular Course, Seminar, Conference, or Meeting indicated in your request. If this license covers a text excerpt or a Full Text Article, access to the reprinted AAAS material must be restricted to attendees of your event only (if you have been granted electronic rights for use of a full text article on your website, your website must be password protected, or access restricted so that only attendees can access the content on your site).

If you are using AAAS Material on a CD, DVD, Flash Drive, or the World Wide Web, you must include the following notice in any electronic versions, either adjacent to the reprinted AAAS material or in the terms and conditions for use of your electronic products: "Readers may view, browse, and/or download material for temporary copying purposes only, provided these uses are for noncommercial personal purposes. Except as provided by law, this material may not be further reproduced, distributed, transmitted, modified, adapted, performed, displayed, published, or sold in whole or in part, without prior written permission from the publisher."

FOR POLICY REPORTS:

These rights are granted only to non-profit organizations and/or government agencies. Permission covers print and electronic versions of a report, provided the required credit line appears in both versions and provided the AAAS material reproduced as permitted herein remains in situ and is not exploited separately.

FOR CLASSROOM PHOTOCOPIES:

Permission covers distribution in print copy format only. Article copies must be freestanding and not part of a course pack. They may not be physically attached to anything or have anything attached to them.

FOR COURSEPACKS OR COURSE WEBSITES:

These rights cover use of the AAAS material in one class at one institution. Permission is valid only for a single semester after which the AAAS material must be removed from the Electronic Course website, unless new permission is obtained for an additional semester. If the material is to be distributed online, access must be restricted to students and instructors enrolled in that particular course by some means of password or access control.

FOR WEBSITES:

You must include the following notice in any electronic versions, either adjacent to the

reprinted AAAS material or in the terms and conditions for use of your electronic products: "Readers may view, browse, and/or download material for temporary copying purposes only, provided these uses are for noncommercial personal purposes. Except as provided by law, this material may not be further reproduced, distributed, transmitted, modified, adapted, performed, displayed, published, or sold in whole or in part, without prior written permission from the publisher."

Permissions for the use of Full Text articles on third party websites are granted on a case by case basis and only in cases where access to the AAAS Material is restricted by some means of password or access control. Alternately, an E-Print may be purchased through our reprints department (brocheleau@rockwaterinc.com).

REGARDING FULL TEXT ARTICLE USE ON THE WORLD WIDE WEB IF YOU ARE AN 'ORIGINAL AUTHOR' OF A SCIENCE PAPER

If you chose "Original Author" as the Requestor Type, you are warranting that you are one of authors listed on the License Agreement as a "Licensed content author" or that you are acting on that author's behalf to use the Licensed content in a new work that one of the authors listed on the License Agreement as a "Licensed content author" has written.

Original Authors may post the 'Accepted Version' of their full text article on their personal or on their University website and not on any other website. The 'Accepted Version' is the version of the paper accepted for publication by AAAS including changes resulting from peer review but prior to AAAS's copy editing and production (in other words not the AAAS published version).

FOR MOVIES / FILM / TELEVISION:

Permission is granted to use, record, film, photograph, and/or tape the AAAS material in connection with your program/film and in any medium your program/film may be shown or heard, including but not limited to broadcast and cable television, radio, print, world wide web, and videocassette.

The required credit line should run in the program/film's end credits.

FOR MUSEUM EXHIBITIONS:

Permission is granted to use the AAAS material as part of a single exhibition for the duration of that exhibit. Permission for use of the material in promotional materials for the exhibit must be cleared separately with AAAS (please contact us at permissions@aaas.org).

FOR TRANSLATIONS:

Translation rights apply only to the language identified in your request summary above. The following disclaimer must appear with your translation, on the first page of the article, after the credit line: "This translation is not an official translation by AAAS staff, nor is it endorsed by AAAS as accurate. In crucial matters, please refer to the official English-language version originally published by AAAS."

FOR USE ON A COVER:

Permission is granted to use the AAAS material on the cover of a journal issue, newsletter issue, book, textbook, or annual report in print and electronic formats provided the AAAS material reproduced as permitted herein remains in situ and is not exploited separately. By using the AAAS Material identified in your request, you agree to abide by all the terms and conditions herein.

Questions about these terms can be directed to the AAAS Permissions department

permissions@aaas.org.

Other Terms and Conditions:

v 2

Questions? customercare@copyright.com or +1-855-239-3415 (toll free in the US) or +1-978-646-2777.

**JOHN WILEY AND SONS LICENSE
TERMS AND CONDITIONS**

Oct 20, 2018

This Agreement between Miss. Stefanie Mellon ("You") and John Wiley and Sons ("John Wiley and Sons") consists of your license details and the terms and conditions provided by John Wiley and Sons and Copyright Clearance Center.

License Number	4445521198390
License date	Oct 10, 2018
Licensed Content Publisher	John Wiley and Sons
Licensed Content Publication	Limnology and Oceanography
Licensed Content Title	Sedimentation, bioturbation, and Hg uptake in the sediments of the estuary and Gulf of St. Lawrence
Licensed Content Author	J. N. Smith, C. T. Schafer
Licensed Content Date	Jan 29, 1999
Licensed Content Volume	44
Licensed Content Issue	1
Licensed Content Pages	13
Type of use	Dissertation/Thesis
Requestor type	University/Academic
Format	Print and electronic
Portion	Figure/table
Number of figures/tables	1
Original Wiley figure/table number(s)	Figure 4
Will you be translating?	No
Title of your thesis / dissertation	INVESTIGATING THE 13C SUESS EFFECT IN THE NORTHWESTERN NORTH ATLANTIC
Expected completion date	Oct 2018
Expected size (number of pages)	1
Requestor Location	Miss. Stefanie Mellon 1-6539 Chebucto Rd. Halifax, NS B3L1L6 Canada Attn: Miss. Stefanie Mellon
Publisher Tax ID	EU826007151
Total	0.00 CAD

[Terms and Conditions](#)

TERMS AND CONDITIONS

This copyrighted material is owned by or exclusively licensed to John Wiley & Sons, Inc. or one of its group companies (each a "Wiley Company") or handled on behalf of a society with which a Wiley Company has exclusive publishing rights in relation to a particular work (collectively "WILEY"). By clicking "accept" in connection with completing this licensing transaction, you agree that the following terms and conditions apply to this transaction (along with the billing and payment terms and conditions established by the Copyright Clearance Center Inc., ("CCC's Billing and Payment terms and conditions"), at the time that you opened your RightsLink account (these are available at any time at <http://myaccount.copyright.com>).

Terms and Conditions

- The materials you have requested permission to reproduce or reuse (the "Wiley Materials") are protected by copyright.
- You are hereby granted a personal, non-exclusive, non-sub licensable (on a stand-alone basis), non-transferable, worldwide, limited license to reproduce the Wiley Materials for the purpose specified in the licensing process. This license, **and any CONTENT (PDF or image file) purchased as part of your order**, is for a one-time use only and limited to any maximum distribution number specified in the license. The first instance of republication or reuse granted by this license must be completed within two years of the date of the grant of this license (although copies prepared before the end date may be distributed thereafter). The Wiley Materials shall not be used in any other manner or for any other purpose, beyond what is granted in the license. Permission is granted subject to an appropriate acknowledgement given to the author, title of the material/book/journal and the publisher. You shall also duplicate the copyright notice that appears in the Wiley publication in your use of the Wiley Material. Permission is also granted on the understanding that nowhere in the text is a previously published source acknowledged for all or part of this Wiley Material. Any third party content is expressly excluded from this permission.
- With respect to the Wiley Materials, all rights are reserved. Except as expressly granted by the terms of the license, no part of the Wiley Materials may be copied, modified, adapted (except for minor reformatting required by the new Publication), translated, reproduced, transferred or distributed, in any form or by any means, and no derivative works may be made based on the Wiley Materials without the prior permission of the respective copyright owner. **For STM Signatory Publishers clearing permission under the terms of the [STM Permissions Guidelines](#) only, the terms of the license are extended to include subsequent editions and for editions in other languages, provided such editions are for the work as a whole in situ and does not involve the separate exploitation of the permitted figures or extracts**, You may not alter, remove or suppress in any manner any copyright, trademark or other notices displayed by the Wiley Materials. You may not license, rent, sell, loan, lease, pledge, offer as security, transfer or assign the Wiley Materials on a stand-alone basis, or any of the rights granted to you hereunder to any other person.
- The Wiley Materials and all of the intellectual property rights therein shall at all times remain the exclusive property of John Wiley & Sons Inc, the Wiley Companies, or their respective licensors, and your interest therein is only that of having possession of and the right to reproduce the Wiley Materials pursuant to Section 2 herein during the continuance of this Agreement. You agree that you own no right, title or interest in or to the Wiley Materials or any of the intellectual property rights therein. You shall have no rights hereunder other than the license as provided for above in Section 2. No right, license or interest to any trademark, trade name, service mark or other branding ("Marks") of WILEY or its licensors is granted hereunder, and you agree that you shall not assert any such right, license or interest with respect thereto
- NEITHER WILEY NOR ITS LICENSORS MAKES ANY WARRANTY OR REPRESENTATION OF ANY KIND TO YOU OR ANY THIRD PARTY, EXPRESS, IMPLIED OR STATUTORY, WITH RESPECT TO THE MATERIALS OR THE ACCURACY OF ANY INFORMATION CONTAINED IN THE MATERIALS, INCLUDING, WITHOUT LIMITATION, ANY IMPLIED WARRANTY OF MERCHANTABILITY, ACCURACY, SATISFACTORY QUALITY, FITNESS FOR A PARTICULAR PURPOSE, USABILITY, INTEGRATION OR NON-INFRINGEMENT AND ALL SUCH WARRANTIES ARE HEREBY EXCLUDED BY WILEY AND ITS LICENSORS AND WAIVED BY YOU.
- WILEY shall have the right to terminate this Agreement immediately upon breach of this Agreement by you.

- You shall indemnify, defend and hold harmless WILEY, its Licensors and their respective directors, officers, agents and employees, from and against any actual or threatened claims, demands, causes of action or proceedings arising from any breach of this Agreement by you.
- IN NO EVENT SHALL WILEY OR ITS LICENSORS BE LIABLE TO YOU OR ANY OTHER PARTY OR ANY OTHER PERSON OR ENTITY FOR ANY SPECIAL, CONSEQUENTIAL, INCIDENTAL, INDIRECT, EXEMPLARY OR PUNITIVE DAMAGES, HOWEVER CAUSED, ARISING OUT OF OR IN CONNECTION WITH THE DOWNLOADING, PROVISIONING, VIEWING OR USE OF THE MATERIALS REGARDLESS OF THE FORM OF ACTION, WHETHER FOR BREACH OF CONTRACT, BREACH OF WARRANTY, TORT, NEGLIGENCE, INFRINGEMENT OR OTHERWISE (INCLUDING, WITHOUT LIMITATION, DAMAGES BASED ON LOSS OF PROFITS, DATA, FILES, USE, BUSINESS OPPORTUNITY OR CLAIMS OF THIRD PARTIES), AND WHETHER OR NOT THE PARTY HAS BEEN ADVISED OF THE POSSIBILITY OF SUCH DAMAGES. THIS LIMITATION SHALL APPLY NOTWITHSTANDING ANY FAILURE OF ESSENTIAL PURPOSE OF ANY LIMITED REMEDY PROVIDED HEREIN.
- Should any provision of this Agreement be held by a court of competent jurisdiction to be illegal, invalid, or unenforceable, that provision shall be deemed amended to achieve as nearly as possible the same economic effect as the original provision, and the legality, validity and enforceability of the remaining provisions of this Agreement shall not be affected or impaired thereby.
- The failure of either party to enforce any term or condition of this Agreement shall not constitute a waiver of either party's right to enforce each and every term and condition of this Agreement. No breach under this agreement shall be deemed waived or excused by either party unless such waiver or consent is in writing signed by the party granting such waiver or consent. The waiver by or consent of a party to a breach of any provision of this Agreement shall not operate or be construed as a waiver of or consent to any other or subsequent breach by such other party.
- This Agreement may not be assigned (including by operation of law or otherwise) by you without WILEY's prior written consent.
- Any fee required for this permission shall be non-refundable after thirty (30) days from receipt by the CCC.
- These terms and conditions together with CCC's Billing and Payment terms and conditions (which are incorporated herein) form the entire agreement between you and WILEY concerning this licensing transaction and (in the absence of fraud) supersedes all prior agreements and representations of the parties, oral or written. This Agreement may not be amended except in writing signed by both parties. This Agreement shall be binding upon and inure to the benefit of the parties' successors, legal representatives, and authorized assigns.
- In the event of any conflict between your obligations established by these terms and conditions and those established by CCC's Billing and Payment terms and conditions, these terms and conditions shall prevail.
- WILEY expressly reserves all rights not specifically granted in the combination of (i) the license details provided by you and accepted in the course of this licensing transaction, (ii) these terms and conditions and (iii) CCC's Billing and Payment terms and conditions.
- This Agreement will be void if the Type of Use, Format, Circulation, or Requestor Type was misrepresented during the licensing process.

- This Agreement shall be governed by and construed in accordance with the laws of the State of New York, USA, without regards to such state's conflict of law rules. Any legal action, suit or proceeding arising out of or relating to these Terms and Conditions or the breach thereof shall be instituted in a court of competent jurisdiction in New York County in the State of New York in the United States of America and each party hereby consents and submits to the personal jurisdiction of such court, waives any objection to venue in such court and consents to service of process by registered or certified mail, return receipt requested, at the last known address of such party.

WILEY OPEN ACCESS TERMS AND CONDITIONS

Wiley Publishes Open Access Articles in fully Open Access Journals and in Subscription journals offering Online Open. Although most of the fully Open Access journals publish open access articles under the terms of the Creative Commons Attribution (CC BY) License only, the subscription journals and a few of the Open Access Journals offer a choice of Creative Commons Licenses. The license type is clearly identified on the article.

The Creative Commons Attribution License

The [Creative Commons Attribution License \(CC-BY\)](#) allows users to copy, distribute and transmit an article, adapt the article and make commercial use of the article. The CC-BY license permits commercial and non-

Creative Commons Attribution Non-Commercial License

The [Creative Commons Attribution Non-Commercial \(CC-BY-NC\) License](#) permits use, distribution and reproduction in any medium, provided the original work is properly cited and is not used for commercial purposes.(see below)

Creative Commons Attribution-Non-Commercial-NoDerivs License

The [Creative Commons Attribution Non-Commercial-NoDerivs License](#) (CC-BY-NC-ND) permits use, distribution and reproduction in any medium, provided the original work is properly cited, is not used for commercial purposes and no modifications or adaptations are made. (see below)

Use by commercial "for-profit" organizations

Use of Wiley Open Access articles for commercial, promotional, or marketing purposes requires further explicit permission from Wiley and will be subject to a fee.

Further details can be found on Wiley Online Library

<http://olabout.wiley.com/WileyCDA/Section/id-410895.html>

Other Terms and Conditions:

v1.10 Last updated September 2015

Questions? customercare@copyright.com or +1-855-239-3415 (toll free in the US) or +1-978-646-2777.

**JOHN WILEY AND SONS LICENSE
TERMS AND CONDITIONS**

Oct 20, 2018

This Agreement between Miss. Stefanie Mellon ("You") and John Wiley and Sons ("John Wiley and Sons") consists of your license details and the terms and conditions provided by John Wiley and Sons and Copyright Clearance Center.

License Number	4445500769400
License date	Oct 10, 2018
Licensed Content Publisher	John Wiley and Sons
Licensed Content Publication	Geophysical Research Letters
Licensed Content Title	Twentieth century warming in deep waters of the Gulf of St. Lawrence: A unique feature of the last millennium
Licensed Content Author	Benoît Thibodeau, Anne de Vernal, Claude Hillaire-Marcel, et al
Licensed Content Date	Sep 14, 2010
Licensed Content Volume	37
Licensed Content Issue	17
Licensed Content Pages	5
Type of use	Dissertation/Thesis
Requestor type	University/Academic
Format	Print and electronic
Portion	Figure/table
Number of figures/tables	1
Original Wiley figure/table number(s)	Figure 3
Will you be translating?	No
Title of your thesis / dissertation	INVESTIGATING THE 13C SUESS EFFECT IN THE NORTHWESTERN NORTH ATLANTIC
Expected completion date	Oct 2018
Expected size (number of pages)	1
Requestor Location	Miss. Stefanie Mellon 1-6539 Chebucto Rd. Halifax, NS B3L1L6 Canada Attn: Miss. Stefanie Mellon
Publisher Tax ID	EU826007151
Total	0.00 CAD

[Terms and Conditions](#)

TERMS AND CONDITIONS

This copyrighted material is owned by or exclusively licensed to John Wiley & Sons, Inc. or one of its group companies (each a "Wiley Company") or handled on behalf of a society with which a Wiley Company has exclusive publishing rights in relation to a particular work (collectively "WILEY"). By clicking "accept" in connection with completing this licensing transaction, you agree that the following terms and conditions apply to this transaction (along with the billing and payment terms and conditions established by the Copyright Clearance Center Inc., ("CCC's Billing and Payment terms and conditions"), at the time that you opened your RightsLink account (these are available at any time at <http://myaccount.copyright.com>).

Terms and Conditions

- The materials you have requested permission to reproduce or reuse (the "Wiley Materials") are protected by copyright.
- You are hereby granted a personal, non-exclusive, non-sub licensable (on a stand-alone basis), non-transferable, worldwide, limited license to reproduce the Wiley Materials for the purpose specified in the licensing process. This license, **and any CONTENT (PDF or image file) purchased as part of your order**, is for a one-time use only and limited to any maximum distribution number specified in the license. The first instance of republication or reuse granted by this license must be completed within two years of the date of the grant of this license (although copies prepared before the end date may be distributed thereafter). The Wiley Materials shall not be used in any other manner or for any other purpose, beyond what is granted in the license. Permission is granted subject to an appropriate acknowledgement given to the author, title of the material/book/journal and the publisher. You shall also duplicate the copyright notice that appears in the Wiley publication in your use of the Wiley Material. Permission is also granted on the understanding that nowhere in the text is a previously published source acknowledged for all or part of this Wiley Material. Any third party content is expressly excluded from this permission.
- With respect to the Wiley Materials, all rights are reserved. Except as expressly granted by the terms of the license, no part of the Wiley Materials may be copied, modified, adapted (except for minor reformatting required by the new Publication), translated, reproduced, transferred or distributed, in any form or by any means, and no derivative works may be made based on the Wiley Materials without the prior permission of the respective copyright owner. **For STM Signatory Publishers clearing permission under the terms of the [STM Permissions Guidelines](#) only, the terms of the license are extended to include subsequent editions and for editions in other languages, provided such editions are for the work as a whole in situ and does not involve the separate exploitation of the permitted figures or extracts**, You may not alter, remove or suppress in any manner any copyright, trademark or other notices displayed by the Wiley Materials. You may not license, rent, sell, loan, lease, pledge, offer as security, transfer or assign the Wiley Materials on a stand-alone basis, or any of the rights granted to you hereunder to any other person.
- The Wiley Materials and all of the intellectual property rights therein shall at all times remain the exclusive property of John Wiley & Sons Inc, the Wiley Companies, or their respective licensors, and your interest therein is only that of having possession of and the right to reproduce the Wiley Materials pursuant to Section 2 herein during the continuance of this Agreement. You agree that you own no right, title or interest in or to the Wiley Materials or any of the intellectual property rights therein. You shall have no rights hereunder other than the license as provided for above in Section 2. No right, license or interest to any trademark, trade name, service mark or other branding ("Marks") of WILEY or its licensors is granted hereunder, and you agree that you shall not assert any such right, license or interest with respect thereto
- NEITHER WILEY NOR ITS LICENSORS MAKES ANY WARRANTY OR REPRESENTATION OF ANY KIND TO YOU OR ANY THIRD PARTY, EXPRESS, IMPLIED OR STATUTORY, WITH RESPECT TO THE MATERIALS OR THE ACCURACY OF ANY INFORMATION CONTAINED IN THE MATERIALS, INCLUDING, WITHOUT LIMITATION, ANY IMPLIED WARRANTY OF MERCHANTABILITY, ACCURACY, SATISFACTORY QUALITY, FITNESS FOR A PARTICULAR PURPOSE, USABILITY, INTEGRATION OR NON-INFRINGEMENT AND ALL SUCH WARRANTIES ARE HEREBY EXCLUDED BY WILEY AND ITS LICENSORS AND WAIVED BY YOU.
- WILEY shall have the right to terminate this Agreement immediately upon breach of this Agreement by you.

- You shall indemnify, defend and hold harmless WILEY, its Licensors and their respective directors, officers, agents and employees, from and against any actual or threatened claims, demands, causes of action or proceedings arising from any breach of this Agreement by you.
- IN NO EVENT SHALL WILEY OR ITS LICENSORS BE LIABLE TO YOU OR ANY OTHER PARTY OR ANY OTHER PERSON OR ENTITY FOR ANY SPECIAL, CONSEQUENTIAL, INCIDENTAL, INDIRECT, EXEMPLARY OR PUNITIVE DAMAGES, HOWEVER CAUSED, ARISING OUT OF OR IN CONNECTION WITH THE DOWNLOADING, PROVISIONING, VIEWING OR USE OF THE MATERIALS REGARDLESS OF THE FORM OF ACTION, WHETHER FOR BREACH OF CONTRACT, BREACH OF WARRANTY, TORT, NEGLIGENCE, INFRINGEMENT OR OTHERWISE (INCLUDING, WITHOUT LIMITATION, DAMAGES BASED ON LOSS OF PROFITS, DATA, FILES, USE, BUSINESS OPPORTUNITY OR CLAIMS OF THIRD PARTIES), AND WHETHER OR NOT THE PARTY HAS BEEN ADVISED OF THE POSSIBILITY OF SUCH DAMAGES. THIS LIMITATION SHALL APPLY NOTWITHSTANDING ANY FAILURE OF ESSENTIAL PURPOSE OF ANY LIMITED REMEDY PROVIDED HEREIN.
- Should any provision of this Agreement be held by a court of competent jurisdiction to be illegal, invalid, or unenforceable, that provision shall be deemed amended to achieve as nearly as possible the same economic effect as the original provision, and the legality, validity and enforceability of the remaining provisions of this Agreement shall not be affected or impaired thereby.
- The failure of either party to enforce any term or condition of this Agreement shall not constitute a waiver of either party's right to enforce each and every term and condition of this Agreement. No breach under this agreement shall be deemed waived or excused by either party unless such waiver or consent is in writing signed by the party granting such waiver or consent. The waiver by or consent of a party to a breach of any provision of this Agreement shall not operate or be construed as a waiver of or consent to any other or subsequent breach by such other party.
- This Agreement may not be assigned (including by operation of law or otherwise) by you without WILEY's prior written consent.
- Any fee required for this permission shall be non-refundable after thirty (30) days from receipt by the CCC.
- These terms and conditions together with CCC's Billing and Payment terms and conditions (which are incorporated herein) form the entire agreement between you and WILEY concerning this licensing transaction and (in the absence of fraud) supersedes all prior agreements and representations of the parties, oral or written. This Agreement may not be amended except in writing signed by both parties. This Agreement shall be binding upon and inure to the benefit of the parties' successors, legal representatives, and authorized assigns.
- In the event of any conflict between your obligations established by these terms and conditions and those established by CCC's Billing and Payment terms and conditions, these terms and conditions shall prevail.
- WILEY expressly reserves all rights not specifically granted in the combination of (i) the license details provided by you and accepted in the course of this licensing transaction, (ii) these terms and conditions and (iii) CCC's Billing and Payment terms and conditions.
- This Agreement will be void if the Type of Use, Format, Circulation, or Requestor Type was misrepresented during the licensing process.

- This Agreement shall be governed by and construed in accordance with the laws of the State of New York, USA, without regards to such state's conflict of law rules. Any legal action, suit or proceeding arising out of or relating to these Terms and Conditions or the breach thereof shall be instituted in a court of competent jurisdiction in New York County in the State of New York in the United States of America and each party hereby consents and submits to the personal jurisdiction of such court, waives any objection to venue in such court and consents to service of process by registered or certified mail, return receipt requested, at the last known address of such party.

WILEY OPEN ACCESS TERMS AND CONDITIONS

Wiley Publishes Open Access Articles in fully Open Access Journals and in Subscription journals offering Online Open. Although most of the fully Open Access journals publish open access articles under the terms of the Creative Commons Attribution (CC BY) License only, the subscription journals and a few of the Open Access Journals offer a choice of Creative Commons Licenses. The license type is clearly identified on the article.

The Creative Commons Attribution License

The [Creative Commons Attribution License \(CC-BY\)](#) allows users to copy, distribute and transmit an article, adapt the article and make commercial use of the article. The CC-BY license permits commercial and non-

Creative Commons Attribution Non-Commercial License

The [Creative Commons Attribution Non-Commercial \(CC-BY-NC\) License](#) permits use, distribution and reproduction in any medium, provided the original work is properly cited and is not used for commercial purposes.(see below)

Creative Commons Attribution-Non-Commercial-NoDerivs License

The [Creative Commons Attribution Non-Commercial-NoDerivs License](#) (CC-BY-NC-ND) permits use, distribution and reproduction in any medium, provided the original work is properly cited, is not used for commercial purposes and no modifications or adaptations are made. (see below)

Use by commercial "for-profit" organizations

Use of Wiley Open Access articles for commercial, promotional, or marketing purposes requires further explicit permission from Wiley and will be subject to a fee.

Further details can be found on Wiley Online Library

<http://olabout.wiley.com/WileyCDA/Section/id-410895.html>

Other Terms and Conditions:

v1.10 Last updated September 2015

Questions? customercare@copyright.com or +1-855-239-3415 (toll free in the US) or +1-978-646-2777.

**SPRINGER NATURE LICENSE
TERMS AND CONDITIONS**

Oct 20, 2018

This Agreement between Miss. Stefanie Mellon ("You") and Springer Nature ("Springer Nature") consists of your license details and the terms and conditions provided by Springer Nature and Copyright Clearance Center.

License Number	4385110269691
License date	Jul 09, 2018
Licensed Content Publisher	Springer Nature
Licensed Content Publication	Nature
Licensed Content Title	Anomalously weak Labrador Sea convection and Atlantic overturning during the past 150 years
Licensed Content Author	David J. R. Thornalley et al
Licensed Content Date	Apr 11, 2018
Type of Use	Thesis/Dissertation
Requestor type	academic/university or research institute
Format	print and electronic
Portion	figures/tables/illustrations
Number of figures/tables/illustrations	1
High-res required	no
Will you be translating?	no
Circulation/distribution	<501
Author of this Springer Nature content	no
Title	INVESTIGATING THE 13C SUESS EFFECT IN THE NORTHWESTERN NORTH ATLANTIC
Instructor name	Dr. Markus Kienast
Institution name	Dalhousie University
Expected presentation date	Oct 2018
Portions	Fig. 3: Proxy reconstructions of AMOC changes over the past 1,600 years.
Requestor Location	Miss. Stefanie Mellon 1-6539 Chebucto Rd. Halifax, NS B3L1L6 Canada Attn: Miss. Stefanie Mellon
Billing Type	Invoice
Billing Address	Miss. Stefanie Mellon 1-6539 Chebucto Rd. Halifax, NS B3L1L6 Canada Attn: Miss. Stefanie Mellon
Total	0.00 CAD
Terms and Conditions	

Springer Nature Terms and Conditions for RightsLink Permissions

Springer Customer Service Centre GmbH (the Licensor) hereby grants you a non-exclusive, world-wide licence to reproduce the material and for the purpose and requirements specified in the attached copy of your order form, and for no other use, subject to the conditions below:

1. The Licensor warrants that it has, to the best of its knowledge, the rights to license reuse of this material. However, you should ensure that the material you are requesting is original to the Licensor and does not carry the copyright of another entity (as credited in the published version).

If the credit line on any part of the material you have requested indicates that it was reprinted or adapted with permission from another source, then you should also seek permission from that source to reuse the material.
2. Where **print only** permission has been granted for a fee, separate permission must be obtained for any additional electronic re-use.
3. Permission granted **free of charge** for material in print is also usually granted for any electronic version of that work, provided that the material is incidental to your work as a whole and that the electronic version is essentially equivalent to, or substitutes for, the print version.
4. A licence for 'post on a website' is valid for 12 months from the licence date. This licence does not cover use of full text articles on websites.
5. Where '**reuse in a dissertation/thesis**' has been selected the following terms apply: Print rights for up to 100 copies, electronic rights for use only on a personal website or institutional repository as defined by the Sherpa guideline (www.sherpa.ac.uk/romeo/).
6. Permission granted for books and journals is granted for the lifetime of the first edition and does not apply to second and subsequent editions (except where the first edition permission was granted free of charge or for signatories to the STM Permissions Guidelines <http://www.stm-assoc.org/copyright-legal-affairs/permissions/permissions-guidelines/>), and does not apply for editions in other languages unless additional translation rights have been granted separately in the licence.
7. Rights for additional components such as custom editions and derivatives require additional permission and may be subject to an additional fee. Please apply to Journalpermissions@springernature.com/bookpermissions@springernature.com for these rights.
8. The Licensor's permission must be acknowledged next to the licensed material in print. In electronic form, this acknowledgement must be visible at the same time as the figures/tables/illustrations or abstract, and must be hyperlinked to the journal/book's homepage. Our required acknowledgement format is in the Appendix below.
9. Use of the material for incidental promotional use, minor editing privileges (this does not include cropping, adapting, omitting material or any other changes that affect the meaning, intention or moral rights of the author) and copies for the disabled are permitted under this licence.
10. Minor adaptations of single figures (changes of format, colour and style) do not require the Licensor's approval. However, the adaptation should be credited as shown in Appendix below.

Appendix — Acknowledgements:

For Journal Content:

Reprinted by permission from [**the Licensor**]: [**Journal Publisher** (e.g. Nature/Springer/Palgrave)] [**JOURNAL NAME**] [**REFERENCE CITATION** (Article name, Author(s) Name), [**COPYRIGHT**] (year of publication)]

For Advance Online Publication papers:

Reprinted by permission from [**the Licensor**]: [**Journal Publisher** (e.g. Nature/Springer/Palgrave)] [**JOURNAL NAME**] [**REFERENCE CITATION** (Article name, Author(s) Name), [**COPYRIGHT**] (year of publication), advance online publication, day month year (doi: 10.1038/sj.[**JOURNAL ACRONYM**].)]

For Adaptations/Translations:

Adapted/Translated by permission from [**the Licensor**]: [**Journal Publisher** (e.g. Nature/Springer/Palgrave)] [**JOURNAL NAME**] [**REFERENCE CITATION** (Article name, Author(s) Name), [**COPYRIGHT**] (year of publication)

Note: For any republication from the British Journal of Cancer, the following credit line style applies:

Reprinted/adapted/translated by permission from [**the Licensor**]: on behalf of Cancer Research UK: : [**Journal Publisher** (e.g. Nature/Springer/Palgrave)] [**JOURNAL NAME**] [**REFERENCE CITATION** (Article name, Author(s) Name), [**COPYRIGHT**] (year of publication)

For Advance Online Publication papers:

Reprinted by permission from The [**the Licensor**]: on behalf of Cancer Research UK: [**Journal Publisher** (e.g. Nature/Springer/Palgrave)] [**JOURNAL NAME**] [**REFERENCE CITATION** (Article name, Author(s) Name), [**COPYRIGHT**] (year of publication), advance online publication, day month year (doi: 10.1038/sj.[**JOURNAL ACRONYM**])

For Book content:

Reprinted/adapted by permission from [**the Licensor**]: [**Book Publisher** (e.g. Palgrave Macmillan, Springer etc)] [**Book Title**] by [**Book author(s)**] [**COPYRIGHT**] (year of publication)

Other Conditions:

Version 1.0

Questions? customercare@copyright.com or +1-855-239-3415 (toll free in the US) or +1-978-646-2777.
